HOST UNIVERSITY: The University of Maryland

FACULTY: School of Engineering

DEPARTMENT: Department of Fire Protection Engineering

Academic Year 2016-2017

INFLUENCE OF DOUBLE-SKIN FACADES ON FIRE SAFETY

Cui Wuquan

Promoters:

Professor Michael J. Gollner

Professor Bart Merci

Professor Andre W. Marshall

Master thesis submitted in the Erasmus+ Study Programme

International Master of Science in Fire Safety Engineering

DISCLAIMER

This thesis is submitted in partial fulfilment of the requirements for the degree of *The International Master of Science in Fire Safety Engineering (IMFSE)*. This thesis has never been submitted for any degree or examination to any other University/programme. The author(s) declare(s) that this thesis is original work except where stated. This declaration constitutes an assertion that full and accurate references and citations have been included for all material, directly included and indirectly contributing to the thesis. The author(s) gives (give) permission to make this master thesis available for consultation and to copy parts of this master thesis for personal use. In the case of any other use, the limitations of the copyright have to be respected, in particular with regard to the obligation to state expressly the source when quoting results from this master thesis. The author and thesis supervisor must be informed when data or results are used.

April 30, 2017

ABSTRACT

A combined experimental and numerical approach for fire modeling is developed and examined in this research. Salt water modeling experiments are successfully conducted in laboratory in a 1/20 scaled acrylic model to simulate the smoke transportation in the configuration of louver double-skin facade. Utilizing blue dye and PIV/PLIF measurements assisting with dimensionless analysis, dimensionless front arrival time, dimensionless velocity, and dimensionless density difference of the salt water flow could be obtained to evaluate CFD full-scale models in FDS in which velocity, temperature, mass fraction, mass flow and particles are tracked in the domain. The measurements from these two methods show a great agreement in predicting smoke spread rate in the cavity and smoke filling process in the adjacent floor. Totally four cases with four different louver angles are tested, from which the most critical case 135 degrees along with its mechanism is highlighted. Results and conclusions could be referenced by fire consultants and architects when making designs and even fire fighters when making tactics. The advantages and disadvantages of applying salt water modeling and CFD modeling in fire research are summarized for future reference.

论文摘要 (Abstract in Chinese)

本篇论文在火灾研究中结合了实验模拟与电脑模拟。研究烟气在双层幕墙结构中传播的盐水实验在实验室二十分之一比例的模型中成功完成。实验分别利用蓝色染料和PIV/PLIF 激光技术获取盐水流动数据，辅以无因次分析得到无因次流动时间、无因次速度和无因次密度差。实验结果与在软件 FDS 中的计算流体动力学模型进行对比并得到理想的契合。两种方法皆成功预测烟气在双层幕墙空间的传播速率以及烟气在相邻楼层的填充过程。此次研究使用两种方法对四种外层幕墙角度进行了分析并得出最不利角度及其机理。实验结果和结论可以为将来性能化防火设计、建筑结构设计以及消防等方面提供建议。同时盐水模拟和数字模拟这两种火灾模拟的优缺点也在文中进行了论述，为将来火灾分析提供参考。

ACKNOWLEDGEMENTS

I would like to thank IMFSE program first for providing me such a splendid two-year studying experience and giving me this opportunity to finish my graduation thesis in the University of Maryland.

Then very special thanks to Professor Michael J. Gollner for all his guidance in my thesis. And I would like to thank Professor Andre W. Marshall for his significant suggestions and instructions on my research. I really learned a lot and improved a lot in these four months.

Moreover, I would like to express my gratitude to the Department of Fire Protection Engineering in the University of Maryland. I really enjoyed my stay here, all new things I know from here and all new friends I met from here. I would like to thank Mr. Pietro Maisto for his help in laser diagnose technology and some help when I arrived here and thank all colleagues in this department and Michael's group. How I want to continue the weekly lab meeting every Wednesday.

This research was funded by the DHS/FEMA/USFA Assistance to Firefighters Grant program, award EMW-2012-FP-01336. All previous works on this experimental setup are great assets to my research, including the works done by Professor Andre W. Marshall's students, Xiaobo Yao and Chan Chau Siang, and the model and nozzle built by Jan Felix Zimlich and Jens Triller, whose reports greatly helped me to understand the model design and basic setup at the beginning when I prepare the experiments. The report on year one progress for this funding also helped me a lot to understand the principles throughout these researches.

At last, I would like to say thanks to my father and mother who supported me in these two years. The United States of America is the 41st country I have been to, and I know I have two years not back to home. Without their support I cannot travel so far and further in future. As a self-funded student, it is a big expense to finish my study and research, but I am proud to tell that it is worth.

TABLE OF CONTENTS

APPENDICES

LIST OF TABLES

LIST OF FIGURES

NOMENCLATURE

$\dot{Q}^*$ dimensionless source strength for fire

$\dot{m}_{sw}^*$ dimensionless source strength for salt water

x_i^* dimensionless position

t^* dimensionless time

u_j^* dimensionless velocity

θ^* dimensionless density difference

$\dot{w}^*$ dimensionless volumetric mass release rate

$\dot{Q}$ heat release rate

$\dot{m}_{salt}$ salt release rate

x_i position

t time

u_j velocity

T temperature

T_0 ambient temperature

Y_{smoke} smoke mass fraction

y_{smoke} smoke mass fraction at source

Y_{salt} salt mass fraction

β volumetric expansion coefficient

L characteristic compartment height

ρ_0 ambient fluid density

c_p ambient fluid heat capacity

ΔH_c calorific value of fuel

Re Reynolds number

Gr Grashof number

Pr Prandtl number

Sc Schimidt number

ν kinematic viscosity

α thermal diffusivity

D mass diffusivity

Subscript

sw salt water

s salt

f fire

CHAPTER 1

Introduction

1.1 Motivation

New building features present many challenges to the fire safety of buildings. In order to improve the efficiency of heating and cooling in buildings, features long serving to protect structures and residents from fire, separation and smaller spaces, are violated in new designs. The double-skin facade, used as part of new natural ventilation schemes in high-rise buildings or skyscrapers improve the efficiency of lighting and sound insulation in the meantime, is rated as the most critical green-certified feature that may have adverse influence on fire safety from the interviews to fire protection consultants or engineers and the reviews to plenty of fire incidents [22]. As there is a general principal for fire protection designs that fire should be resisted to the floor of origin, the implication of double-skin facades may represent a feasible fire hazard transporting smoke and hot gasses between compartments of adjacent floors. At least when this feature is widespread in modern buildings, the fire risks are still not primely verified and well covered by literature. Thus, on the perspective of building design, architects who did not pour attention into this issue may be jeopardized by laggard fire research in double-skin facade.

On the side of fire safety engineering and fire fighting, due to the inhalation and visibility hazard of smoke in fire evacuation, smoke spread and smoke filing in different configurations are extremely important topics to study. In Chow's report on performance-based fire safety design for green and sustainable buildings [12], two fire accidents in green buildings are reviewed which gave a conclusion that the operating fire suppression system in these buildings cannot make the heat released in a room under the estimated rate, which means the unexamined green feature may post an unexpected influence on fire safety. As double-skin facade is a newly developed feature which is also related to building ventilation system, the study on this topic could provide guidance on smoke and heat control and prevent unforeseen hazard in fire evacuation and fire fighting.

From the view of society, the use of double-skin facade could improve the living comfort of residents, reduce the energy consumption and related costs, and minimize the impact on environment from building. The motivation of studying the influence of double-skin facade on fire safety could well match and guarantee the benefits of this green feature in protecting the life safety of occupants, decreasing the threaten on structure failure and related economic losses, and controlling the diffusion of toxic gases to the environment.

In fire research, a combination of experimental and numerical approaches is often applied, mostly using fire tests and CFD modeling. The method of salt water modeling is a commendable way to study smoke movement in different configurations as proven by some literatures. This method along with scaling theory is examined again in the configuration with double-skin facade.

1.2 Literature Review

1.2.1 Double-skin Facade

The double-skin facade is a kind of building envelop system with two layers of facades creating an air cavity in between. As described in the Best Practice for Double Skin Facades [28], the most classical classification methods for double-skin facades are depend on the type of ventilation, the ventilation mode of cavity and the partitioning of the facade, of which the most common-applied type in modern high-rise buildings is the multiple-storey louver double facade with natural ventilation and outdoor air curtain. The Gherkin (more formally known as 30 St Mary Axe) is a very classical example of it. It is common recognized and examined by many researchers that the use of double-skin facade could significantly improve the energy utilization in high rise buildings [1].

In the field of fire research in double-skin facade, Chow has contributed a great deal of effort by applying CFD modeling with full-scale fire tests [8,9,10,11]. In the full-scale fire tests on an enclosure with double-skin facade of 6m's height [9], temperatures along the height of cavity are recorded and it is found that the inner glazing is very easily broken above the fire room. After that another full-scale fire test is done in a fire enclosure with double-skin facade of 15m's height and how the width of cavity could influence the smoke spread is also studied [11]. Then numerical study on the same topic was conducted which was validated by the results of full-scale fire tests [8]. Based on above research, Chow developed a set of correlations between the temperature in the cavity with the height above the ceiling of fire room to predict the window breakage in fire [10]. It could be concluded that the adding of cavity in a building can extremely influence the fire safety conditions, especially the high-rise building with double-skin facade for the entire height which allow smoke to travel up or down to all other floors.

Some other researchers also studied different factors of double-skin facade that may influence the smoke spread in cavity. For example, O'Connor studied the influence of the angle of inner-skin facade and horizontal projection between floors [23]. Li used numerical method to simulate the effect of cavity width [16]. Ding focused on the principal of natural ventilation and proposed to use methods to reduce the temperature of cavity to prevent smoke spreading into the adjacent floor [14].

However, no literature is found about the influence of louver angle in outer-skin facade on the smoke vertical movement or stack effect.

Moreover, as stated in Acknowledgements, all previous works on this experimental setup are great assets to my research, including the works done by Professor Andre W. Marshall's students, Xiaobo Yao and Chan Chau Siang's thesis on scaling theory, and Jan Felix Zimlich and Jens Triller's lab reports on model design and basic setup.

1.2.2 Salt Water Modeling

The development of salt water modeling cannot be divided from the development of scaling theory. In 1988, Steckler developed the scaling relations for salt water flow connecting this method to fire modeling in quantitative study and a complex ship model is used in experiment to examine the theory for smoke simulations [27]. Then Quintiere developed and summarized the scaling laws in fire research which laid a foundation for further studies using salt water modeling [24].

With the development of this method, new technologies are applied to assist the analysis. Laser diagnose technology made it possible for better data recording. Yao's research is another cornerstone which developed the detailed dimensionless equations for salt water analog model and examined the reliability and repeatability using PLIF and LDV in experiments modeling the fire induced flow moving along the ceiling [32]. Siang conducted the salt water experiment assisting with PIV and PLIF techniques on the topic of smoke dispersion for ceilings with deep beam, which showed a great agreement with full-scale test by using the equation developed by Yao for dimensionless analysis [26].

Salt water modeling became a commendable method in fire research with several advantages over the traditional methods of fire tests and CFD modeling. Only two literatures are found about the comparison between salt water modeling and CFD modeling. Clement used the results of salt water experiments to verify the hydrodynamic models in FDS (Fire Dynamics Simulator) for three different types of configuration [7]. Kelly applied blue dye salt water tests to compare the front arrival time to certain locations in a two-floor compartment connecting by a horizontal opening on the second storey floor with the result of FDS simulations [15]. Both researches showed great match in results for these two methods.

1.2.3 CFD (Computational Fluid Dynamics) Modeling

CFD based fire modeling is used extensively at present not only in universities or institutions but also in fire services, fire litigations and fire designs. As mentioned before, a combination of numerical and experimental approach is widely used in fire research, as this way could confirm the reliability of results. Many practical problems in fire were studied by using CFD modeling validated by fire tests. Barowy used this

way to study the heat and smoke transportation in a live fire training facility [3]. Yang applied this method to investigate a storehouse fire accident [30]. Yan followed this principle to examine the fire safety performance of building external insulation system [34]. The combination of these methods could contribute to more complex fire researches and the validation process could improve the function of CFD modeling tools.

Although CFD based fire modeling is useful for dealing with engineering problems, there are still quite a lot of limitations. Babrauskas summarized six limitations of computer-based fire modeling when studying zone fire models, including no flame spread, no heat release rate, no fire and smoke chemistry, absence of realistic layer mixing and no suppression, then gave a conclusion that nowadays computer-based fire modeling is useful but conditionally trustful [5]. What's more, CFD based fire modeling is very user-dependent, as concluded by the famous round-robin study of a priori modeling prediction in Dalmarnock Test in which ten international independent groups simulate the same fire tests but big discrepancies are found in final comparison [25].

Thus, it is extremely important to conduct validation and verification studies for fire models to minimize the limitations and unreliability which is an often discussed topic in fire modeling [21, 29]. Users should pay attention to some conditions when using computer fire modeling. Those conditions are commendably summarized by Beard in the "Fire Design Triangle" [6].

1.3 Research Objective

In this research, a detailed analysis of smoke movement inside the cavity of double-skin facades and smoke filling in the second floor compartment are provided by using salt water modeling and CFD (Computational Fluid Dynamics) modeling. The quantitative saltwater modeling is a prominent physical model to simulate smoke movement within complex building configurations, connecting inverse saltwater flow with fire induced flow by dimensionless analysis. Implementing this methodology, a two-floor acrylic model with louvered double-skin facades in a reduced scale is built based on the configuration of a quintessential architecture using this green feature, the Gherkin in London, UK. In laboratory saltwater blue dye tests were conducted first to provide qualitative comparison for 4 cases with different angled louvers. Then these 4 cases were carried on by applying both PIV (Particle Image Velocimetry) and PLIF (Planar Laser Induced Fluorescence) to determine velocity and concentration fields in order to study the transport of smoke and hot produce between building facades. In addition to experimental approach, numerical method of CFD modeling by FDS-SMV is applied to study the same cases as salt water modeling. The combination of these two methods could foster advantages of both approaches while circumvent disadvantages of separate models. The comparison of results from each method could

give more reliable conclusions for this research and more valuable suggestions for studies in future using these methods in other topics.

The specific objective of this research are listed below.

- Further develop and examine the method of salt water modeling in applying to complex configurations (double-skin facades) assisted with PIV (Particle Image Velocimetry) and PLIF (Planar Laser Induced Fluorescence) technology.
- Use FDS (Fire Dynamics Simulator) to simulate the smoke movement in a two-floor compartment with double-skin facade.
- Compare the results of salt water modeling and CFD modeling using dimensionless analysis.
- Determine the influence of louver double-skin facade on velocity, temperature, and mass fraction of smoke in vertical transportation.
- Give suggestions on applying louver double facade in building design and related fire safety issues.
- Give suggestions on the combining method of salt water modeling and CFD modeling in future study.

CHAPTER 2

Methodology

The researches on real compartment fires or the development of these fire theories cannot leave methods of full-scale fire testing and fire modeling. Costly and time-consuming, limited numbers of real scale fire tests could be conducted. On the other hand, with the extensive application of CFD (Computational Fluid Dynamics) Modeling, very limited numbers of fire test records could meet the standards for model validation, while the accuracy and reliability of CFD modeling are still need to be deliberated. Under this circumstance, salt water modeling, a physical simulation method with infinite resolution, is developed for fire research and comparison with the result of CFD Modeling.

In this research, two methods are applied to study the topic (Figure 2.1), which are CFD (Computational Fluid Dynamics) modeling using the software of FDS-SMV (Fire Dynamics Simulator & Smokeview) and salt water modeling assisting with laser diagnose technology, PIV (Particle Image Velocimetry) and PLIF (Planar Laser Induced Fluorescence). Generally, both methods linked by scaling theory could provide records for quantitative and qualitative analysis, of which influence of the louver angle in double-skin facade on smoke spread in cavity and smoke filing in adjacent floor are two main points to investigate. Moreover, the results of these two methods are compared and evaluated by dimensionless analysis, which could ensure the reliability of this research.

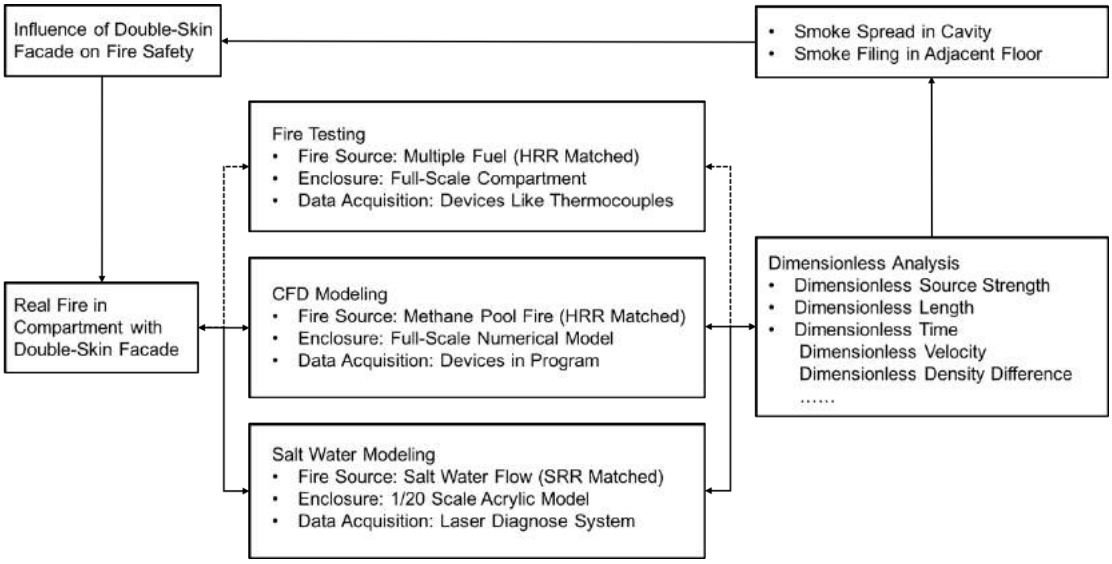

Figure 2.1 General View of Methods to Study the Topic

2.1 Dimensionless Analysis

In scientific research, dimensionless analysis is a widely-used method to simplify calculations or qualify comparisons. Fire-induced flow and salt water flow could be linked by this method, of which proper dimensionless parameter should be chosen to make them comparable. Quintiere verified the scaling application in fire research by applying dimensionless derivations for several fire-related parameters [24]. Xiaobo developed this theory for salt water flow by defining dimensionless parameters to solve the governing conservation equations of mass, momentum and salt mass species, which made it possible to use salt water flow to simulate fire-induced flow theoretically [33]. The governing equations and derived dimensionless parameters for fire-induced flow and salt water flow are summarized in Table 2.1.

To apply these equations for data processing, several assumptions need to be noticed:

- The flow is injected from the point source of origin.
- There is no radiative heat loss in the system. Radiation, pressure work and viscosity dissipation are negligible.
- The smoke and hot gases generated by fire source is considered as ideal gas.
- Boussinesq approximation is applied when determining the buoyancy that the term $\frac{\rho-\rho_0}{\rho_0}$ is estimated by $\frac{T-T_0}{T_0}$, then in other places ρ is equal to ρ_0.
- Conductivity k, specific heat c_p, diffusion coefficient D, and viscosity μ are considered as constant.
- The volumetric expansion coefficient of smoke is considered to be the reciprocal of ambient temperature and the volumetric expansion coefficient of salt water is considered to be constant as 0.76.

Dimensionless Analysis		Fire-Induced Flow	Salt Water Flow
Governing Equations	Momentum	$\frac{\partial u_j^*}{\partial t^*} + u_i^* \frac{\partial u_j^*}{\partial x_i^*} =$ $-\frac{\partial p^*}{\partial x_i^*} + \frac{1}{Gr^{1/3}} \frac{\partial^2 u_j^*}{\partial x_i^* \partial x_i^*} + \theta_T^* f_j^*$	$\frac{\partial u_j^*}{\partial t^*} + u_i^* \frac{\partial u_j^*}{\partial x_i^*} =$ $-\frac{\partial p^*}{\partial x_i^*} + \frac{1}{Gr^{1/3}} \frac{\partial^2 u_j^*}{\partial x_i^* \partial x_i^*} + \theta_{sw}^* f_j^*$
	Energy	$\frac{\partial \theta_T^*}{\partial t^*} + u_i^* \frac{\partial \theta_T^*}{\partial x_i^*} =$ $\frac{1}{Gr^{1/3} Pr} \frac{\partial^2 \theta_T^*}{\partial x_i^* \partial x_i^*} + \dot{q}^*$	
	Mass Species	$\frac{\partial \theta_{smoke}^*}{\partial t^*} + u_i^* \frac{\partial \theta_{smoke}^*}{\partial x_i^*} =$ $\frac{1}{Gr^{1/3} Sc} \frac{\partial^2 \theta_{smoke}^*}{\partial x_i^* \partial x_i^*} + \dot{w}_{smoke}^*$	$\frac{\partial \theta_{sw}^*}{\partial t^*} + u_i^* \frac{\partial \theta_{sw}^*}{\partial x_i^*} =$ $\frac{1}{Gr^{1/3} Sc} \frac{\partial^2 \theta_{sw}^*}{\partial x_i^* \partial x_i^*} + \dot{w}_{sw}^*$
Basic Variables		$Gr = \frac{g \dot{Q} {L_f}^2}{\rho_0 c_p T_0 v^3} = Re^3 \dot{Q}^*$ $Pr = \frac{v}{\alpha}$ $Sc = \frac{v}{D}$	$Gr = \frac{\beta_{sw} g \dot{m}_{salt} {L_{sw}}^2}{\rho_0 v^3} = Re^3 \dot{m}_{sw}^*$ $Sc = \frac{v}{D}$
Fixed Variables	Source Strength	$\dot{Q}^* = \frac{\beta_T \dot{Q}}{\rho_0 c_p T_0 g^{1/2} {L_f}^{5/2}}$ $\beta_T = \frac{1}{T_0}$	$\dot{m}_{sw}^* = \frac{\beta_{sw} \dot{m}_{salt}}{\rho_0 g^{1/2} {L_{sw}}^{5/2}}$ $\beta_{sw} = 0.76$
Independent Variables	Position	$x_i^* = \frac{x_i}{L_f}$	$x_i^* = \frac{x_i}{L_{sw}}$
	Time	$t_f^* = t_f (g/L_f)^{1/2} (\dot{Q}^*)^{1/3}$	$t_{sw}^* = t_{sw} (g/L_{sw})^{1/2} (\dot{m}_{sw}^*)^{1/3}$
Dependent Variables	Velocity	$u_j^* = \frac{u_j}{(\dot{Q}^*)^{1/3} (g L_f)^{1/2}}$	$u_j^* = \frac{u_j}{(\dot{m}_{sw}^*)^{1/3} (g L_{sw})^{1/2}}$
	Density Difference	$\theta_T^* = \frac{\beta_T (T - T_0)}{(\dot{Q}^*)^{2/3}}$ $\theta_{smoke}^* = \frac{\beta_T Y_{smoke} \Delta H_c}{y_{smoke} c_p (\dot{Q}^*)^{2/3}}$	$\theta_{sw}^* = \frac{\beta_{sw} Y_{salt}}{(\dot{m}_{sw}^*)^{2/3}}$

Table 2.1 Dimensionless Analysis for Fire-Induced Flow and Salt Water Flow

2.2 Salt Water Modeling

2.2.1 Analogue Method

The vertical spread of smoke and hot gases generated by fire source is dominant by buoyancy, while buoyancy depends upon the difference between upward and downward pressure which is related to density difference between smoke and ambient air. In salt water analogue system, salt water induced by nozzle has a higher

density than ambient fresh water, which creates an inverse analogue system to model the smoke spread to ambient air. The schematic of salt water analogue modeling compared with smoke spread is shown in Figure 2.2. With an upside-down scaled building model residing in a large tank full of fresh water, this method can be utilized to simulate smoke movement within complex building configurations. The process of enclosure model design for studying the influence of double-skin facade on fire safety is described in 2.2.2.

As shown in Figure 2.2, the function of both systems rely on the density difference between injected flow and its ambient environment. However, fire plume is not only a buoyancy-dominant flow but also a turbulent flow as concerned by Steckler [27]. Turbulence is one of the most important and difficult characteristics to reproduce or simulate in different models, which is also a key element to make the model repeatable and reliable. An appropriate flow source design could maximum the feature of turbulence in model, which is introduced in 2.2.3.

As proved by plenty of researches [7, 15, 26, 33], the method of salt water modeling can be applied to different complex configurations and results are well-matched with real fire measurements. Using laser diagnose technology, salt water flow can be tracked and recorded. Using dimensionless analysis, the output of salt water modeling can be compared to real fire-induced flow in different configurations. The experiments of salt water modeling are conducted in the laboratory of the Department of Fire Protection Engineering in the University of Maryland. All setups and devices used in these experiments are listed in 2.2.4. In general, there are three phases of experiments in this research. Firstly, blue dye tests (stated in 2.2.5) are performed to visualize the flow and find the areas of vital interest for further investigation. Then Particle Image Velocimetry (PIV) experiments (stated in 2.2.6) are conducted to examine the influence on the velocity of salt water flow. At last, the density changes of key areas are recorded using Planar Laser Induced Fluorescence (PLIF) technology (stated in 2.2.6).

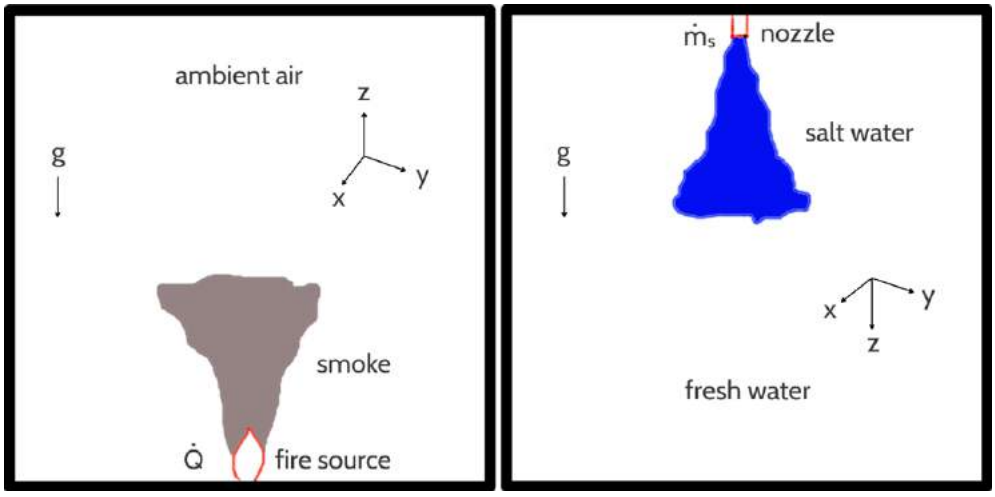

Figure 2.2 Schematic of Salt Water Analogue Modeling

2.2.2 Enclosure Design

As models with complex configurations can be effectively tested using salt water analogue method, it becomes primarily important to design and build a typical enclosure which represents the research objective. In this research, the angle of louvers which compose the outer-skin facade is the analogue variable to study the smoke movement in the small vertical cavity, thus a two-floor compartment with adjustable outer-skin facade is built based on the dimension scale of a famous double-skin facade architecture, the Gherkin (Figure 2.3).

Figure 2.3 The Gherkin [Photo from http://www.fosterandpartners.com/projects/30-st-mary-axe/]

The Gherkin (more formally known as 30 St Mary Axe), which is located in the heart of London's primary financial district, is renowned as the first ecological building in UK. With the application of double-skin facade system, ventilation performance or air flow of the whole building could be controlled by adjusting angles of exterior facade panels. Following researches on this glazing configuration, plenty of researchers repeatedly claimed that as much as fifty percent of the energy consumption could be saved compared with other similar office buildings without this feature [2].

Based on the elevation drawing (shown in Figure 2.4) and floor plan (shown in Figure 2.5) of the Gherkin, a room in level 22 is randomly chosen as the prototype of the acrylic model. The room size and distance between facades of the model are scaled from the real dimensions of the Gherkin, while the openings and type of louver is simplified to more classical design. The dimensions of the real building and scaled

model are listed in Table 2.2. The CAD draft of the acrylic model to show the configuration in design is also shown in Figure 2.6.

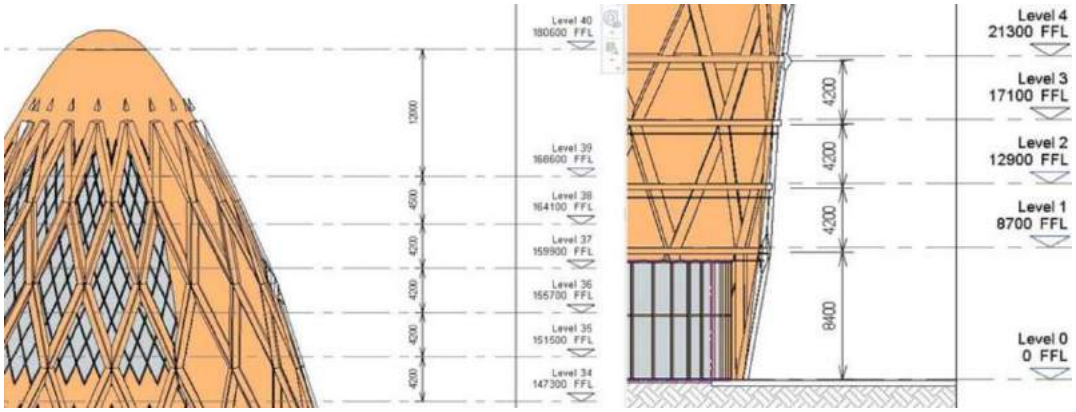

Figure 2.4 Part of the Elevation Drawing (The Gherkin) [Photo from http://www.fosterandpartners.com/projects/30-st-mary-axe/]

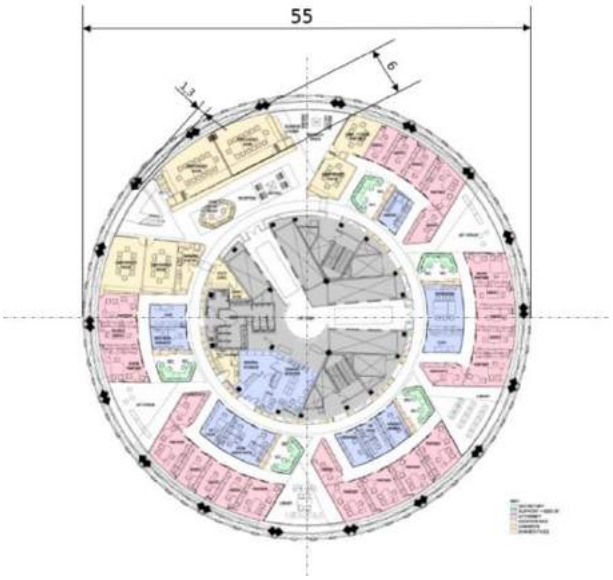

Figure 2.5 Floor Plan of Level 22 (The Gherkin) [Photo from http://www.fosterandpartners.com/projects/30-st-mary-axe/]

	Room			Window (Opening)		Cavity	Louver	
	Length	Width	Height	Height 1	Height 2	Width	Width	Distance
Real Building	6.000	4.000	3.900	1.000	1.900	1.300	0.860	0.720
Scaled Model	0.280	0.190	0.180	0.046	0.090	0.060	0.040	0.033
Scale	0.047	0.047	0.046	0.046	0.047	0.046	0.047	0.046

Table 2.2 Dimensions of the Real Building and Scaled Model (m)

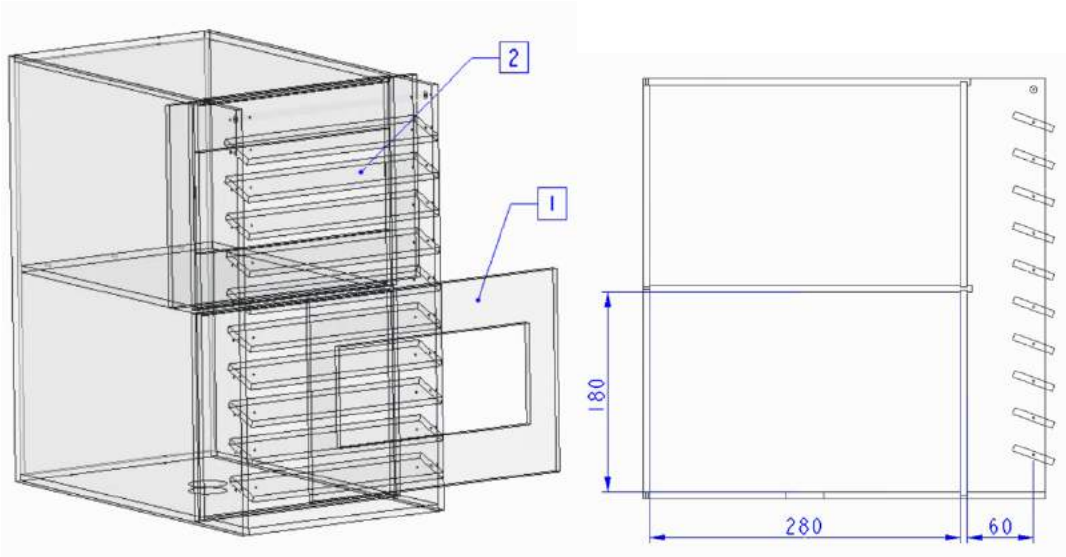

Figure 2.6 CAD Draft of the Model [(1) Inner-skin facade; (2) Outer-skin facade.] Notes: (1) The inner-skin facade of the model is designed to be replaceable, of which three acrylic panels with different opening factors (25%, 50% and 75%) are produced as another variable for research in future. In this research, an opening factor of 25% is used in first floor (refer to Height 1 in Table 2.2) and 50% is used in second floor (refer to Height 2 in Table 2.2). (2) The angle of outer-skin facade or louver of the model is designed to be adjustable. In this research, 0°, 45°, 90° and 135° are tested in salt water experiments. For the convenience of fabrication, same type of acrylic plate is used for this model, so the thickness of louver is not in the same scale as other dimensions. [Photo from Jan and Jen's lab report]

According to the design of this 1/20 scale model, 8 pieces of ACRYLITE® Optical mar resistant acrylic sheets, 590×450 mm^2 each with a thickness of 6 mm, are ordered and cut in laboratory using VLS 3.60 Universal Laser System (shown in Figure 2.7). The laser cutter is set to a relatively low power of 40% and a speed of 100% to reduce the defusing heat around the laser beam and avoid an unsolicited chamfering of the edges caused by the asymmetrical melting of the acrylic. In order to achieve the impermeability of the model, 3 steps are applied when assembling the sculpted plates ahead of leak-proof tests. Firstly, the indentation method is used in laser system after cutting the acrylic plates, a depth of 1.5 mm indentation for two-side-connection plates by setting a power of 10% and a speed of 90% and a depth of 3 mm indentation for one-side-connection plates by setting a power of 18% and a speed of 85%. Then Weld-On 16, a very high strength, clear, fast curing and solvent-type acrylic cement, is exploited to bond those plates into designed configuration and Weld-On 4, a water-thin, moderately fast setting and blush-resistant acrylic cement, is exploited to seal the remaining leakages. At last, additional bolts are applied at joints where adhesive stress could be reduced caused by acrylic cement. The accomplished acrylic model for salt water experiment is shown in Figure 2.8.

Figure 2.7 VLS 3.60 Universal Laser System [Photo from https://www.ulsinc.com/]

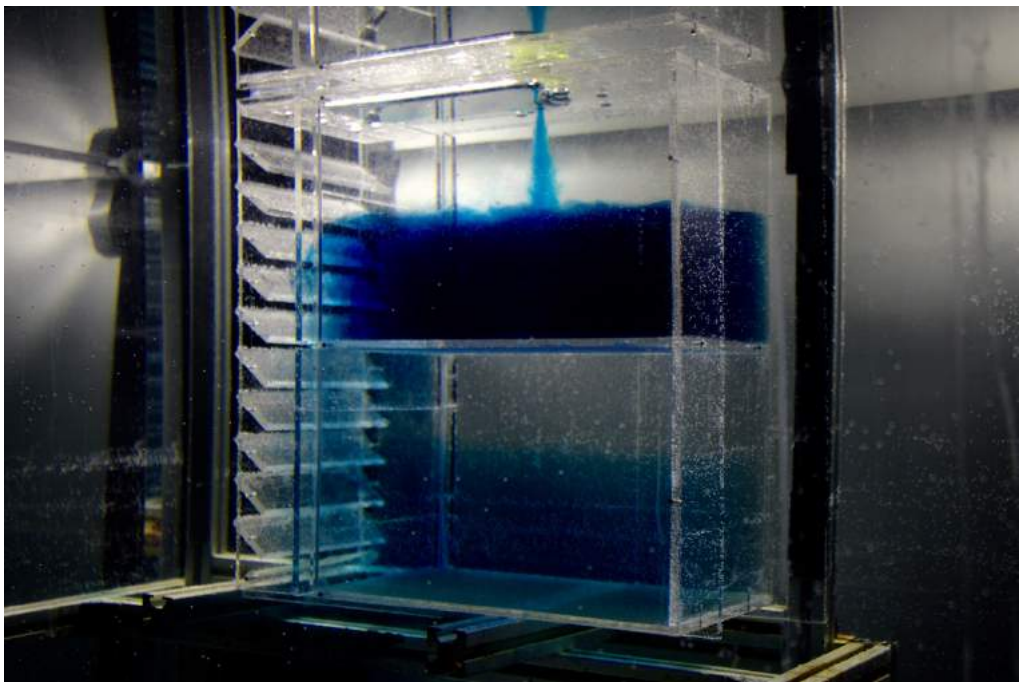

Figure 2.8 Acrylic Model for Salt Water Experiment

2.2.3 Flow Source Design

As stated in 2.2.1, salt water flow injected from the nozzle should be buoyancy-driven turbulent flow theoretically which is dependent on the velocity of injection. To achieve turbulence, a relative high velocity is required, but a certain distance of flow from injector will be momentum-driven. To get buoyancy-driven, a relative low velocity is needed, but a certain distance of flow from nozzle will be laminar flow. Thus the first problem of nozzle design is to determine which factor is more important for this simulation. From the target of this research, smoke movement in cavity and smoke filling in adjacent floor are two main points of interest to study. Obviously spilling flow

from the window of source-origin compartment is buoyancy-driven since there is no downward velocity when salt water flows just reach the opening, which means the flow source of cavity and adjacent compartment could provide buoyancy-driven flow. The momentum-driven flow may affect the smoke filling time of the first compartment and the location of point source, but the compartment with flow source is not the field to be focused on. The reference time can be set to the start of spilling flow from opening when calculating the dimensionless time to compare with the result of FDS modeling. Therefore, in this research appropriate turbulence scaling of the flow is chosen as the first requirement in the nozzle design, while the second condition is ensured from cavity to be buoyancy-driven.

The nozzle should also be designed to prevent back flow and recirculation at the outlet. A small outlet diameter of 4.3 mm and a larger inlet diameter of 5.9 mm are chosen (shown in Figure 2.9) to avoid those effects. The structure of the flow exiting the nozzle can be greatly affected by the geometry of the nozzle. Therefore, an overall consideration of salt mass fraction, volumetric flow rate and nozzle diameter should be taken to achieve the desired flow characteristics.

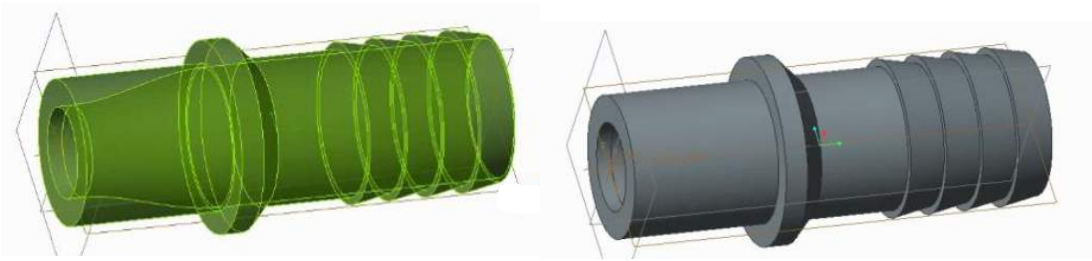

Figure 2.9 3D Draft of the Nozzle [Photo from Jan and Jen's lab report]

Based on the basic principles of flow source design, the nozzle to be used as flow source for salt water modeling is manufactured by 3D-printing and stereolithography techniques. The nozzle manufactured by stereolithography is characterized by transparent yellow sunburned surface due to the high UV-sensitivity of the photopolymer material and the exposure time for the hardening process. The advantage in applying the stereolithography compared with 3D printing is to get a smoother inner surface of the nozzle. The same product could be obtained after the manufacturing process by polishing the 3D-printed component using acetone. Although the 3D printing technique ensured high fidelity of the details, the acetone-smoothing procedure compromised the effectiveness of the designed inner surface by melting the material. Therefore, the nozzle employed for the measurements is manufactured by stereolithography, while the adaptor to fit nozzle into the model is manufactured by 3D printing. Moreover, the nozzle is painted with black color on purpose to reduce laser scattered reflections during PIV and PLIF applications. The nozzle with adaptor produced for salt water experiments are shown in Figure 3.0.

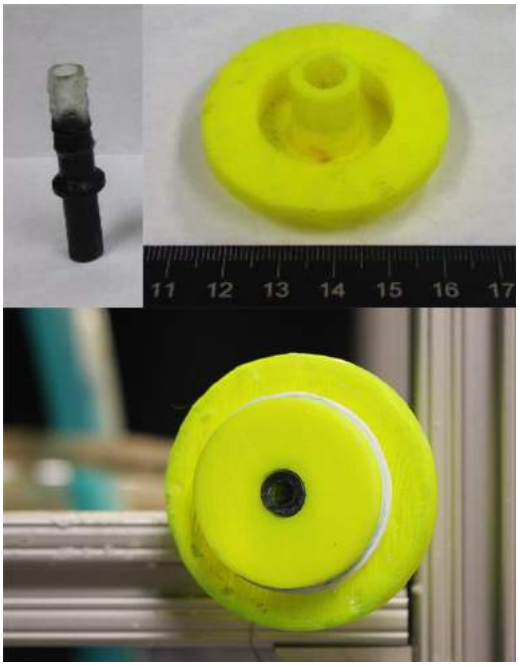

Figure 2.10 Nozzle with Adapter

To bring salt water into the nozzle, a gravity-driven source system is applied which consists of two 10-gallon polyethylene tanks vertically placed in a frame shelf (shown in Figure 2.11). A pump bringing salt water from the bottom tank to the top is used to keep the salt water well-mixed, and a vertical tube connecting two tanks is used to keep salt water level constant in order to provide a constant pressure in the outlet of injector.

Figure 2.11 Gravity-Driven Source System

The volume flow rate of this flow system is set to be 3×10^{-5} m^3/s which is tested by a rotameter. 4 kg salt is weighed to be well-mixed into 10 gallon fresh water, which provides a salt mass fraction of 0.10. Knowing these values, dimensionless source strength of this salt flow system can be calculated using the equation stated in Table 2.1, which is equivalent to 600 kw fire. More parameters of the flow source design are listed in Table 2.3.

Injector Diameter, D (m)	4.3×10^{-3}
Volumetric Flow Rate, $\dot{V}$ (m^3/s)	3.1×10^{-5}
Injection Velocity, U_i (m/s)	2.1
Reynolds Number, Re	8600
Salt Mass Fraction, Y_{salt}	0.1
Salt Water Density, ρ_{sw} (kg/m^3)	1.1×10^{3}
Salt Release Rate, $\dot{m}_{salt}$ (kg/s)	3.5×10^{-3}
Dimensionless Source Strength, $\dot{m}^*_{sw}$	6.2×10^{-5}

Table 2.3 Salt Water Tests Matrix

2.2.4 Experimental Setup

The experiments of salt water modeling are conducted in the laboratory of the Department of Fire Protection Engineering in the University of Maryland. All setups and devices used in these experiments are shown in Figure 2.12. The experiments of salt water modeling include three phases in this research, Blue dye tests, Particle Image Velocimetry (PIV) experiments and Planar Laser Induced Fluorescence (PLIF) experiments. The experiment procedures and special setups of these three phases are explained in the following three sections. In this section, basic setups for salt water modeling experiments are introduced.

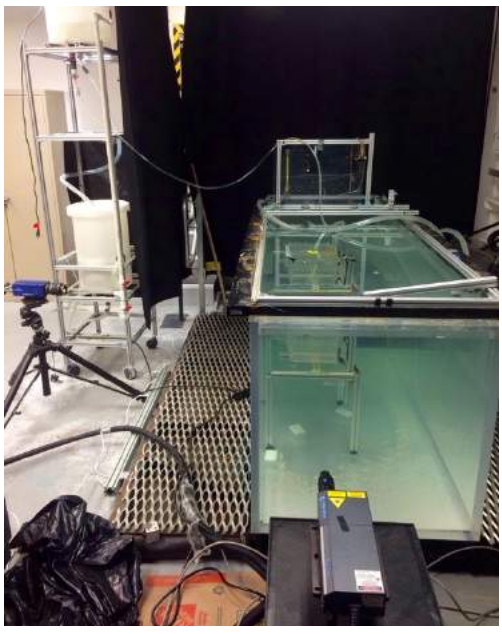

Figure 2.12 Experimental Setups for Salt Water Tests

As shown in Figure 2.13, all devices in salt water experiments can be divided into three parts. The first part is salt water source system, which is introduced in 2.2.3. Two 10-gallon tanks connected to nozzle can provide turbulent salt water flow with steady volumetric flow rate. The salt water source is connected with double-skin facade model which is located in the second part, a large fresh water tank with dimensions of $2.375 \times 0.79 \times 0.85$ m^3. This tank is filled with fresh water which is filtered by 0.5 μm cotton filter in each test. Since the salt water plume is very sensitive to small movement in the tank, a quiescent environment should be ensured prior to experiments. A stilling time of at least 1 hour is given after the tank is filled which could restrain the movement of ambient water flow in the tank caused by the filling process. The flow source is calibrated first in the tank and different source strengths are tested to choose one with the best effect. At last, a salt mass fraction of 0.1 and a volumetric flow rate of 3.1×10^{-5} m^3/s are chosen for the following experiments. The third part is devices for data acquisition. Since devices and principles are different for blue dye tests, PIV and PLIF experiments, more details are described in the next couple of sections. In PIV and PLIF experiments, devices are all coated with black opaque paint to avoid noise in the form of back reflected light and the area using laser is screened by a special blackout curtain by ThorLabs to protect the sensitivity of devices to light and prevent the harmful reflection of laser [20].

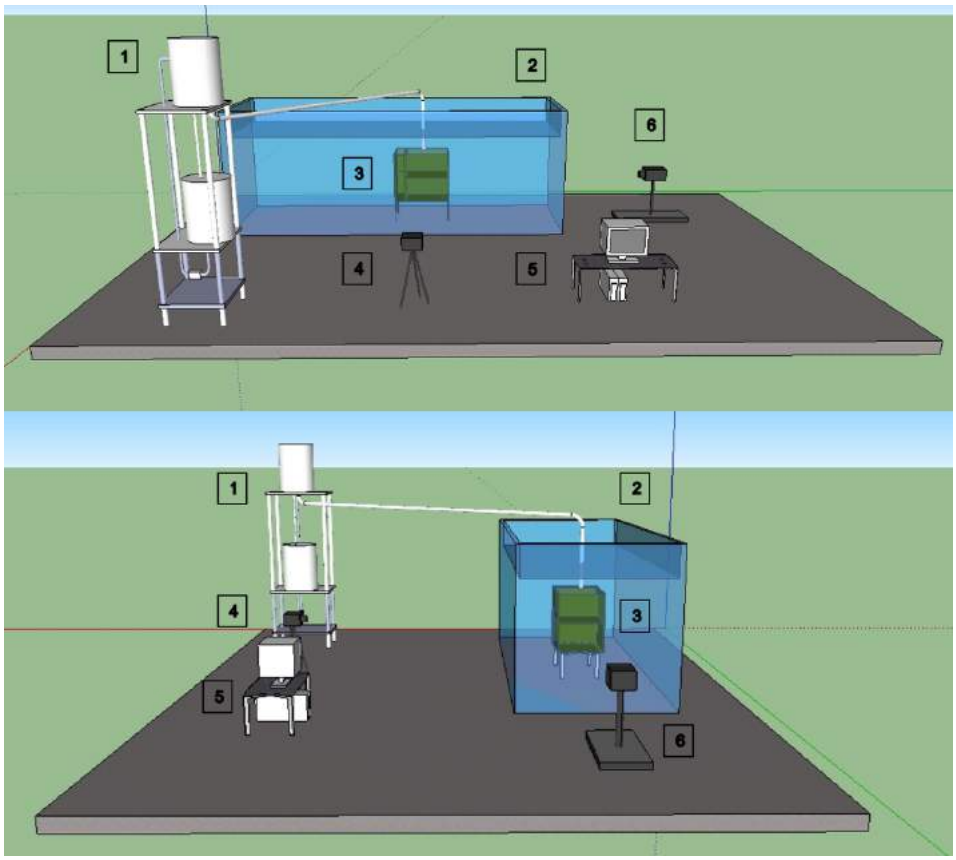

Figure 2.13 Experimental Facilities for Salt Water Tests [(1) Salt water source system; (2) Fresh water tank; (3) Double-skin facade model; (4) Camera (Nikon D7100 or CCD camera, listed in Table 2.4); (5) Computer for data acquisition; (6) Laser system.]

2.2.5 Blue Dye Tests

Blue dye test is an easy but efficient method to investigate the characteristics of salt water flow in complex configurations. The visualization could help to fix the critical case and interest region for further study, including PIV and PLIF experiments and CFD modeling. Other than qualitative study, the front arrival time for a certain location in the model recorded by camera is an important quantitative parameter to simulate the smoke arrival time. As mentioned in 2.2.3, blue dye tests could also be used to calibrate or choose a flow source before all salt water experiments.

In blue dye tests, blue dye powder (0.03% by weight) is added to salt water source and the circulation system makes the blue color of salt water homogeneous. A Nikon D7100 camera with an 18-105 mm f/1-3.5 lens is used to record the images (4000 × 6000 pixels^2) of experiments in a time interval of 2 seconds until the blue color is steady in the second floor compartment. The camera is fixed by a tripod setting parameters to 40 for focal length, 4.5 for f-number, 1/50 for exposure time and 800 for ISO. To reduce the reflection of glass and water, neon lights are installed above the tank in the experiments. In total, 4 blue dye tests are carried on for four different louver angles, 135°, 90°, 45° and 0° which are named as M1, M2, M3 and M4 (shown in Figure 2.14).

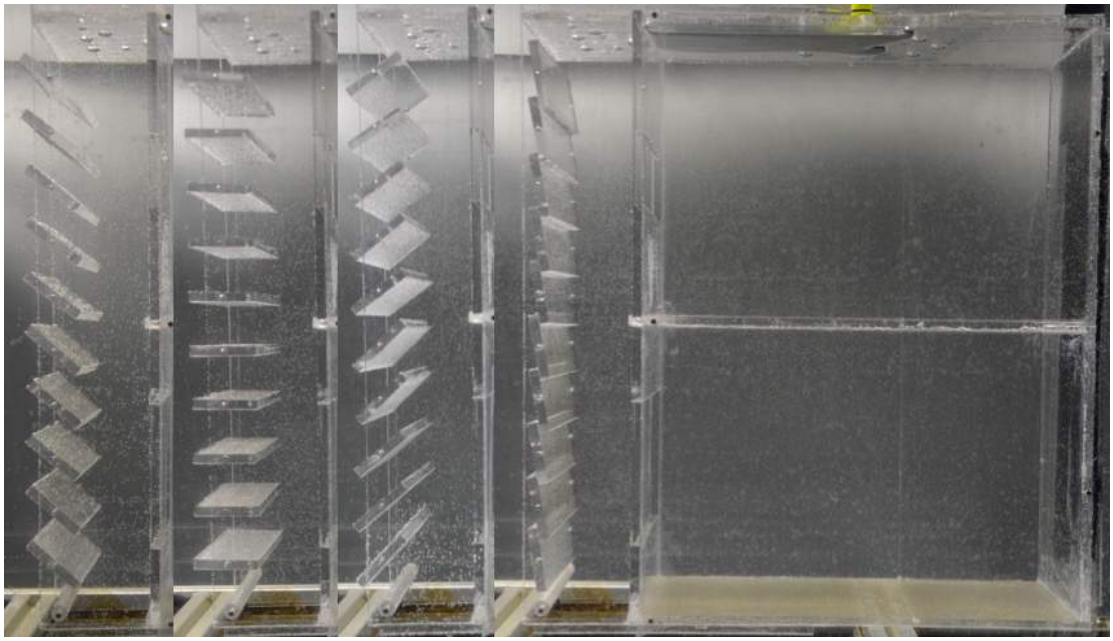

Figure 2.14 Models with Different Louver Angles in Salt Water Experiments
Note: These four cases are named as M1, M2, M3 and M4 from left to right according to the changes of louver angle. The part of two-floor compartment in images from M1 to M3 are abbreviated, remaining the area of double-skin facade only.

2.2.6 PIV (Particle Image Velocimetry) Experiments

After blue dye tests, interest areas are chosen for further investigations using laser diagnose technology. The flow pattern in cavity around the louver is the first interest point to study as this could prove the influence of louver angle on the movement of flow in this region. To study the flow pattern in cavity, the flow source of cavity which is the spilling flow from the opening of compartment with source origin is a critical factor to start a certain flow pattern and the flow into the adjacent compartment is also important which could reflect the impact of louver. PIV technique can be used to estimate the flow velocity field by tracking the displacement of the particles, setting on a double pulse mode which means the camera records one image per pulse with a known time gap. By tracking the displacement of particles, stream lines of salt water flow can be drawn which could be an unexceptionable way to describe the flow pattern. Then results obtained in PIV experiments could be used to validate the CFD modeling.

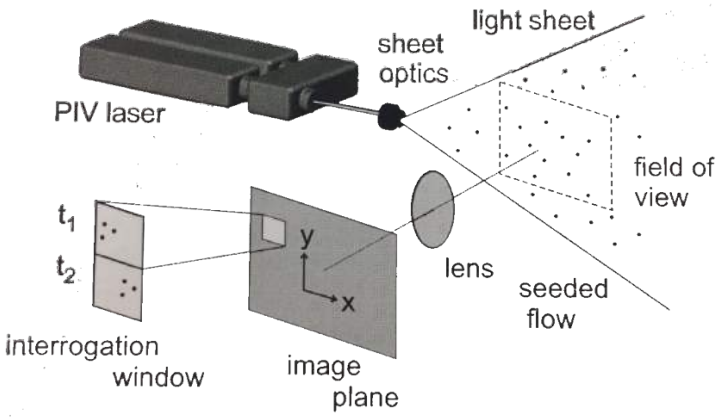

Figure 2.15 General Setup of a 2D PIV System [17]

The general setup of a 2D PIV system is shown in Figure 2.15. In this research, a 30 MJ double-pulse 532 nm Nd/YAG laser by New Wave is used to provide the light sheet across the symmetrical central planar of the acrylic model. Two cylindrical lenses of f = -10 mm and f = -20 mm focal length are attached to the laser system as a part of the optical arrangement. One is used to form the planar sheet out of the original 1.5 mm diameter laser beam and another is used to adjust the thickness of the laser sheet at the probe volume which could optimize the intensity of laser sheet. The salt water flow is seeded by 50 μm polyamide seeding particles (0.6% by weight) which are illuminated twice with a small time gap in between. The displacement of these tiny tracers is recorded by a LaVision ProX 4M CCD camera placed perpendicular to the planar of laser sheet with a resolution of 2048 × 2048 pixels^2. Since PIV is very sensitive to the spatial resolution of the images and their quality, a relatively high resolution is set for post-processing. The sensor size is 15.6 × 15.3 mm^2 and the maximum imaging frequency is 14.7 Hz, allowing the double-

frame PIV images to be taken at a maximum rate of 7 Hz. Moreover, a Nikon 60 mm f/2.8 lens with a field of view of 300 mm which is set to wide open for better light input and a 532 nm pass-filter which only collect the light back-scattered from the particles are chosen to add on the camera. In this research the field of view is set to the region of cavity between two openings and the second floor compartment. The velocity vectors in this field of view can be calculated using the displacement of particles and the time gap in pulse separation. The PIV system is calibrated before experiments (shown in Figure 2.16) following the procedure in the manual of DaVis FlowMaster [17].

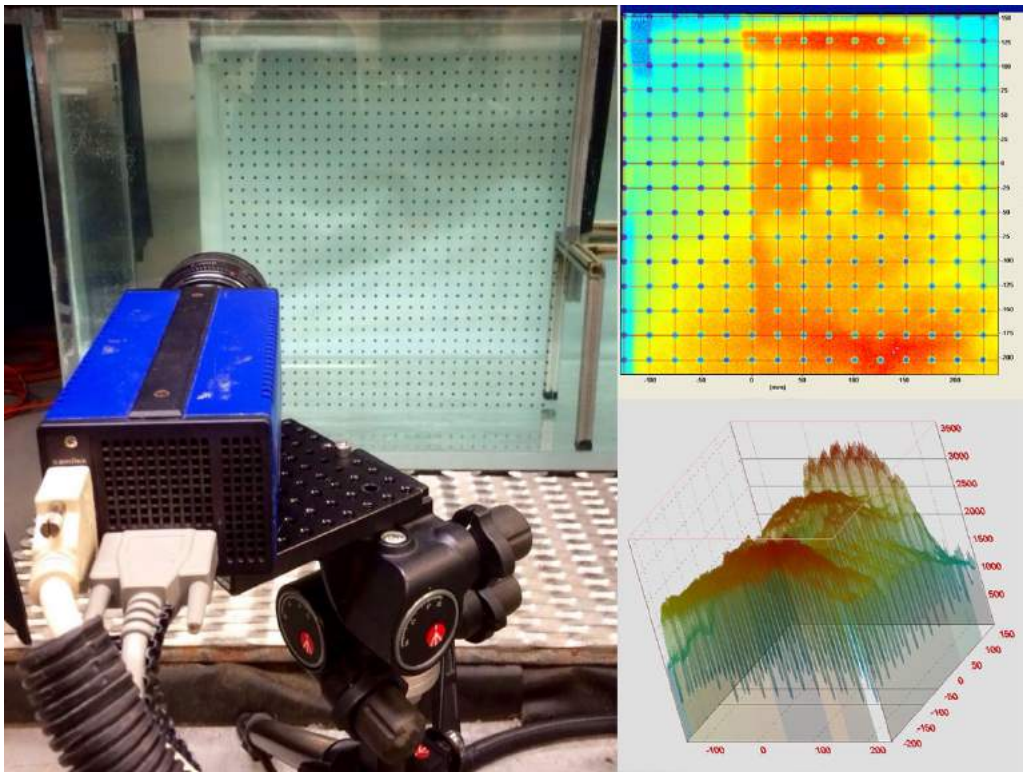

Figure 2.16 Calibration of PIV System

2.2.7 PLIF (Planar Laser Induced Fluorescence) Experiments

The second interest point to study is the smoke filing of the second floor compartment, which could be the result of flow pattern influenced by louver angle. The investigation of the smoke filling process is also very practical to provide suggestions for occupants' evacuation, fire fighting tactics and even for performance-based design. PLIF technique can be applied to obtain the changes of salt water concentration in the field of interest, simulating the smoke fraction in real compartment fire.

The general setup of the PLIF system is similar to PIV. The tracer of salt water flow is different in PLIF experiments which is the Rhodamine 6G dye tracer. A single pulse mode is applied and a laser sheet is provided throughout the whole period of experiment. A 532nm block-filter is used to collect the fluorescence signal

demonstrated by Rhodamine 6G dye tracer only. The intensity of this kind of signal captured by PLIF system could provide quantitative measurements of density difference. The differences between setups of data acquisition of blue dye tests, PIV and PLIF experiments are shown in Table 2.4.

	Blue Dye	PIV	PLIF
Camera type	Nikon D7100	CCD camera	CCD camera
Image Size (Pixels^2)	4000 × 6000	2048 × 2048	2048 × 2048
Lens	18-105mm f/1-3.5	60mm f/2.8	60mm f/2.8
Filter	-	532 nm pass-filter	532nm block-filter
Focal Length (mm)	40	60	60
F-Number	4.5	2.8	2.8
Exposure Time (s)	1/50	1/20000	1/100
Laser Mode	-	Double pulse	Single pulse
Tracer	Blue dye	50 μm polyamide	Rhodamine 6G dye
Interest Region	Overall View	Cavity	2nd Floor

Table 2.4 Setups of Data Acquisition Systems

2.3 CFD (Computational Fluid Dynamics) Modeling

CFD (Computational Fluid Dynamics) is a numerical tool to provide solutions for the governing equations of fluid mechanics, including Navier-Stokes equations and conservation equations, which is based on numerical modeling in computer program. FDS (Fire Dynamics Simulator), an open-source software first released in 2000 by NIST, is one of the most widely used CFD model to solve and analyze problems related to fire-driven fluid flow, especially smoke and heat transport from fire [18, 19]. SMV (Smokeview) is a separate program to visualize the result of FDS. In this research, the most current release version, FDS 6.5.3 and SMV 6.4.4, is used to model the fire phenomenon in a two-floor compartment with louver double-skin facade. A sample FDS input is listed in Appendix 1.

2.3.1 Computational Model Design

As introduced in 2.2.2, a two-floor compartment with adjustable louver double facade is designed based on the dimension scale of the Gherkin. In FDS, full-scale enclosure models are built following dimensions of the real building in Table 2.2. In total, five simulations are run for four different louver angles, 135°, 90°, 45° and 0° which are named as M1, M2, M3 and M4 (same order as salt water modeling) and one without outer-skin louver facade for comparison which is named as M5. The geometry of these five models are shown in Figure 2.17.

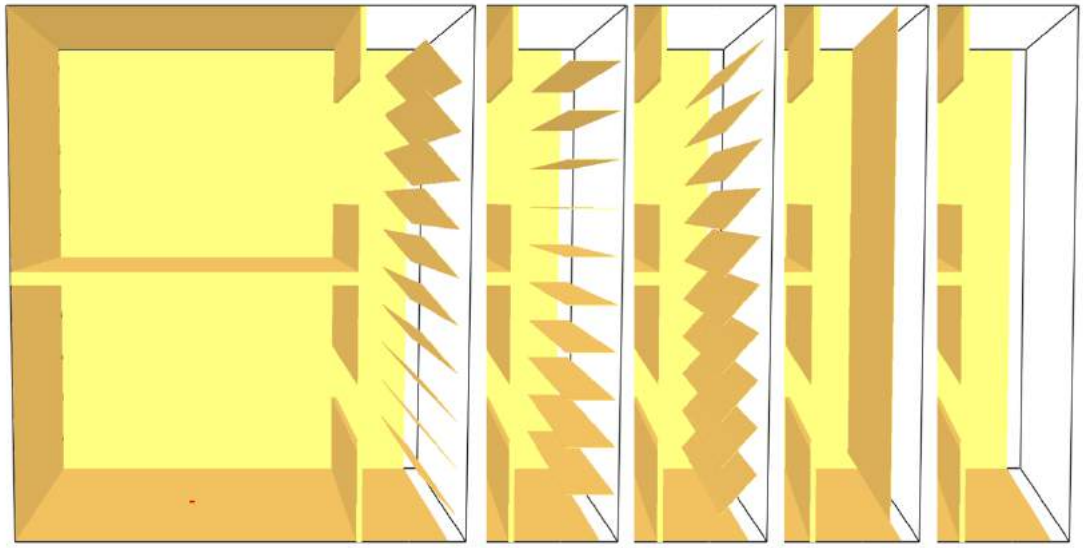

Figure 2.17 Computational Models with Different Louver Angles in FDS-SMV
Note: These five cases are named as M1, M2, M3, M4 and M5 from left to right according to the changes of louver angle. The part of two-floor compartment in images from M2 to M5 are abbreviated, remaining the area of double-skin facade only.

According to the geometry of these numerical models, the size of computational domain is set to be 8 × 4 × 8 m^3. The boundaries that overlap with the model are set to default, while other parts are set to open. The domain is divided into two parts, two-floor compartment (6 × 4 × 8 m^3) and double-skin facade (2 × 4 × 8 m^3), with two different mesh size. The mesh size of two-floor compartment is chosen to be 0.1 × 0.1 × 0.1 m^3, because the compartment dimensions can be easily divided by it and the thicknesses of floor and wall are 0.1 m. Since the thickness of louver facade is 0.01 m and there are two cases with slope configuration, the mesh size of double-skin facade is set to be 0.01 × 0.02 × 0.01 m^3. Setting two different mesh sizes can save computational time and model the configuration as accurate as possible. In the cases of M1 and M3, the obstacles of louvers in slope are defined cell by cell. Totally 620 obstacles are defined to form the structure of 10 angled louvers. The disadvantages of FDS are obvious here due to the limitation of grid resolution and fixed grid arrangement for modeling slope configuration. Since it takes months to finish the simulation using a finer mesh and a coarser mesh cannot accurately describe the structure, grid resolution study is replaced by comparison with the result of salt water modeling which shows a great agreement with full-scale fire experiments in previous researches [26, 31, 32].

The fire source is simplified as a methane pool fire located in the center of the first floor. According to dimensionless analysis as introduced in 2.1, the fire source strength should match the salt water source strength which is calculated to be 600 kW by using equations for dimensionless source strength in Table 2.1 to make $\dot{Q}^* = \dot{m}_{sw}^*$. Since there are no matched features of radiation and heat loss in salt water modeling, these functions are turned off in FDS for better comparison. Moreover, Lagrangian particles

are introduced in fire source to show the smoke transportation with a randomly subgrid-diffusivity-based movement, which is a useful feature to match the flow tracers in salt water modeling.

2.3.2 Data Acquisition

As there are two main targets in this research, one is to combine salt water modeling with CFD modeling to investigate how the angle of louver can influence the smoke movement in the cavity of double-skin facade and another is to make comparisons between these two methods of modeling to give suggestions for future studies in other topics, data desired to obtain in FDS by setting devices in certain locations should be representative enough for fire research and matchable enough for comparison with salt water modeling by dimensionless analysis.

In blue dye tests, front arrival time of salt water flow to certain locations are recorded in camera. In FDS simulations, front arrival time of smoke to critical positions could also be visualized in SMV. As introduced in 2.1, dimensionless front arrival time can be calculated for both modeling methods. As shown in Figure 2.17, point 0 located at the top line of first floor opening which is the start point of spilling flow is set to be the reference time. Dimensionless front arrival time to point 1 (bottom of the second floor opening), 2 (center of the second floor ceiling), 3 (left side wall), 4 (bottom of the second floor opening), and 5 (center of the room with the same height as point 1) are compared for both methods to examine the time scale. The front arrival time can also indicate the speed of smoke filling to give a ranking of critical cases for further study.

In PIV experiments, velocity vectors at the interest field, cavity area between first floor opening and second floor opening and second floor enclosure, can be plotted with high resolution. In FDS simulations, velocity vectors in these regions could also be obtained in SMV from the SLCF file which is set to the same location as the planar of laser sheet in PIV experiments. Images of streak line can be generated by both methods for comparison and the part around louvers are valuable to investigate or explain the influence of louver angle on speed of smoke transportation. Furthermore, devices are set in FDS to record the velocity values at points along the center line of first floor opening (O1_1-9), second floor opening (O2_1-18) and second floor compartment (C2_1-18). Locations of these points are shown in Figure 2.17 and more details are listed in Appendix 2. Using equations in Table 2.1, dimensionless velocity correlated with dimensionless time or location could be obtained for further comparison.

In PLIF experiments, variations of salt water concentration in second floor compartment are recorded by CCD camera. As stated in 2.1, there are two ways to calculate the dimensionless density difference, one is based on temperature difference and another is based on smoke mass fraction. In FDS simulations, devices are set to record temperature and mass fraction at points along the center line of first

floor opening (O1_1-9), second floor opening (O2_1-18) and second floor compartment (C2_1-18). Locations of these points are shown in Figure 2.18 and more details are listed in Appendix 2. Thus, the average smoke mass fraction and smoke layer height in second floor enclosure correlated with time for different cases of louver angle could be obtained. The differences in comparison between cases are caused by positions of double-skin facade. Using dimensionless analysis, dimensionless density difference based on temperature and smoke mass fraction can be compared with the dimensionless value in salt water modeling based on salt mass fraction.

Moreover, in FDS simulations mass flow out of the first floor opening, mass flow in to the second floor opening and mass flow up through the cavity for case M1 to M5 are also recorded by devices.

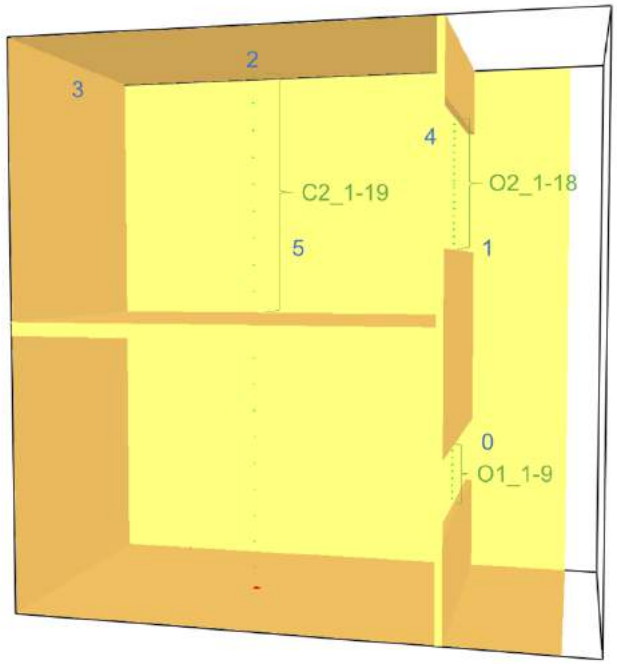

Figure 2.18 Locations of Devices in FDS-SMV

CHAPTER 3

Results

3.1 Results of Blue Dye Tests

Blue dye tests provide flow visualization recorded by camera with 2 second time interval. Figure 3.1 shows the overall view images selected at 10 s, 50 s, 100 s and 200 s for cases from M1 to M4 in blue dye tests.

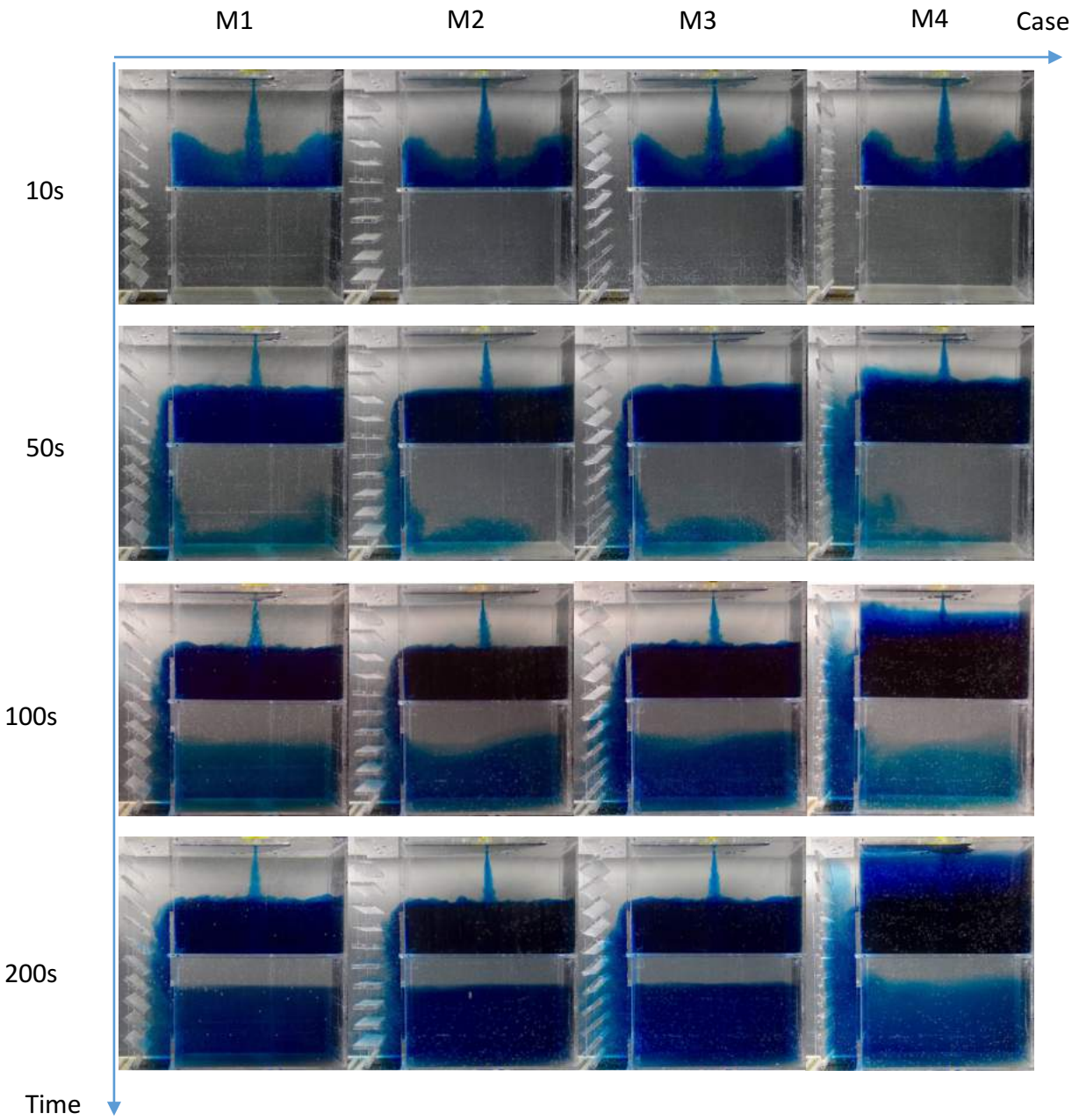

Figure 3.1 Images of Blue Dye Tests

Comparing images by cases in Figure 3.1, M4 with closed louver facade obviously looks different. The salt water modeling simulates that the first floor compartment with fire source contains a ventilation controlled fire in M4. No clear blue dye layer is formed compared with other cases, since the supply of ambient fresh water is insufficient. In real fire cases, it is harmful to stack a so big volume of smoke in a room at the beginning of fire for evacuation and the outer-skin facade could be broken down due to high temperature. Buchanan states this dangerous situation in the section of fire spread to other floors that glass materials could shrink and melt at high temperatures [4]. This case, louver double facade with closed louver, is similar to the type of double facade of which the outer-skin facade is a single glazing curtain wall. Many researchers published their findings using full-scale tests or computational simulations on how this kind of double glazing facade could influence fire safety, including how different factors matter like the width of cavity and the horizontal partition [14, 16, 23]. However, no literature about how the angle of louver can affect the smoke spread in louver double-skin facade is found. Apparently in images of blue dye tests in 50 s and 100 s (shown in Figure 3.1), the extent of blue dye spread is the evidence that the angle of louver facade is also an important factor for further study.

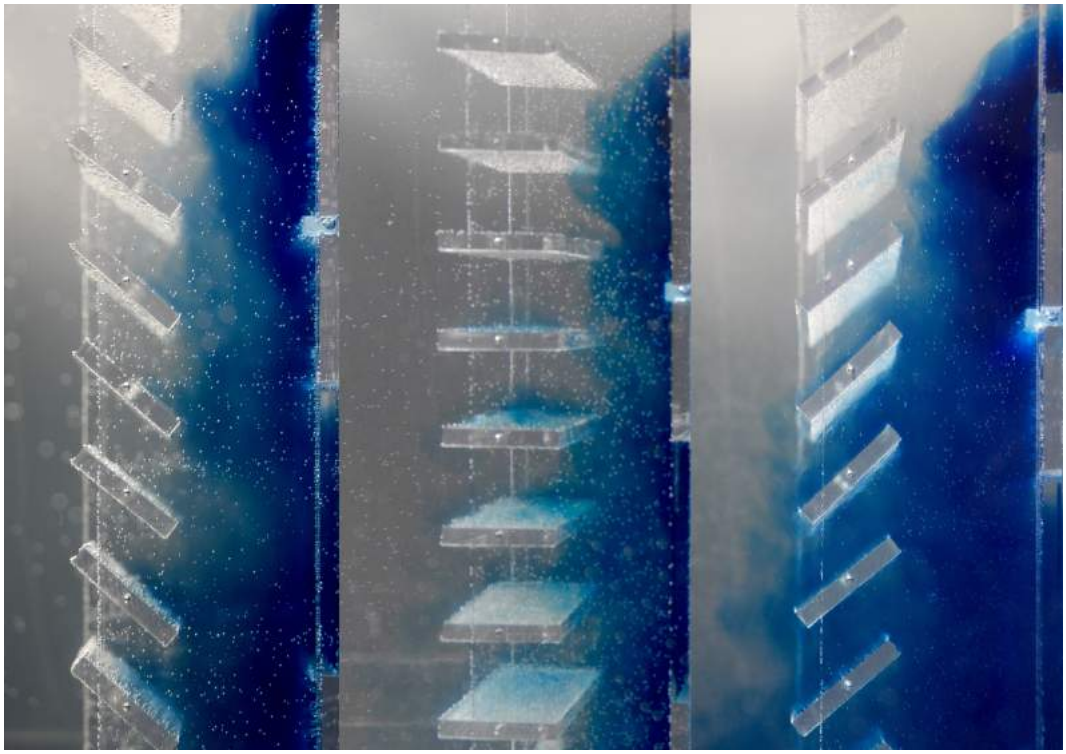

Figure 3.2 Details of Salt Water Flow Around Louvers in Blue Dye Tests

According to the overall view, salt water flow in case M1 spread faster than M2 and M3, while the difference between M2 and M3 are not that obvious. Focusing on the local details of salt water flow around louvers (shown in Figure 3.2), in case M1 louvers largely blocked the outspread of salt water flow from cavity to the outside. More salt water flows are contained in the cavity due to the phenomenon of

backflow compared with M2 and M3. In case M3, the part of salt water flows with louver-wise spread direction slide down along the louvers which result in more extraction of salt water from the cavity. In case M2, the opening factor of outer-skin facade is the biggest in all possible angles, while the width between louver edge and inner-skin facade is the smallest in all cases. From blue dye tests, a certain amount of salt water flow is recorded to flow out of the outer-skin facade in M2, but the difference cannot be quantified compared with M3. So the comparison between M2 and M3 could be a concern-point in further studies.

3.2 Results of FDS Simulations

3.2.1 Velocity

As introduced in 2.3.2, the velocities along the center line of the first floor opening, second floor opening and second floor compartment are recorded in FDS simulations (locations are indicated in 2.3.2). Figure 3.3 to 3.5 give a set of example plots for velocity with time in case M1. It is shown in these figures that a neutral plane could be formed at steady state not only in the first floor opening, but also in the opening and enclosure of the second floor where there is no fire source. The steady state stated in this research is referred to steady state in the first floor enclosure after smoke filing the second floor enclosure where velocity, temperature and mass fraction are at a steady level ignoring the fluctuation. Similar results could be obtained for case M2 to M5 (shown in Appendix C). The comparison between cases could be valuable. The mean velocities at steady state along the height of the center line in the first floor opening, second floor opening and second floor compartment are plotted in Figure 3.6 to 3.8 for case M1 to M5 in which the locations of neutral plane in different cases could also be compared. Due to the poor ventilation condition in case M4, the neutral planes are lower than other cases at the first floor opening and second floor opening. No big difference could be found at steady state for M1, M2, M3 and M5 which could be examined by Figure 3.9 in which the mean velocity values at steady state for VO2_1 are compared, so it could be assumed that the height of neutral plane is depend on the opening factor of inner-skin facade and outer-skin facade at the adjacent floor. The angle of outer-skin louvers may have more influence on the velocity distribution at the higher floors, but not the adjacent floor or have more influence on the development period of velocity distribution, but not the steady state. This inference needs to be verified in the following research.

In the second floor compartment, at steady state case M2 has a higher velocity towards the opening and lower velocity towards the left side wall along the ceiling. M4 still has the lowest values, while M1, M3 and M5 are at the similar level. There are high fluctuations at the second floor opening and enclosure, which could be explained by the U-velocity slice shortcut in SMV. In Figure 3.10, it could be found that the flow in to the second floor compartment and the flow out of the second floor compartment

cross at the opening forming a conflict of counter flow. This effect is driven by buoyancy at first then dominated by momentum at steady state when temperature increases at the compartment without fire source.

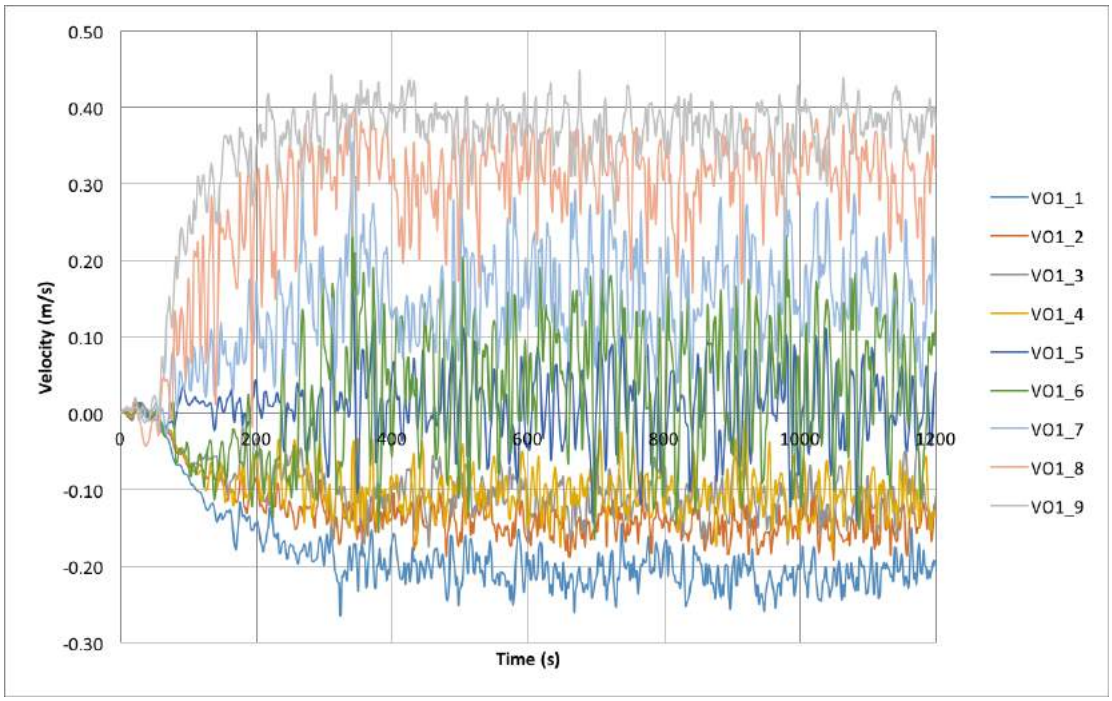

Figure 3.3 Velocities along the Center Line of the First Floor Opening in M1

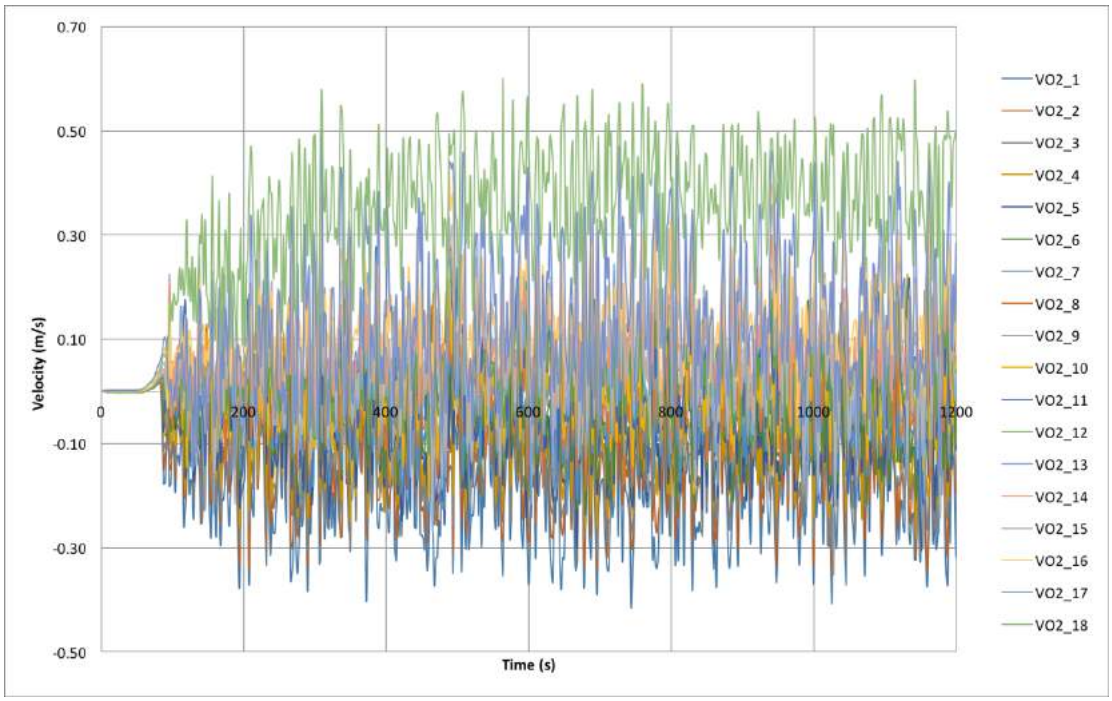

Figure 3.4 Velocities along the Center Line of the Second Floor Opening in M1

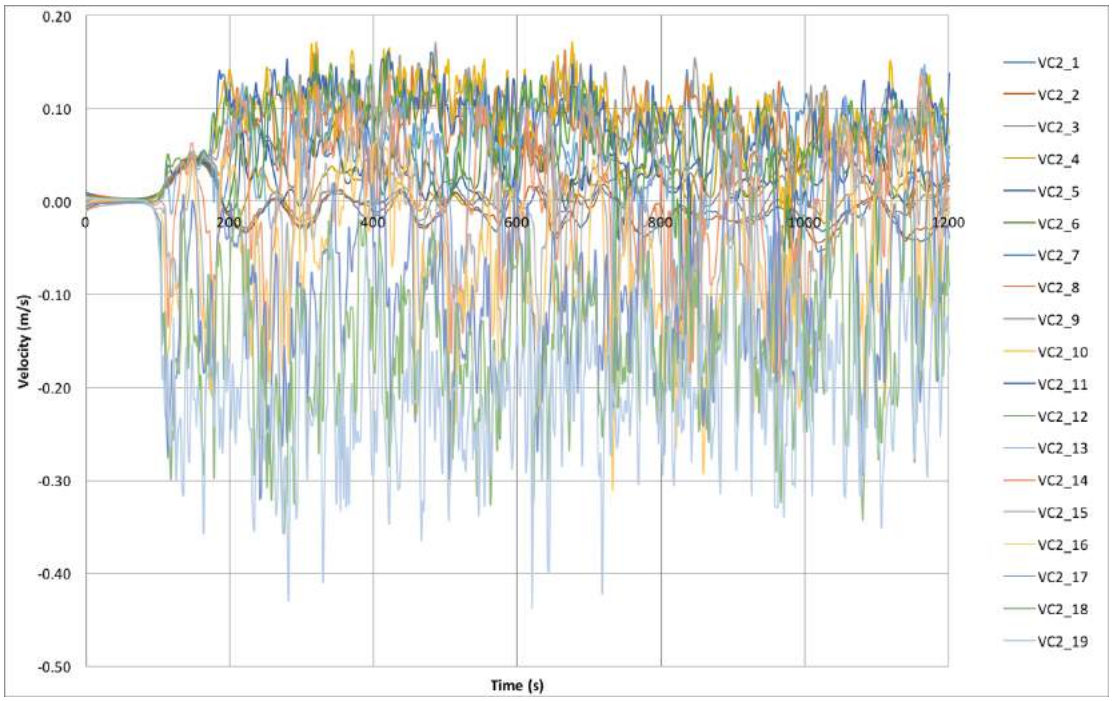

Figure 3.5 Velocities along the Center Line of the Second Floor Compartment in M1

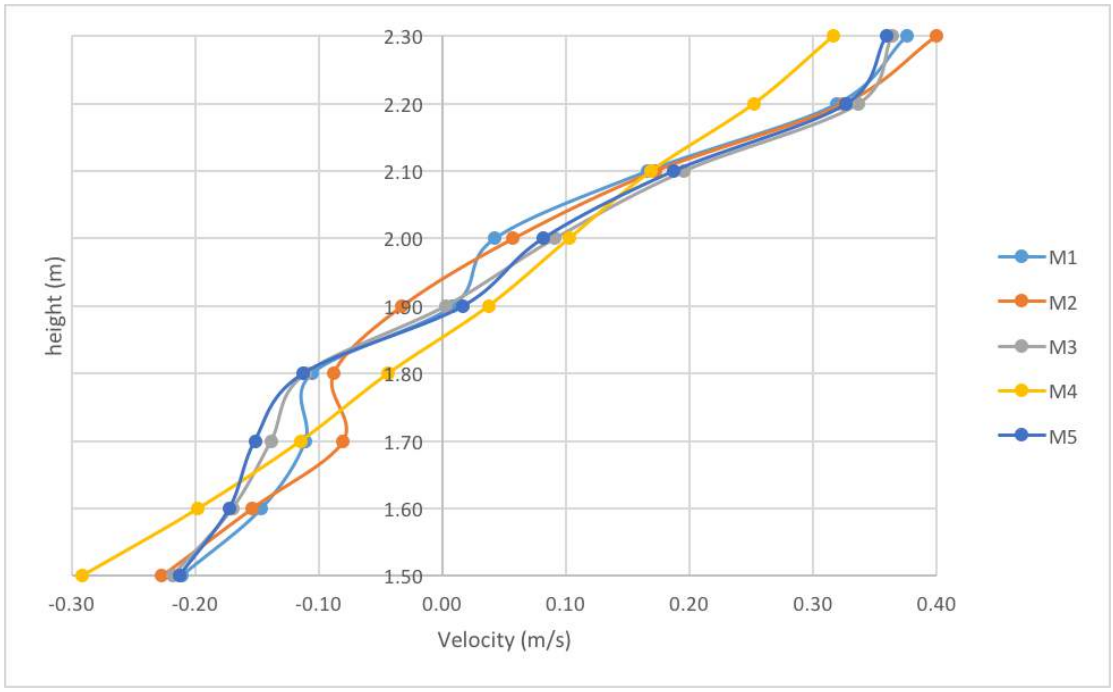

Figure 3.6 Mean Velocities along the Center Line of the First Floor Opening at Steady State for M1 to M5

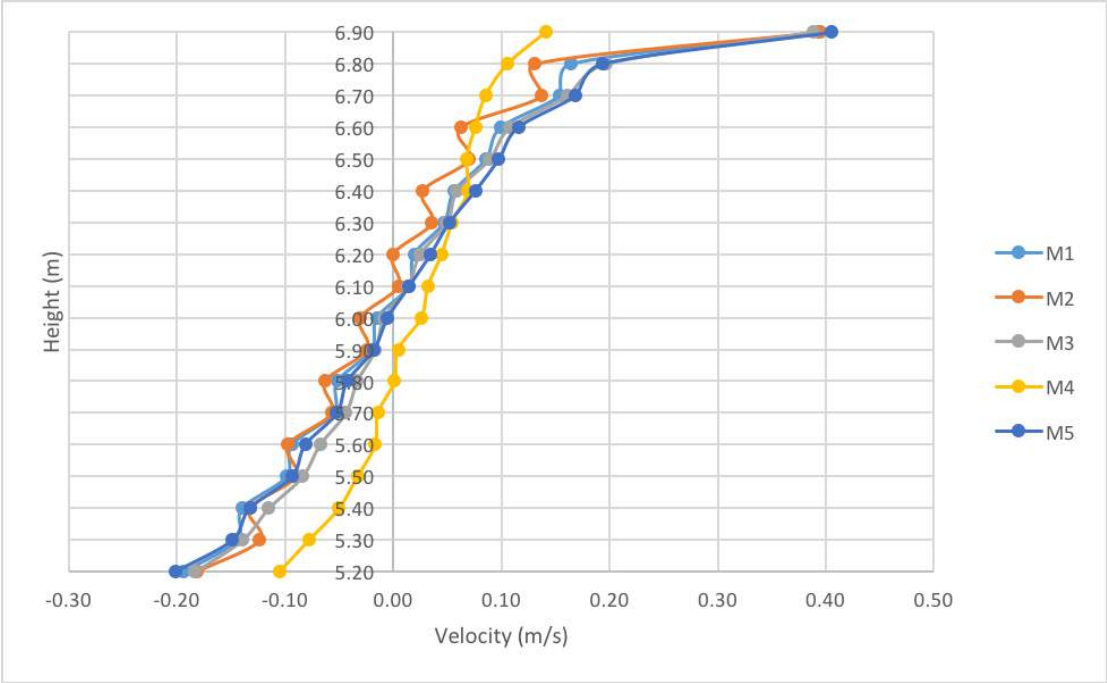

Figure 3.7 Mean Velocities along the Center Line of the Second Floor Opening at Steady State for M1 to M5

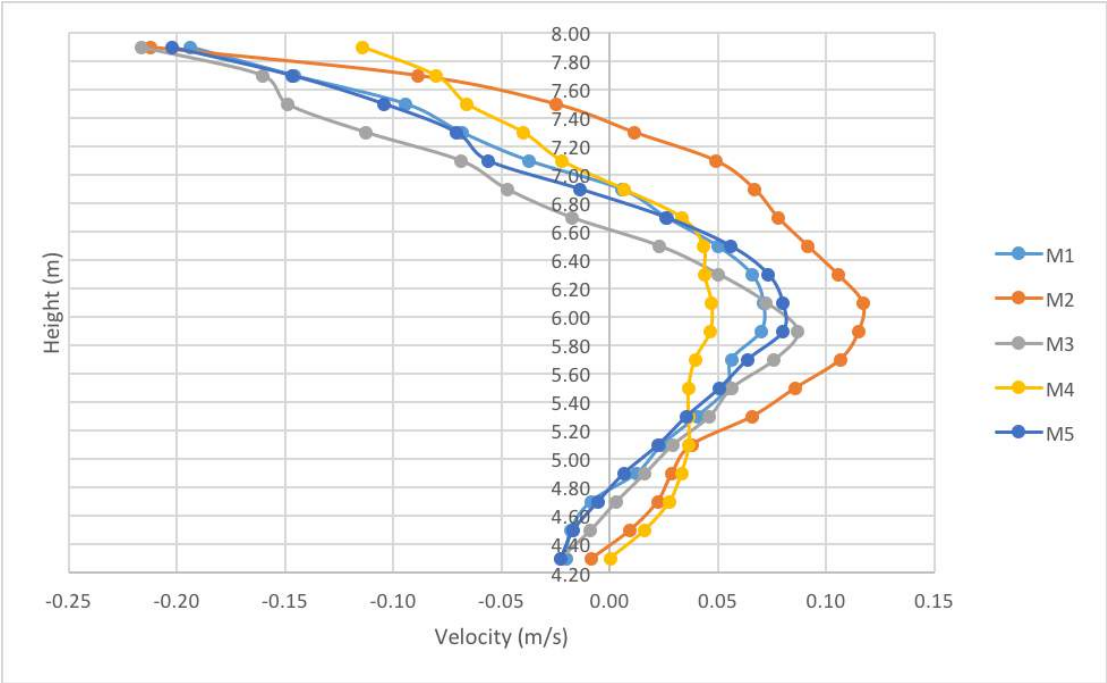

Figure 3.8 Mean Velocities along the Center Line of the Second Floor Compartment at Steady State for M1 to M5

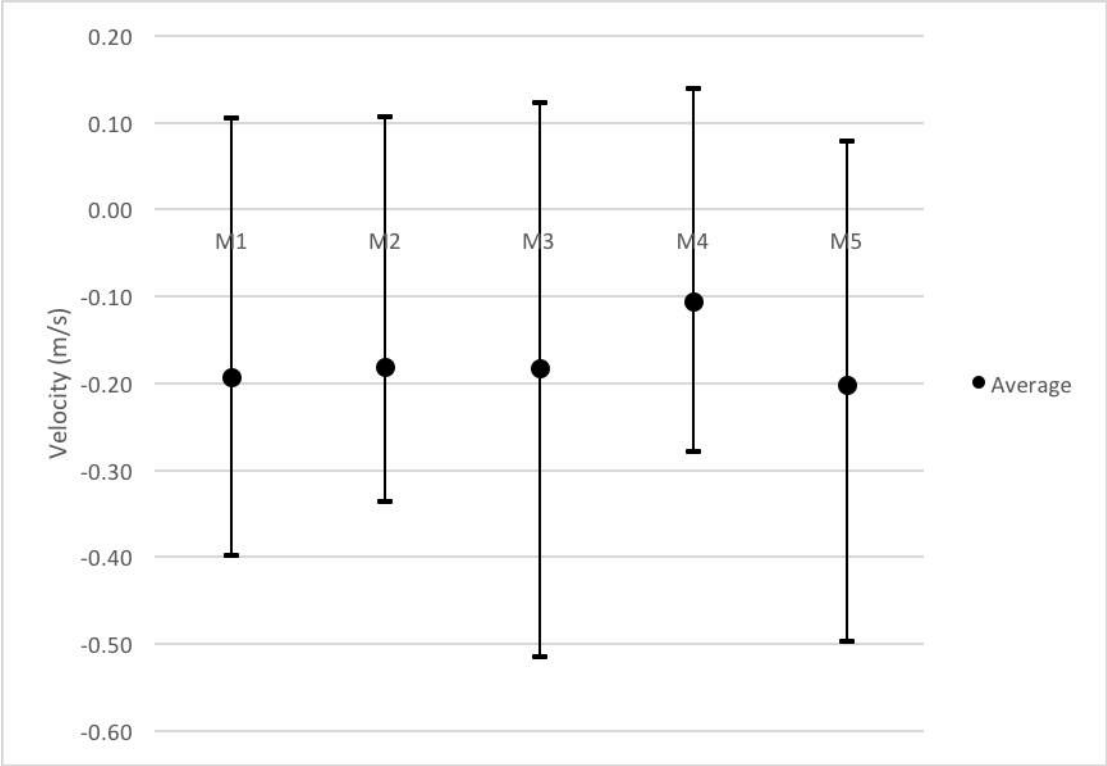

Figure 3.9 Max-Ave-Min Chart of Velocity VO2_1 at Steady State for M1 to M5

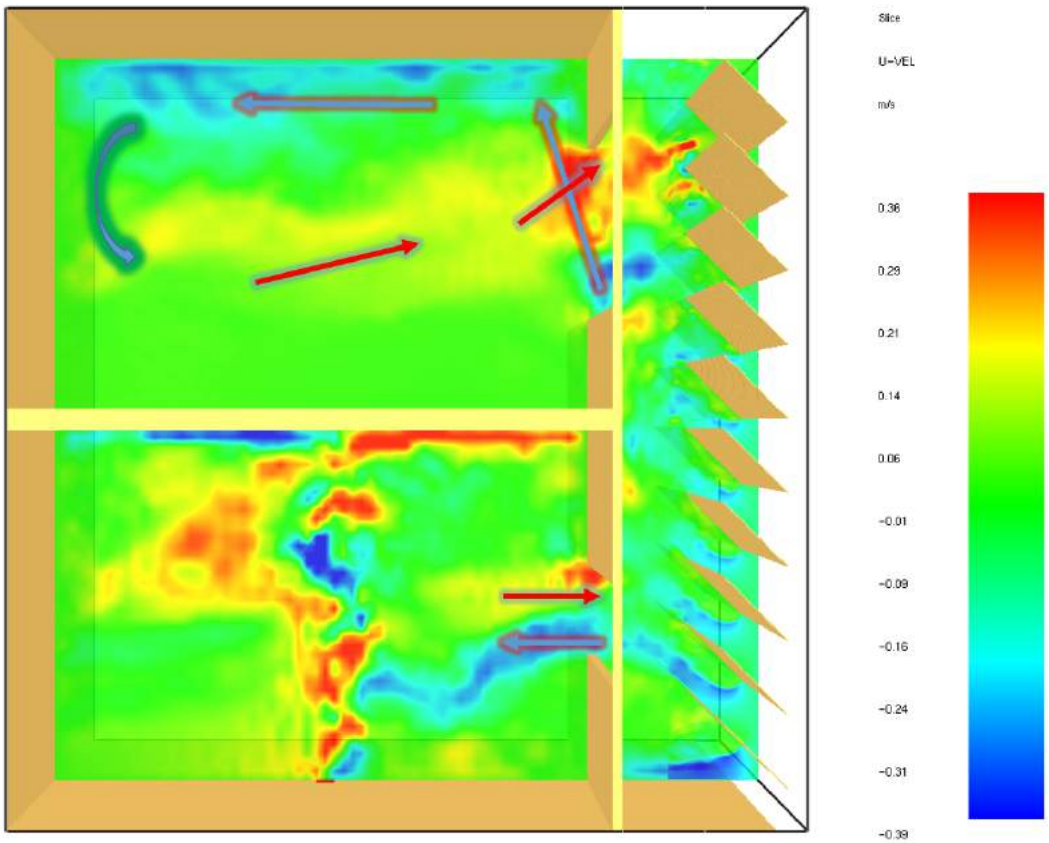

Figure 3.10 Slice Image of U-Velocity at Steady State for Case M1

3.2.2 Temperature

As introduced in 2.3.2, the temperatures along the center line of the first floor opening, second floor opening and second floor compartment are recorded in FDS simulations (locations are indicated in 2.3.2). Figure 3.11 to 3.13 give the plots of the values with time for case M1 and similar plots are also drawn for other cases (shown in Appendix C). Figure 3.12 shows a high variation of temperature at the steady state at the second floor opening which is due to the effect of conflict flow introduced in 3.2.1. Then in the second floor compartment, the temperature increases layer by layer which is followed by the accumulation of smoke.

Taking TC2_9 as example, temperature increases at the second floor compartment are compared between cases, which is shown in Figure 3.14. In this graph M4 has the lowest temperature compared with others, while the differences between other cases are not clear. As there are two stages in this process of smoke filing, comparisons are drawn separately for the growth period of the first 300 seconds (shown in Figure 3.15) and the steady state of the last 300 seconds (shown in Figure 3.16). The trend of temperature increase is related to the process of smoke filling and the difference between cases is caused by the angle of outer-skin louvers which have influences on flow direction and ventilation condition. According to Figure 3.15, M1 has the highest temperature and the highest growth rate at the growth period and M2 is almost at the same level as M1. The reason could be that louvers in M1 block a big part of smoke spreading towards the outside of cavity and the backflow effects make more smoke flowing into the second floor compartment, while M2 has higher ventilation factor which means more smoke are generated and louvers also can contain a certain amount of smoke which result in a roughly same level as M1. M3 is lower than M1 and M2 but higher than M5, since a big part of smoke spilling from the first floor opening spreads out of cavity along the direction of outer-skin louvers, while the existence of outer-skin facade still has the effect to hold smoke compared with M5. M4 is the lowest because of the poor ventilation.

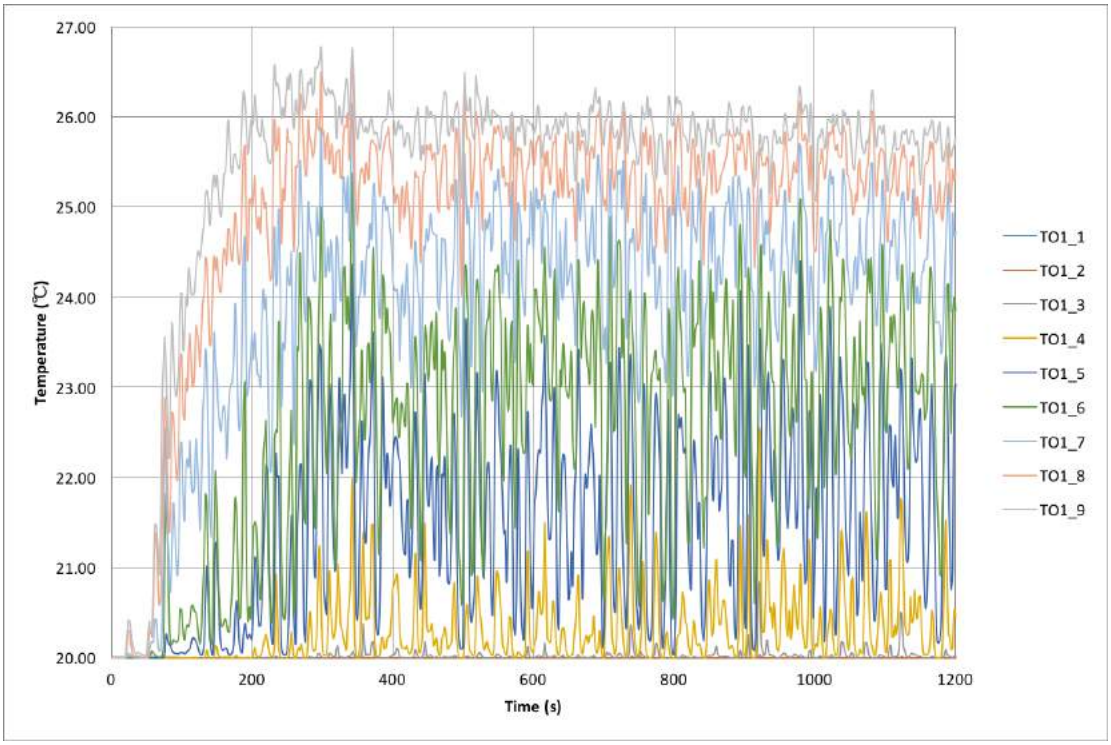

Figure 3.11 Temperatures along the Center Line of the First Floor Opening in M1

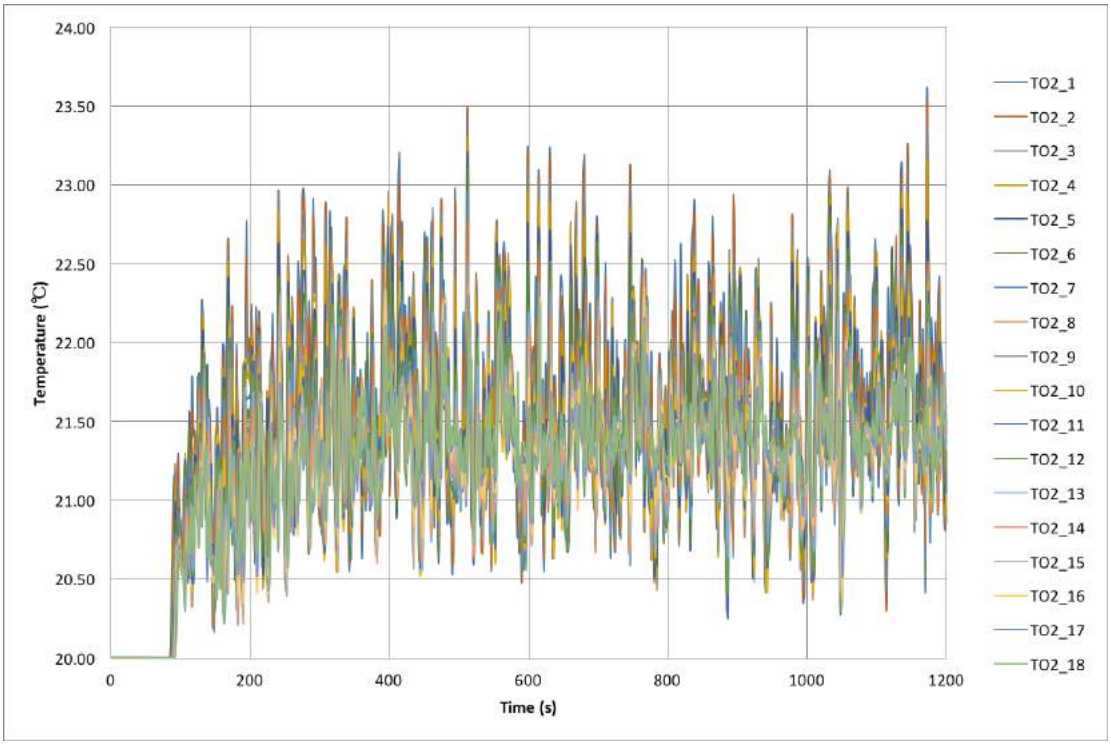

Figure 3.12 Temperatures along the Center Line of the Second Floor Opening in M1

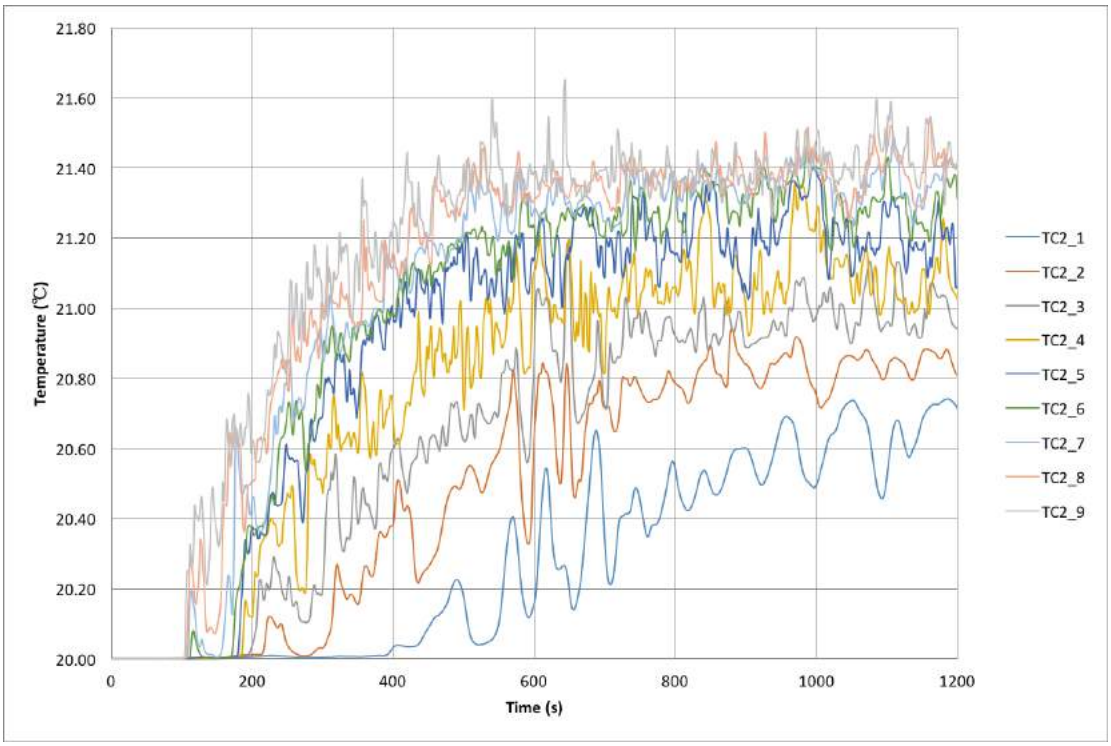

Figure 3.13 Temperatures along the Center Line of the Second Floor Enclosure in M1

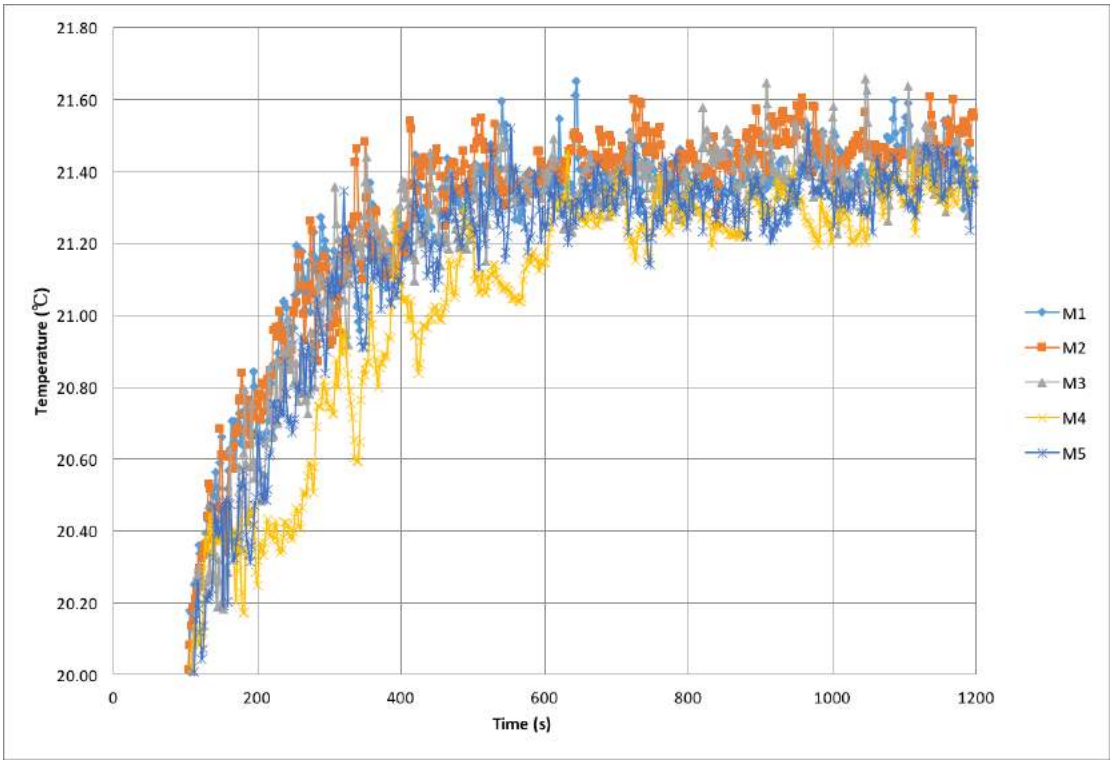

Figure 3.14 Plots of Temperature TC2_9 for M1 to M5

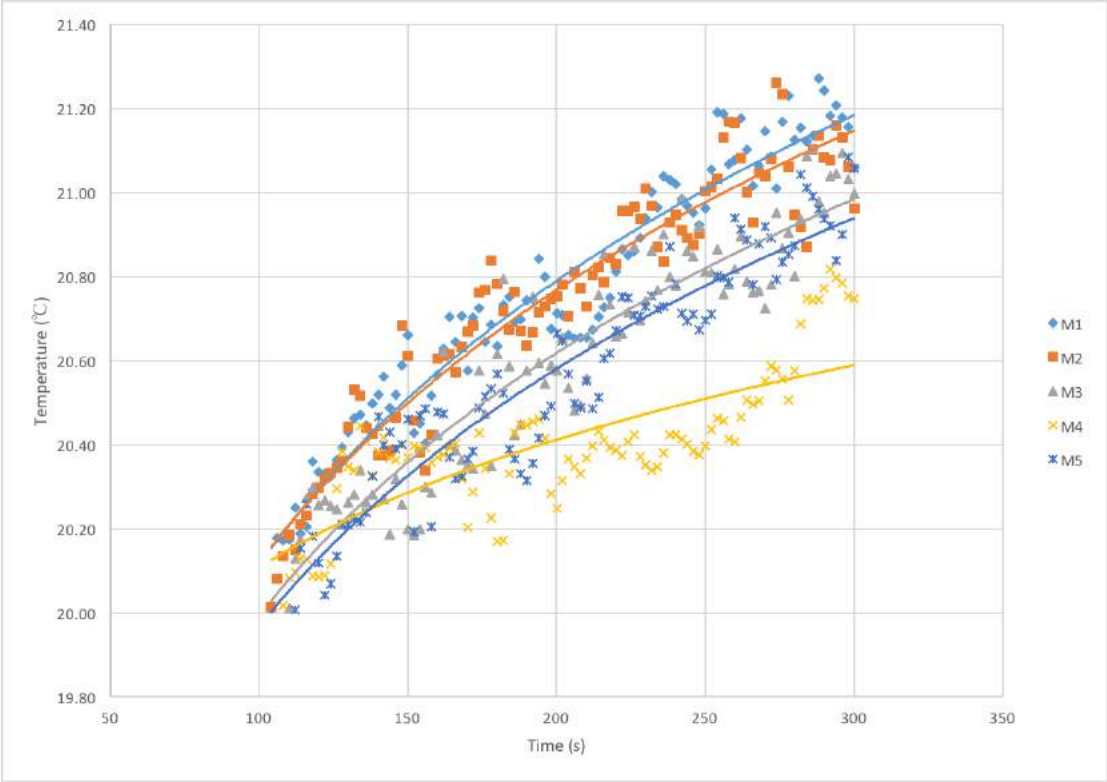

Figure 3.15 Trend Plots of Temperature TC2_9 at the First 300s for M1 to M5

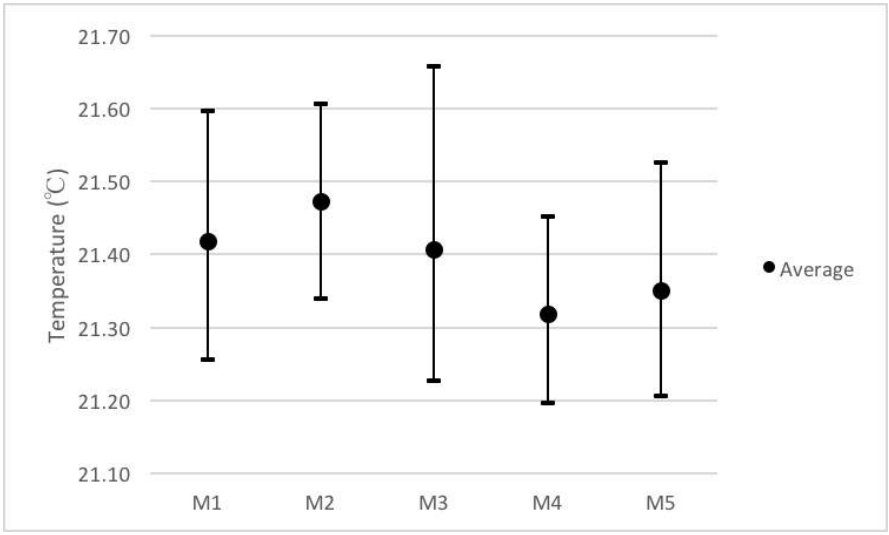

Figure 3.16 Max-Ave-Min Chart of Temperature TC2_9 at Steady State for M1 to M5

3.2.3 Mass Fraction

Mass fraction which is directly related to smoke accumulation has the same trend in plots as temperature. Figure 3.17 shows the plots of mass fraction along the center line at the second floor compartment in M1 (plots of M2 to M5 are shown in Appendix C). The height of smoke layer decreases along with the rising of smoke fraction. The rising of average smoke fraction as well as the decreasing of smoke layer height in the second floor enclosure with time for case M1 to M5 are plotted in

Figure 3.18.

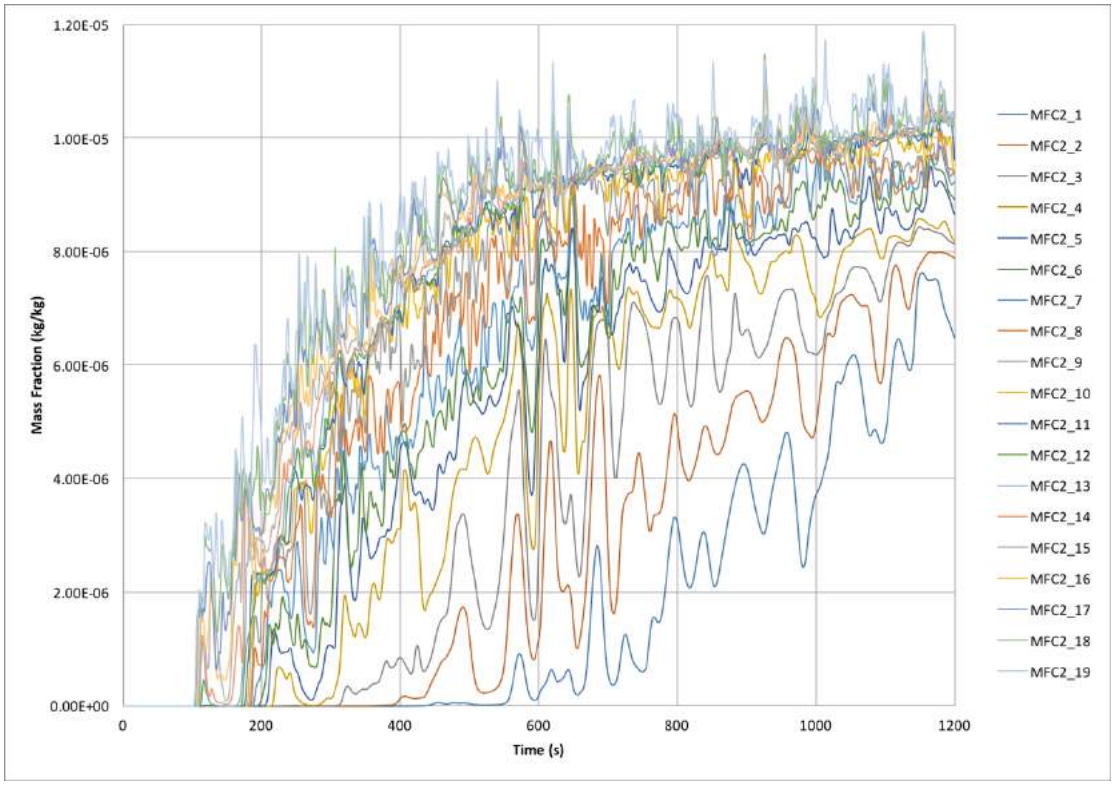

Figure 3.17 Mass Fraction along the Center Line of the Second Floor Enclosure in M1

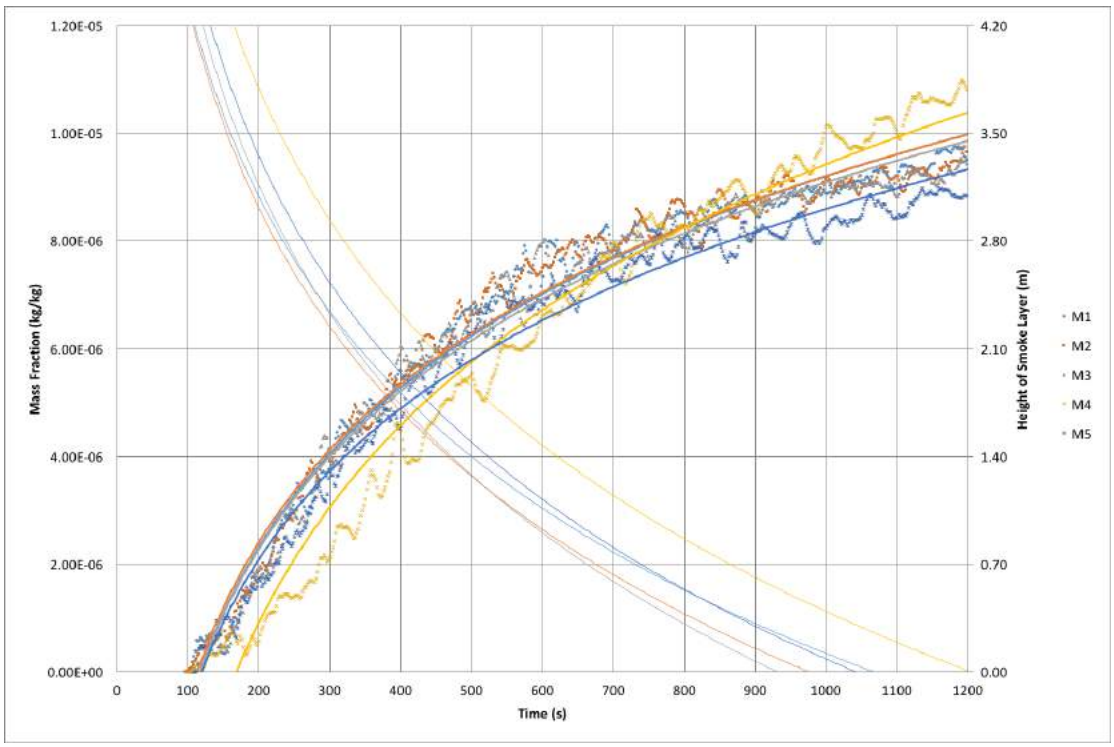

Figure 3.18 Trend lines of Average Mass Fraction and Smoke Layer Height at the Second Floor Enclosure

3.2.4 Mass Flow

Figure 3.19 – 3.21 shows the plots of mass flow out of the first floor opening, mass flow in to the second floor opening and mass flow up through the cavity with time for case M1 to M5 using the output files of FDS simulations. To better compare the results of these cases, average-max-min charts are drawn for steady state at these three locations (shown in Figure 3.22 and 3.23). Based on Figure 3.22, the mass flow out of the first floor opening and mass flow in to the second floor opening in M1, M2, M3 and M5 are at the almost same level at the steady state. By contrast, obvious differences are found in Figure 3.23 which shows the mass flow up through the cavity at steady state decreases from M1 to M4 with the changing of louver angle. Figure 3.24 with a visualization of particles represent smoke indicates the influence of louvers in different cases which is also described in 3.2.2. This finding proves the inference in 3.2.1 to a certain extent that the angle of outer-skin louvers may have more influence on the velocity and temperature distribution at higher floors which contribute to the stack effect, but not much at the adjacent floor and have more influence on the development period of these parameters, but not the steady state at the adjacent floor when fresh air drawing through the gaps of louvers into the cavity continuously because of the steady temperature difference below the opening of the adjacent floor. (The cause of stack effect is introduced in Drysdale's book of An Introduction to Fire Dynamics [13].)

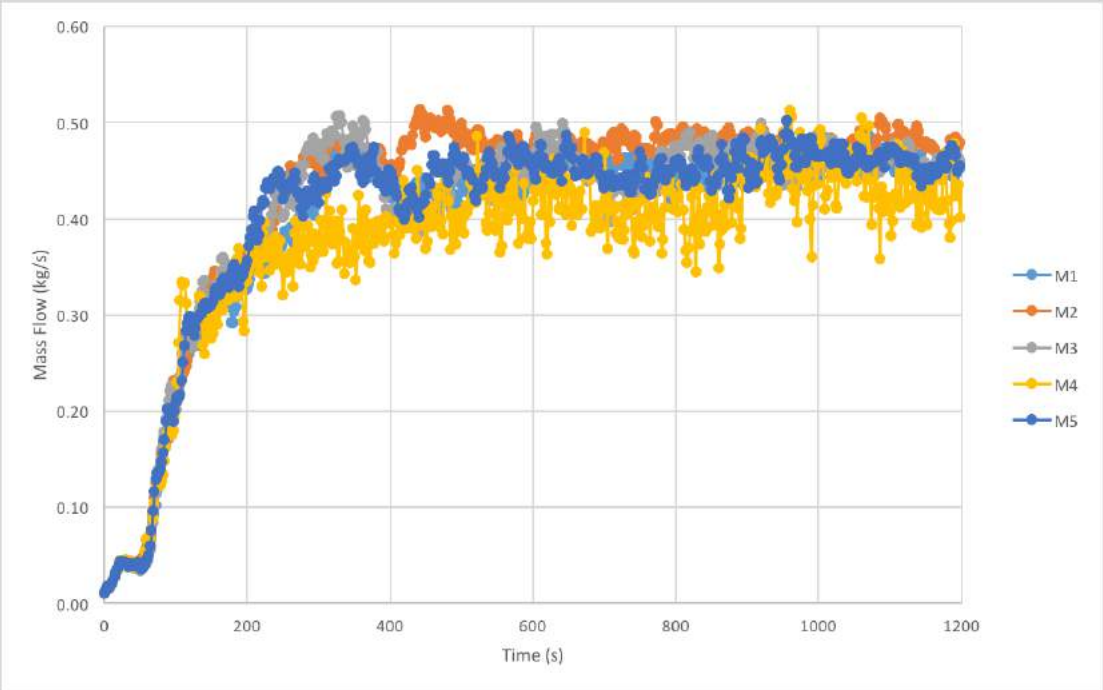

Figure 3.19 Mass Flow Out of the First Floor Opening for M1 to M5

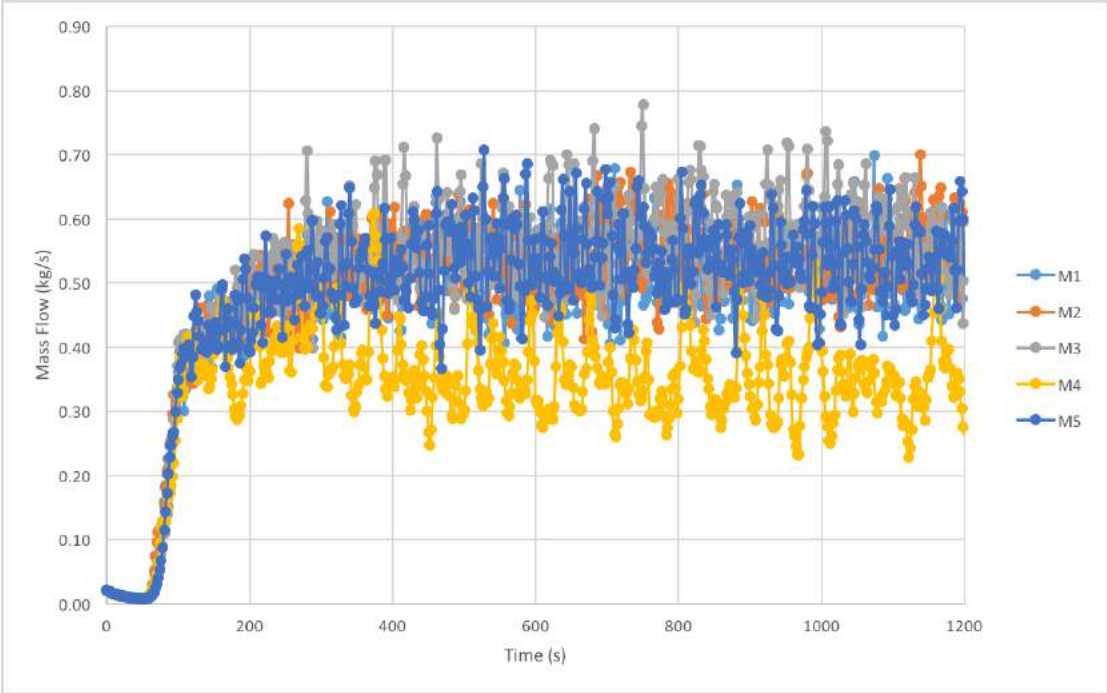

Figure 3.20 Mass Flow In to the Second Floor Opening for M1 to M5

Figure 3.21 Mass Flow Up through the Cavity for M1 to M4

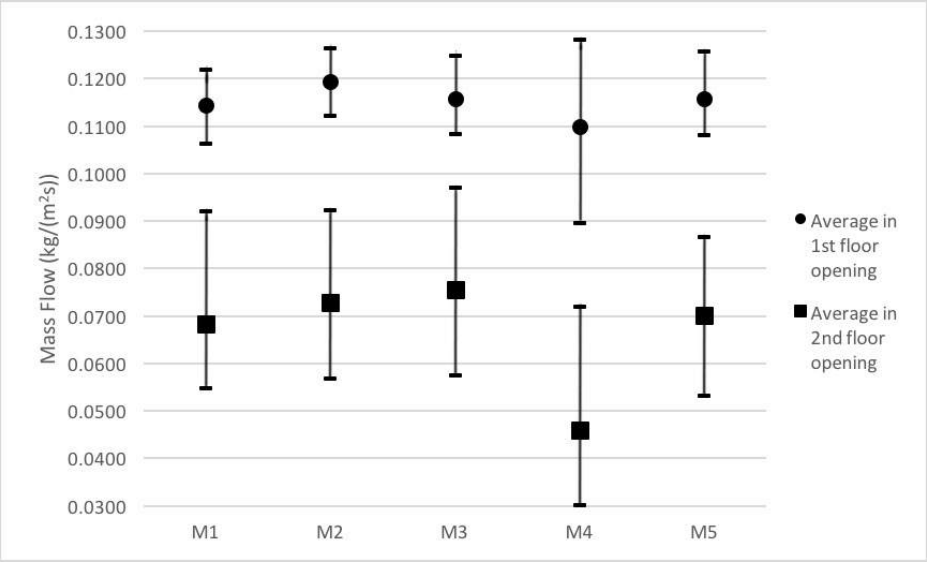

Figure 3.22 Average-Max-Min Chart for Mass Flow Through the First and Second Floor Openings at the Steady State

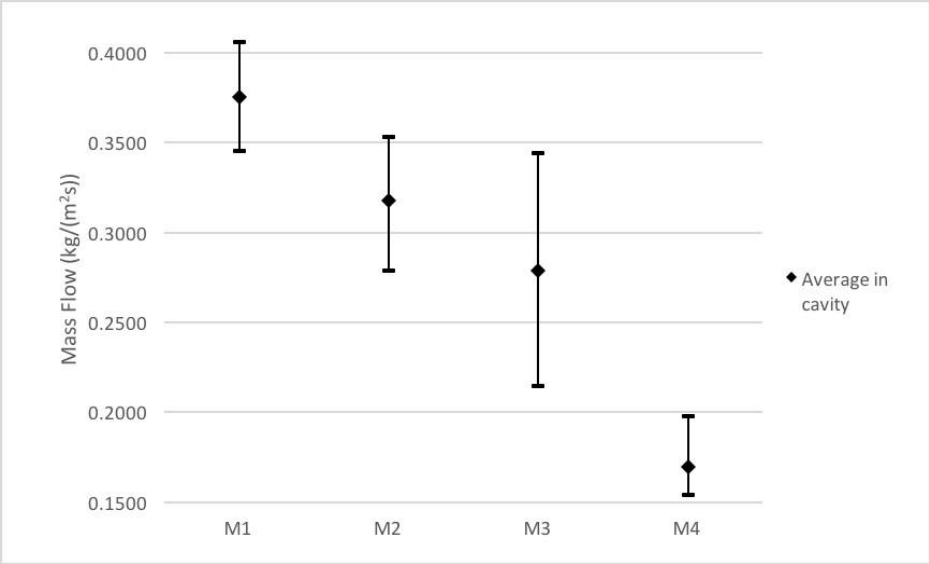

Figure 3.23 Average-Max-Min Chart for Mass Flow Through the Cavity at Steady State

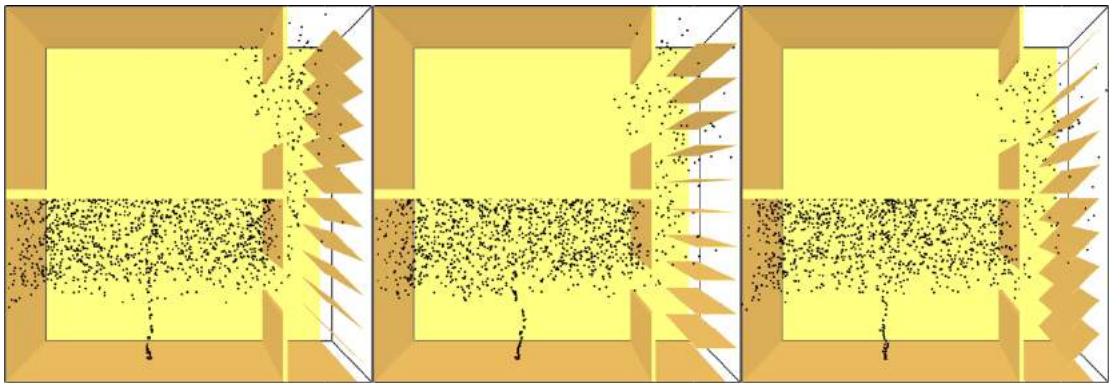

Figure 3.24 Status of Particle Accumulation in 20 Seconds for M1 to M3 in SMV

3.3 Results of PIV/PLIF Experiments

PIV experiments are conducted with a focusing region of second floor compartment and cavity. Figure 3.25 shows the images combining contours and vectors of salt water flow at steady state in the experiments for M1 to M4 exported from PIV system. Values of velocity at different locations could be extracted from the output file as well. In this analysis, expelling the data at the top and bottom edges of opening due to the inaccuracy, values of velocity at eight locations along the height of opening from 0.055 m to 0.125 m are interpreted. Applying the same method as FDS, mean velocity values of the last 50 frames recorded are plotted along the height of opening in Figure 3.26 (mean velocity values are shown in Appendix 4). Similar results are found in these figures compared with the results of FDS simulations. Comparisons are in Chapter 4.

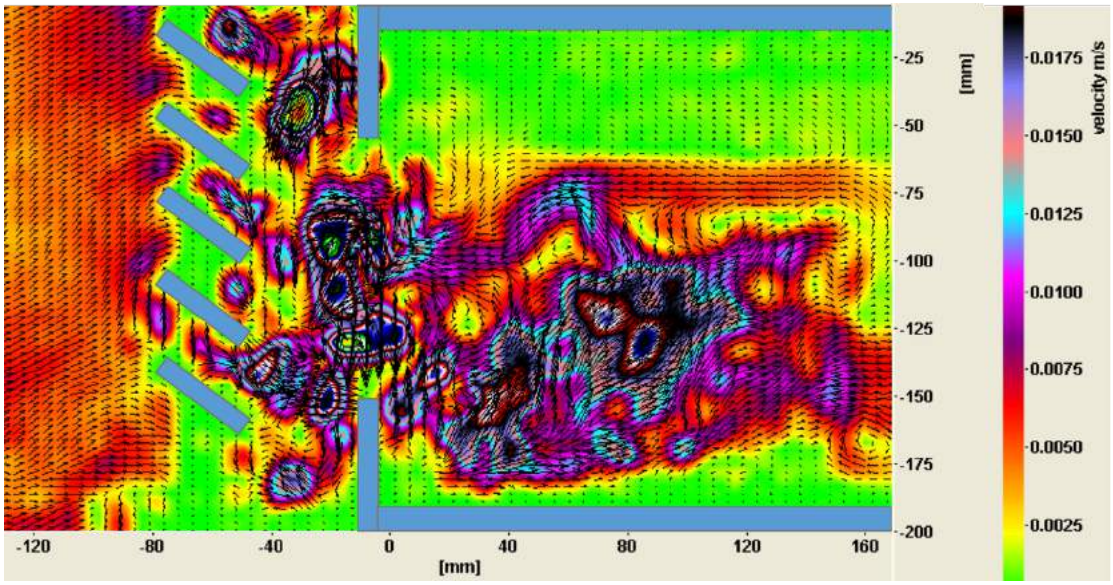

(a)

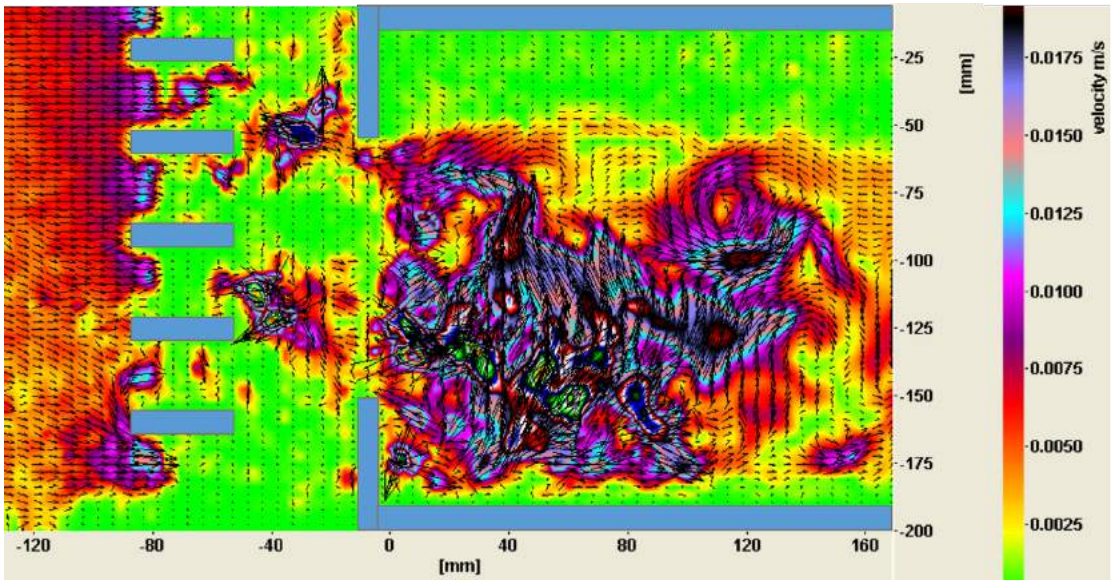

(b)

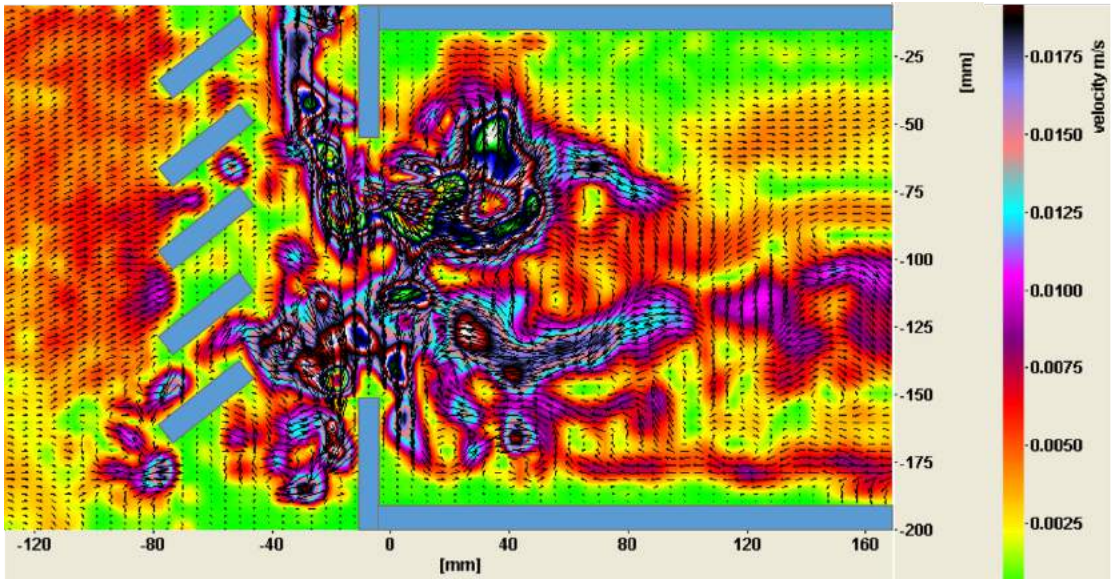

(c)

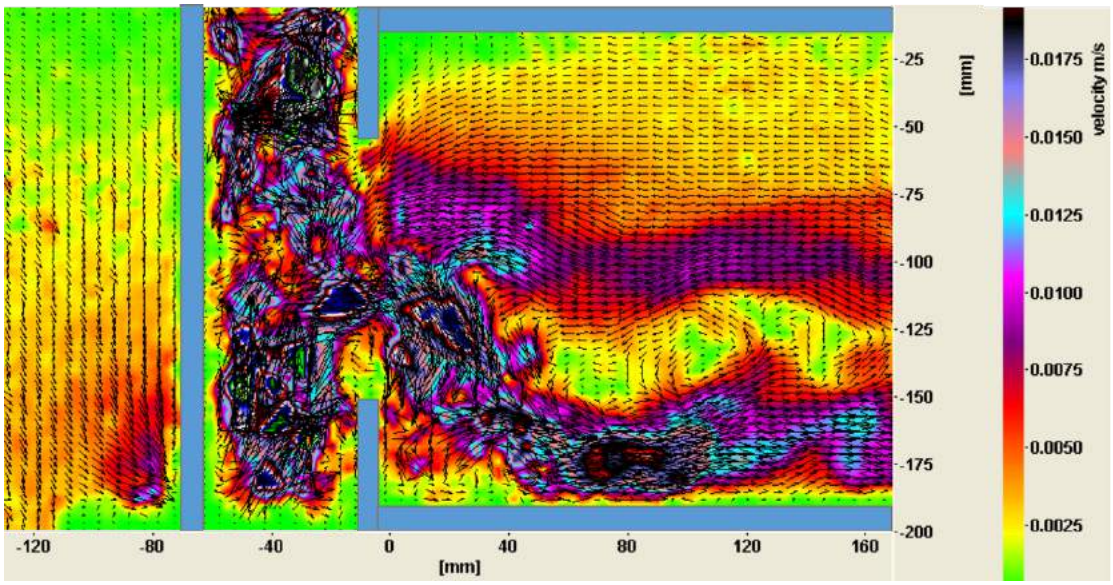

(d)

Figure 3.25 Contour and Vector Images of Salt Water Flow at Steady State Exported from PIV System (a) M1 (b) M2 (c) M3 (d) M4

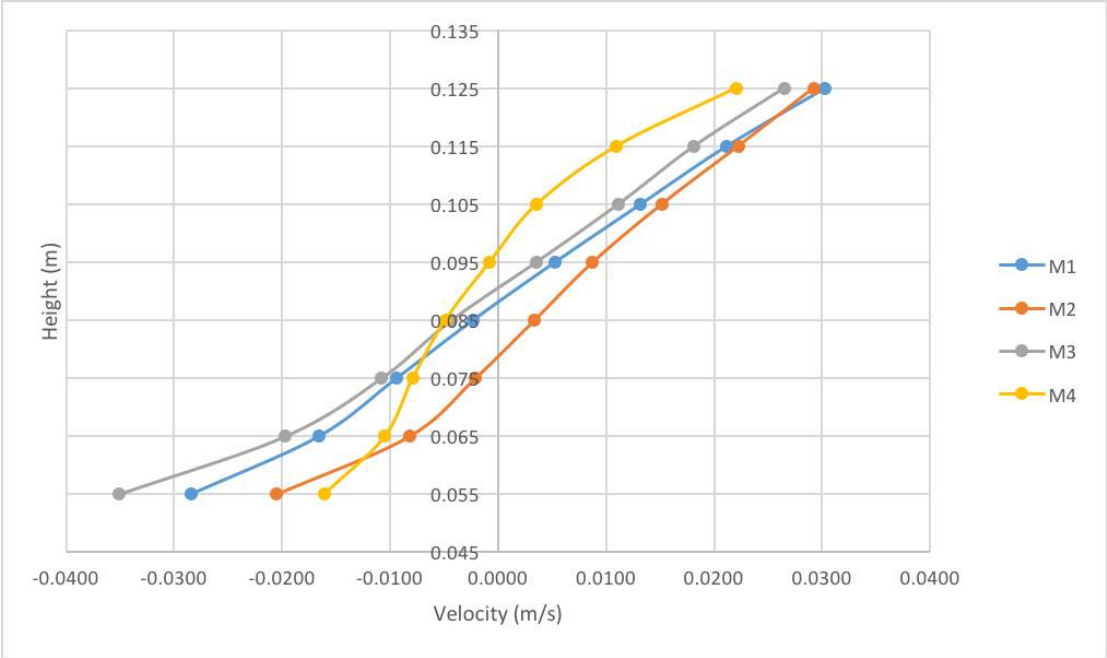

Figure 3.26 Plots of the Mean Velocity at Steady State along the Height of the Center Line at the Second Floor Opening Exported from PIV System for M1 to M4

Chapter 4

Discussion

4.1 Comparisons between the Results of FDS and Blue Dye Tests

Blue dye test is a tool for qualitative study, but one quantitative parameter, the front arrival time to certain locations is recorded by camera. Using dimensionless analysis, the front arrival time for blue dye tests and FDS simulations could be compared. It shows a great match in Kelly's thesis studying the smoke spread in a two-floor compartment connecting with an opening [15]. In this research, five critical locations are chosen (shown in Figure 4.1) with a reference point at the beginning of the spilling flow. Figure 4.2 shows the comparison of dimensionless front arrival time between blue dye tests and FDS simulations for M1 to M4. In this figure, blue dye test has a slightly higher value than FDS simulation in M1 to M3 and has a slightly lower value than FDS simulation in M4, while the trend of increase for dimensionless front arrival time matches very well.

Additionally, an important difference at the steady state for smoke filing is found (shown in Figure 4.2) that a steady blue dye layer could be formed at the second floor enclosure in blue dye tests, while the smoke could fill up the whole enclosure in FDS simulations which is more realistic. This difference could be from the properties of air and liquid like the difference in viscosity and dispersion rate.

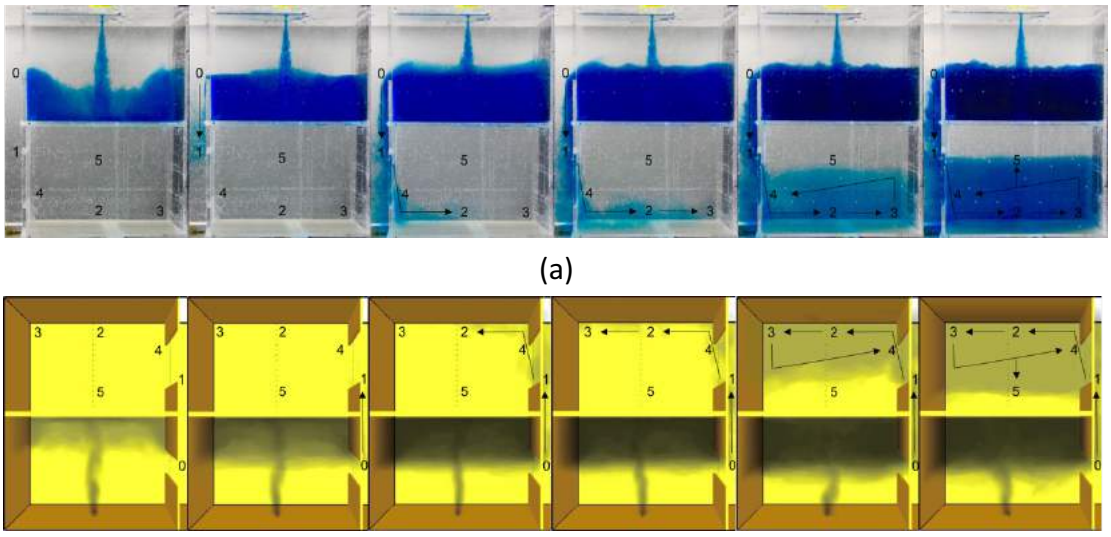

(a)

(b)

Figure 4.1 Critical Locations for Studying Dimensionless Front Arrival Time (a) Blue Dye Test (b) FDS Simulation

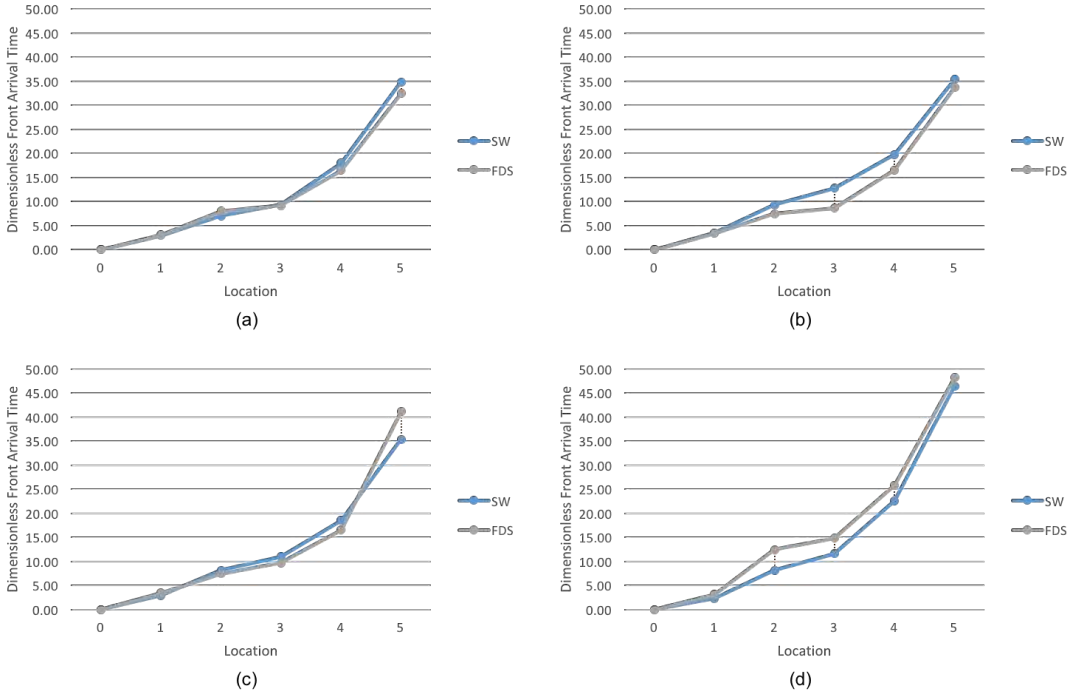

Figure 4.2 Comparison of Dimensionless Front Arrival Time to Critical Locations Between Blue Dye Tests and FDS Simulations (a) M1 (b) M2 (c) M3 (d) M4

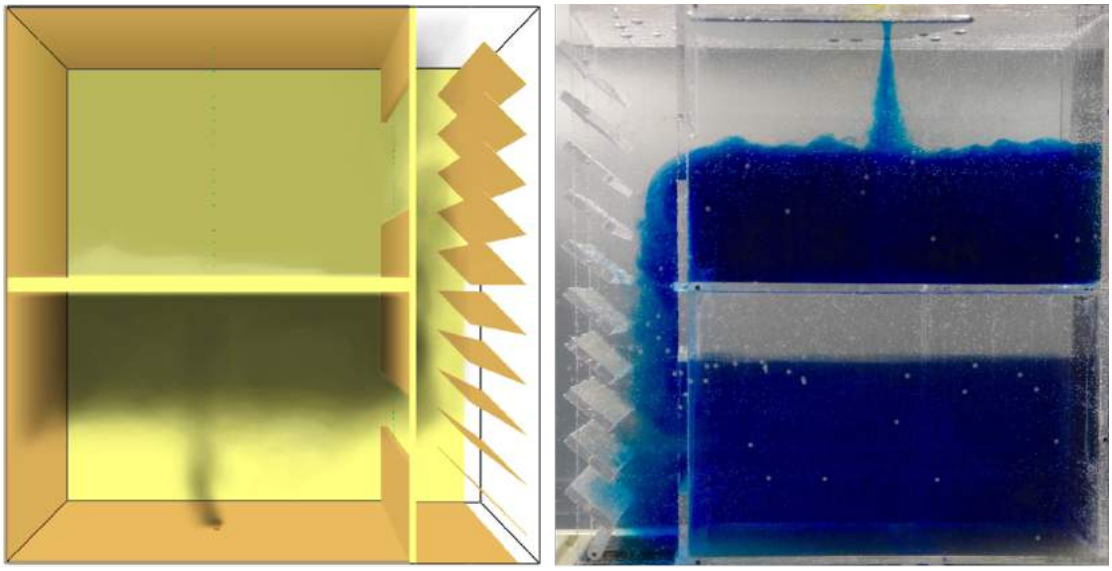

Figure 4.3 Comparison of Smoke Filing Status at the Second Floor Enclosure between FDS Simulation and Blue Dye Test (a) FDS Simulation for M1 (b) Blue Dye Test for M1

4.2 Comparisons between the Results of FDS and PIV/PLIF Experiments

Applying dimensionless analysis for values of velocity along the height of the center line points at the second floor opening, velocity could be compared between models

in FDS simulations and PIV experiments. Figure 4.4 shows the plots of dimensionless velocity at steady state for the output values of both methods in M1 to M4. In this figure results of PIV experiments have a good agreement with FDS simulations. The dimensionless locations of neutral plane obtained from PIV experiments are slightly higher than FDS simulations and the status of velocity distribution along the opening looks less fluctuating in salt water modeling.

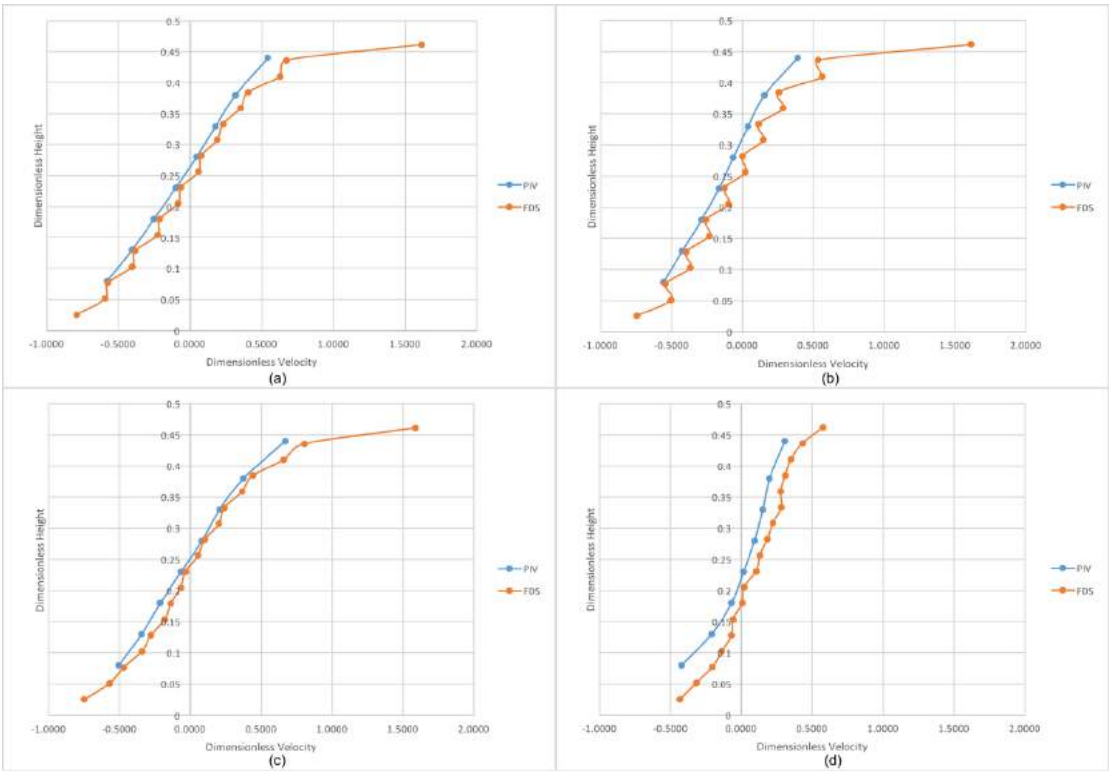

Figure 4.4 Comparison of Dimensionless Velocity at Steady State along the Dimensionless Height of the Center Line Points at the Second Floor Opening Between PIV Experiments and FDS Simulations (a) M1 (b) M2 (c) M3 (d) M4

4.3 Advantages and Disadvantages of Both Methods

As introduced in 1.1.3, CFD modeling is very useful but conditionally trustful due to the limitations of the relevant software. The limitations of FDS simulation are from the deficiency of fire chemistry and physics settings fundamentally. On the other hand, this tool is very user-dependent and relies on the processor and memory support of computer. For example, it takes months to finish one resolution study with finer mesh in this research which is too time-consuming.

Saltwater modeling can be envisioned as a physical simulation of infinite resolution, overcoming the main hurdle of numerical modeling, limited grid resolution. It also overcomes another resolution with many CFD codes, such as the Fire Dynamics Simulator (FDS) which is unable to accurately simulate features such as sloped

structure due to a fixed grid arrangement in the software. However, the differences between liquid flow and air flow like parameters of viscosity and dispersion rate could bring uncertainties in results. Moreover, it takes time to design and build an acrylic model and the size of scaled model is restricted by the size of water tank. On the aspect of data acquisition, it also takes time to setup and calibrate the laser diagnose system and the reflection in experiment can be greatly influence the results.

4.4 The Study on Stack Effect

The cause of stack effect is introduced in Drysdale's book of An Introduction to Fire Dynamics [13]. In general, stack effect is driven by buoyancy in structures like shaft because of the density difference between inner space and outer space in ventilation. Double-skin facade with long vertical cavity spaces used in natural ventilation could be a typical building feature to produce stack effect. The study on stack effect in fire is so important since it could greatly influence the transportation of smoke and hot gases in vertical spread to other floors. And in a broad view, double skin facade is usually a linking space to all structure floor main openings which increases the hazard of stack effect in potential. When studying stack effect, a neutral plane where the pressure difference between inner space and outer space is equal to zero, is a very important parameter to derive which could be used to assess the indoor mass flow, velocity, temperature, visibility and air quality.

In this thesis, two-floor compartment within fire source in a high-rise building is focused on to study the influence of double-skin facade on fire safety in a specific detail part of the building. From the result and analysis in Chapter 3, the status of several fire parameters of the adjacent floor to the floor of fire source is not significantly influenced by louver angle, while it is found that there is a big difference in smoke transport in cavity vertically. Due to the limitation of experimental spaces, the study on stack effect in higher floors is conducted in FDS simulations. As shown in Figure 4.5, Same angle one-to-one correspondent to five cases before with an extended cavity structure and more louvers to influence the smoke movement. Simplifications are made that a flashover fire occurs in the third floor in a ten-floor building. More detailed setups of these models will be introduced in another publication and the simulation results and equations derived to get the height of neutral plane for different louver angles will also be stated in that paper. Figure 4.6 showing the velocity vectors' slice at 100 seconds (steady stage) could help to state the analysis and conclusion of this thesis.

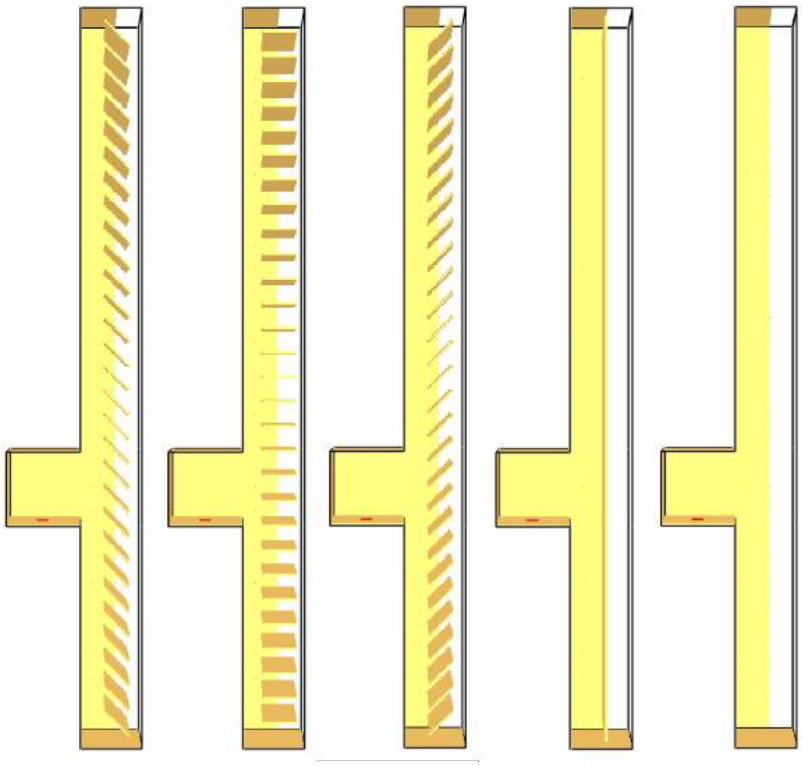

Figure 4.5 Structure Models in FDS-SMV for Extended Study on Stack Effect
Note: These five cases are named as M1s, M2s, M3s, M4s and M5s from left to right one-to-one correspondent to the louver angle of M1, M2, M3, M4 and M5.

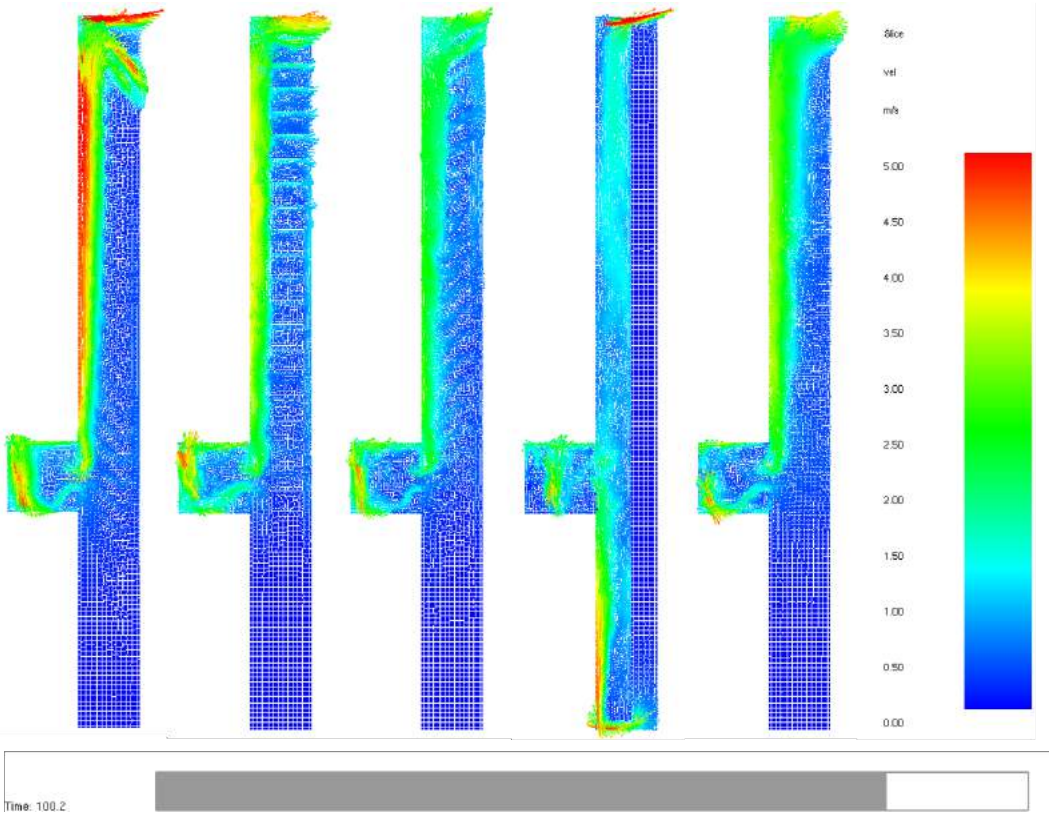

Figure 4.6 Velocity Vectors' Slice in FDS-SMV for Extended Study on Stack Effect

CHAPTER 5

Conclusions

Utilizing the blue dye and PIV/PLIF measurements assisting with dimensionless analysis, dimensionless front arrival time, dimensionless velocity, and dimensionless density difference could be obtained to develop and evaluate CFD full-scale models in FDS in which velocity, temperature, mass fraction, mass flow and particles are tracked in the domain. The measurements from these two methods show a great agreement in predicting smoke spread and smoke filling process in the double-skin facade configuration. Results and conclusions could be referenced by fire consultants, architects when making designs and even fire fighters when making tactics.

Saltwater modeling can be envisioned as a physical simulation of infinite resolution, overcoming the main hurdle of numerical modeling, limited grid resolution. It also overcomes another resolution with many CFD codes, such as the Fire Dynamics Simulator (FDS) which is unable to accurately simulate features such as sloped structure due to a fixed grid arrangement in the software. The combination of these two methods could foster advantages of both approaches while circumvent disadvantages of separate models.

In the study of how louver angle could influence smoke spread and smoke filing based on the analysis of output from these two models, conclusions could be drawn that the application of double-skin facade could hold more smoke in cavity compared with single glazing facade. The angle of 135 degrees calculated from the upward direction of building which is the most common position in louver facade has a significantly adverse effect on smoke diffusion and extraction, since the slots could largely block the way smoke spread out of facade and create backflow effect to induce the part of smoke tends to expel out of cavity back, contributing to stack effect in higher floors and accelerate the speed of smoke filing in adjacent compartments. On the contrary, the angle of 45 degrees could significantly releasing the stack effect in the building and give way for the smoke moving out of cavity easily. At the same time, the ventilation effect, drawing ambient air into the cavity due to temperature difference at lower level, provide adverse velocity vector which could also slow down the vertical spread rate of smoke. Thus, in real fire situation if the angle of outer-skin facade can be easily adjusted, 45 degrees is better than the most commonly-used 135 degrees. What's more, it is found that the angle of outer-skin louvers may have more influence on the velocity and temperature distribution at higher floors which contribute to the stack effect, but not much at the adjacent floor and have more influence on the development period of these parameters, but not the steady state at the adjacent floor when fresh air drawing through the gaps of louvers into the cavity continuously because of the steady temperature difference

below the opening of the adjacent floor.

Furthermore, stack effect in double-skin facade is studied in an extended structure using FDS simulations. More conclusions will be stated in another publication. Meanwhile, the logic of this research could be organized as combining CFD modeling and salt water modeling to investigate the critical part of a large building, normally with fire source at the first step then conducting CFD simulations for the whole body of the large building if the influence of fire is significantly throughout the whole volume. This combined method could substitute for full-scale fire tests to some extent, since salt water modeling, a physical simulation of infinite resolution, could be a great synergic tool to examine or evaluate CFD simulations in fire research.

A vision on future work:

- Change other parameters like opening factor of inner-skin facade and salt water source strength to compare the results.
- Conduct resolution study and sensitivity study in FDS simulations and manage to do full-scale tests if allowed.
- Create more floors in both computational and experimental models for double-skin facade to examine the influence of louver angle on stack effect in the cavity.
- Develop and evaluate the heat transfer model proposed by Yao [33] for salt water modeling in the configuration of double-skin facade.

REFERENCES

[1] M. Azarbayjani, J. Anderson, Beyond arrows: CFD modeling of a new, naturally ventilated double skin facade configuration in a Chicago high-rise office building, SimBuild 2010. (170AD) 170–176.

[2] T.M. Boake, K. Harrison, D. Collins, D., A. Chatham, R. Lee, Understanding the general principles of the double skin facade system, (2003).

[3] A.M. Barowy, Heat and Smoke Transport in A Residential-Scale Live Fire Training Facility: Experiments and Modeling, M.S. Thesis, Worcester Polytechnic Institute, 2010.

[4] A.H. Buchanan, Structural Design for Fire Safety, 2002, pp. 23-25.

[5] V. Babrauskas, Fire Modeling Tools for Fse: Are They Good Enough?, J. Fire Prot. Eng. 8 (1996) 87–93.

[6] A.N. Beard, Fire models and design, Fire Saf. J. 28 (1997) 117–138.

[7] J.M. Clement, Experimental Verification of the Fire Dynamics Simulator Hydrodynamic Model, PHD Thesis, University of Canterbury, 2000.

[8] C.L. Chow, Numerical studies on smoke spread in the cavity of a double-skin facade, J. Civ. Eng. Manag., 17 (2011) 371–392.

[9] C.L. Chow, Full-scale burning tests on double-skin facade fires, Fire Mater. 317 (2013) 17–34.

[10] C.L. Chow, Spread of smoke and heat along narrow air cavity in double-skin facade fires, Thermal Science, 2 (2014): 405-416.

[11] C.L. Chow, A qualitative investigation on double-skin facade fires, MATEC Web of Conferences, EDP Science, 9 (2013): 03007.

[12] W.K. Chow, Design fire in performance based fire safety design for green and sustainable buildings, The 23rd Conference on Passive and Low Energy Architecture, 2006.

[13] D. Drysdale, An Introduction to Fire Dynamics: Third Edition, 2011, pp. 459-469.

[14] W. Ding, Y. Hasemi, T. Yamada, Smoke control using a double-skin facade, in: Fire Saf. Sci., 2005: pp. 1327–1337.

[15] A.A. Kelly, Examination of Smoke Movement in a Two-Story Compartment Using Salt Water and Computational Fluid Dynamics Modeling, M.S. Thesis, University of Maryland, 2001.

[16] J. Li, X. Xing, C. Hu, Y. Li, C. Yin, S. Liu, Numerical studies on effects of cavity width on smoke spread in double-skin facade, in: Procedia Eng., 2012: pp. 695–699.

[17] LaVision GmbH, DaVis FlowMaster – Getting Started Manual for DaVis 7.1, 2005.

[18] K. McGrattan, S. Hostikka, R. McDermott, J. Floyd, C. Weinschenk, K. Overholt, Fire Dynamics Simulator, User's Guide, Sixth Edition, NIST Spec. Publ. 1019. (2013).

[19] K. McGrattan, S. Hostikka, R. McDermott, J. Floyd, C. Weinschenk, K. Overholt, Fire Dynamics Simulator, 2013.

[20] P.M. Maisto, T. Layton, M.J. Gollner, A.W. Marshall, Salt-water modeling to probe sub-grid scale turbulent mixing of fire plumes, Proceedings of the Ninth U.S. National Combustion Meeting, 2015.

[21] W.K. Mok, W.K. Chow, H. Kong, "Verification and Validation" Computational Fluid Dynamics in Fire, Int. J. Archit. Sci. 5 (2004) 58–67.

[22] M.A. Mohammad, The Impact of sustainability on fire safety, M.S. Thesis, Victoria University of Wellington, 2013.

[23] D. O'Connor, Building facade or fire safety facade, CTBUH J. 2008 (2): 30-39.

[24] J.G. Quintiere, Scaling applications in fire research, Fire Saf. J. 15 (1989) 3–29.

[25] G. Rein, J.L. Torero, W. Jahn, J. Stern-Gottfried, N.L. Ryder, S. Desanghere, M. Lázaro, F. Mowrer, A. Coles, D. Joyeux, D. Alvear, J.A. Capote, A. Jowsey, C. Abecassis-Empis, P. Reszka, Round-robin study of a priori modelling predictions of the Dalmarnock Fire Test One, Fire Saf. J. 44 (2009) 590–602.

[26] C.C. Siang, Characterizing Smoke Dispersion Along Beamed Ceilings Using Salt-Water Modeling, M.S. Thesis, University of Maryland, 2010.

[27] K.D. Steckler, H.R. Baum, J.G. Quintiere, Salt water modeling of fire induced flows in multicompartment enclosures, Symp. Combust. 21 (1988) 143–149.

[28] W. Streicher, Best Practice for Double Skin Facades, 2005.

[29] P. Van Hees, Validation and verification of fire models for fire safety engineering, in: Procedia Eng., 2013: pp. 154–168.

[30] P. Yang, X. Tan, W. Xin, Experimental study and numerical simulation for a storehouse fire accident, Build. Environ. 46 (2011) 1445–1459.

[31] X. Yao, A.W. Marshall, Quantitative salt-water modeling of fire-induced flow, Fire Saf. J. 41 (2006) 497–508.

[32] X. Yao, A.W. Marshall, Characterizing turbulent ceiling jet dynamics with salt-water modeling, in: Fire Saf. Sci., 2005: pp. 927–938.

[33] X. Yao, Characterization of Fire Induced Flow Transport Along Ceilings Using Salt-Water Modeling, PHD Thesis, University of Maryland, 2006.

[34] Z. Yan, C. Zhao, Y. Liu, X. Deng, X. Ceng, S. Liu, B. Lan, R. Nilsson, S. Jeansson, Experimental study and advanced CFD simulation of fire safety performance of building external wall insulation system, MATEC Web Conf. 9 (2013).

APPENDICES

APPENDIX A: An Example of FDS input file

```
&HEAD CHID='MODEL1', TITLE='ANGLE 135'/
&MESH ID='MESH1', IJK=60,40,80, XB=0.00,6.00,0.00,4.00,0.00,8.00/
&MESH ID='MESH2', IJK=200,200,800, XB=6.00,8.00,0.00,4.00,0.00,8.00/
&TIME T_END=1200.0/
&DUMP DT_DEVC=2.0/
&REAC FUEL='Methane'
FYI='Methane, C_1 H_4',
C=1.0,
H=4.0,
O=0.0,
N=0.0,
SOOT_YIELD=0.1,
CO_YIELD=0.0,
HEAT_OF_COMBUSTION=50000.0,
IDEAL=.TRUE./
&RADI RADIATION=.FALSE./
&MISC TMPA=20.0/
&PART ID='TRACERS', MASSLESS=.TRUE., SAMPLING_FACTOR=1, AGE=100/
&SURF ID='FIRE', HRRPUA=600, PART_ID='TRACERS', COLOR='RED'/
&VENT ID='BURNER', XB=2.9,3.0,1.9,2.0,0.0,0.0, SURF_ID='FIRE'/
&OBST XB=5.9,6.0,0.0,4.0,0.0,8.0/RIGHT WALL
&HOLE XB=5.8,6.1,0.0,4.0,1.4,2.4/
&HOLE XB=5.8,6.1,0.0,4.0,5.1,7.0/
&OBST XB=0.0,6.0,0.0,4.0,3.9,4.1/FLOOR
&VENT XB=7.5,8.0,0.0,0.0,0.0,8.0, SURF_ID='OPEN'/
&VENT XB=7.5,8.0,4.0,4.0,0.0,8.0, SURF_ID='OPEN'/
&VENT XB=6.0,8.0,0.0,4.0,8.0,8.0, SURF_ID='OPEN'/
&VENT XB=7.5,8.0,0.0,4.0,0.0,0.0, SURF_ID='OPEN'/
&VENT XB=8.0,8.0,0.0,4.0,0.0,8.0, SURF_ID='OPEN'/

&OBST XB=6.99,7.00,0.00,4.00,1.02,1.03/1ST LOUVER
&OBST XB=7.00,7.01,0.00,4.00,1.01,1.02/
&OBST XB=7.01,7.02,0.00,4.00,1.00,1.01/
&OBST XB=7.02,7.03,0.00,4.00,0.99,1.00/
&OBST XB=7.03,7.04,0.00,4.00,0.98,0.99/
&OBST XB=7.04,7.05,0.00,4.00,0.97,0.98/
&OBST XB=7.05,7.06,0.00,4.00,0.96,0.97/
```

```
&OBST XB=7.06,7.07,0.00,4.00,0.95,0.96/
&OBST XB=7.07,7.08,0.00,4.00,0.94,0.95/
&OBST XB=7.08,7.09,0.00,4.00,0.93,0.94/
&OBST XB=7.09,7.10,0.00,4.00,0.92,0.93/
&OBST XB=7.10,7.11,0.00,4.00,0.91,0.92/
&OBST XB=7.11,7.12,0.00,4.00,0.90,0.91/
&OBST XB=7.12,7.13,0.00,4.00,0.89,0.90/
&OBST XB=7.13,7.14,0.00,4.00,0.88,0.89/
&OBST XB=7.14,7.15,0.00,4.00,0.87,0.88/
&OBST XB=7.15,7.16,0.00,4.00,0.86,0.87/
&OBST XB=7.16,7.17,0.00,4.00,0.85,0.86/
&OBST XB=7.17,7.18,0.00,4.00,0.84,0.85/
&OBST XB=7.18,7.19,0.00,4.00,0.83,0.84/
&OBST XB=7.19,7.20,0.00,4.00,0.82,0.83/
&OBST XB=7.20,7.21,0.00,4.00,0.81,0.82/
&OBST XB=7.21,7.22,0.00,4.00,0.80,0.81/
&OBST XB=7.22,7.23,0.00,4.00,0.79,0.80/
&OBST XB=7.23,7.24,0.00,4.00,0.78,0.79/
&OBST XB=7.24,7.25,0.00,4.00,0.77,0.78/
&OBST XB=7.25,7.26,0.00,4.00,0.76,0.77/
&OBST XB=7.26,7.27,0.00,4.00,0.75,0.76/
&OBST XB=7.27,7.28,0.00,4.00,0.74,0.75/
&OBST XB=7.28,7.29,0.00,4.00,0.73,0.74/
&OBST XB=7.29,7.30,0.00,4.00,0.72,0.73/
&OBST XB=7.30,7.31,0.00,4.00,0.71,0.72/
&OBST XB=7.31,7.32,0.00,4.00,0.70,0.71/
&OBST XB=7.32,7.33,0.00,4.00,0.69,0.70/
&OBST XB=7.33,7.34,0.00,4.00,0.68,0.69/
&OBST XB=7.34,7.35,0.00,4.00,0.67,0.68/
&OBST XB=7.35,7.36,0.00,4.00,0.66,0.67/
&OBST XB=7.36,7.37,0.00,4.00,0.65,0.66/
&OBST XB=7.37,7.38,0.00,4.00,0.64,0.65/
&OBST XB=7.38,7.39,0.00,4.00,0.63,0.64/
&OBST XB=7.39,7.40,0.00,4.00,0.62,0.63/
&OBST XB=7.40,7.41,0.00,4.00,0.61,0.62/
&OBST XB=7.41,7.42,0.00,4.00,0.60,0.61/
&OBST XB=7.42,7.43,0.00,4.00,0.59,0.60/
&OBST XB=7.43,7.44,0.00,4.00,0.58,0.59/
&OBST XB=7.44,7.45,0.00,4.00,0.57,0.58/
&OBST XB=7.45,7.46,0.00,4.00,0.56,0.57/
&OBST XB=7.46,7.47,0.00,4.00,0.55,0.56/
&OBST XB=7.47,7.48,0.00,4.00,0.54,0.55/
&OBST XB=7.48,7.49,0.00,4.00,0.53,0.54/
&OBST XB=7.49,7.50,0.00,4.00,0.52,0.53/
```

&OBST XB=7.50,7.51,0.00,4.00,0.51,0.52/
&OBST XB=7.51,7.52,0.00,4.00,0.50,0.51/
&OBST XB=7.52,7.53,0.00,4.00,0.49,0.50/
&OBST XB=7.53,7.54,0.00,4.00,0.48,0.49/
&OBST XB=7.54,7.55,0.00,4.00,0.47,0.48/
&OBST XB=7.55,7.56,0.00,4.00,0.46,0.47/
&OBST XB=7.56,7.57,0.00,4.00,0.45,0.46/
&OBST XB=7.57,7.58,0.00,4.00,0.44,0.45/
&OBST XB=7.58,7.59,0.00,4.00,0.43,0.44/
&OBST XB=7.59,7.60,0.00,4.00,0.42,0.43/
&OBST XB=7.60,7.61,0.00,4.00,0.41,0.42/
&OBST XB=6.99,7.00,0.00,4.00,1.74,1.75/2ND LOUVER
&OBST XB=7.00,7.01,0.00,4.00,1.73,1.74/
&OBST XB=7.01,7.02,0.00,4.00,1.72,1.73/
&OBST XB=7.02,7.03,0.00,4.00,1.71,1.72/
&OBST XB=7.03,7.04,0.00,4.00,1.70,1.71/
&OBST XB=7.04,7.05,0.00,4.00,1.69,1.70/
&OBST XB=7.05,7.06,0.00,4.00,1.68,1.69/
&OBST XB=7.06,7.07,0.00,4.00,1.67,1.68/
&OBST XB=7.07,7.08,0.00,4.00,1.66,1.67/
&OBST XB=7.08,7.09,0.00,4.00,1.65,1.66/
&OBST XB=7.09,7.10,0.00,4.00,1.64,1.65/
&OBST XB=7.10,7.11,0.00,4.00,1.63,1.64/
&OBST XB=7.11,7.12,0.00,4.00,1.62,1.63/
&OBST XB=7.12,7.13,0.00,4.00,1.61,1.62/
&OBST XB=7.13,7.14,0.00,4.00,1.60,1.61/
&OBST XB=7.14,7.15,0.00,4.00,1.59,1.60/
&OBST XB=7.15,7.16,0.00,4.00,1.58,1.59/
&OBST XB=7.16,7.17,0.00,4.00,1.57,1.58/
&OBST XB=7.17,7.18,0.00,4.00,1.56,1.57/
&OBST XB=7.18,7.19,0.00,4.00,1.55,1.56/
&OBST XB=7.19,7.20,0.00,4.00,1.54,1.55/
&OBST XB=7.20,7.21,0.00,4.00,1.53,1.54/
&OBST XB=7.21,7.22,0.00,4.00,1.52,1.53/
&OBST XB=7.22,7.23,0.00,4.00,1.51,1.52/
&OBST XB=7.23,7.24,0.00,4.00,1.50,1.51/
&OBST XB=7.24,7.25,0.00,4.00,1.49,1.50/
&OBST XB=7.25,7.26,0.00,4.00,1.48,1.49/
&OBST XB=7.26,7.27,0.00,4.00,1.47,1.48/
&OBST XB=7.27,7.28,0.00,4.00,1.46,1.47/
&OBST XB=7.28,7.29,0.00,4.00,1.45,1.46/
&OBST XB=7.29,7.30,0.00,4.00,1.44,1.45/
&OBST XB=7.30,7.31,0.00,4.00,1.43,1.44/
&OBST XB=7.31,7.32,0.00,4.00,1.42,1.43/

&OBST XB=7.32,7.33,0.00,4.00,1.41,1.42/
&OBST XB=7.33,7.34,0.00,4.00,1.40,1.41/
&OBST XB=7.34,7.35,0.00,4.00,1.39,1.40/
&OBST XB=7.35,7.36,0.00,4.00,1.38,1.39/
&OBST XB=7.36,7.37,0.00,4.00,1.37,1.38/
&OBST XB=7.37,7.38,0.00,4.00,1.36,1.37/
&OBST XB=7.38,7.39,0.00,4.00,1.35,1.36/
&OBST XB=7.39,7.40,0.00,4.00,1.34,1.35/
&OBST XB=7.40,7.41,0.00,4.00,1.33,1.34/
&OBST XB=7.41,7.42,0.00,4.00,1.32,1.33/
&OBST XB=7.42,7.43,0.00,4.00,1.31,1.32/
&OBST XB=7.43,7.44,0.00,4.00,1.30,1.31/
&OBST XB=7.44,7.45,0.00,4.00,1.29,1.30/
&OBST XB=7.45,7.46,0.00,4.00,1.28,1.29/
&OBST XB=7.46,7.47,0.00,4.00,1.27,1.28/
&OBST XB=7.47,7.48,0.00,4.00,1.26,1.27/
&OBST XB=7.48,7.49,0.00,4.00,1.25,1.26/
&OBST XB=7.49,7.50,0.00,4.00,1.24,1.25/
&OBST XB=7.50,7.51,0.00,4.00,1.23,1.24/
&OBST XB=7.51,7.52,0.00,4.00,1.22,1.23/
&OBST XB=7.52,7.53,0.00,4.00,1.21,1.22/
&OBST XB=7.53,7.54,0.00,4.00,1.20,1.21/
&OBST XB=7.54,7.55,0.00,4.00,1.19,1.20/
&OBST XB=7.55,7.56,0.00,4.00,1.18,1.19/
&OBST XB=7.56,7.57,0.00,4.00,1.17,1.18/
&OBST XB=7.57,7.58,0.00,4.00,1.16,1.17/
&OBST XB=7.58,7.59,0.00,4.00,1.15,1.16/
&OBST XB=7.59,7.60,0.00,4.00,1.14,1.15/
&OBST XB=7.60,7.61,0.00,4.00,1.13,1.14/
&OBST XB=6.99,7.00,0.00,4.00,2.46,2.47/3RD LOUVER
&OBST XB=7.00,7.01,0.00,4.00,2.45,2.46/
&OBST XB=7.01,7.02,0.00,4.00,2.44,2.45/
&OBST XB=7.02,7.03,0.00,4.00,2.43,2.44/
&OBST XB=7.03,7.04,0.00,4.00,2.42,2.43/
&OBST XB=7.04,7.05,0.00,4.00,2.41,2.42/
&OBST XB=7.05,7.06,0.00,4.00,2.40,2.41/
&OBST XB=7.06,7.07,0.00,4.00,2.39,2.40/
&OBST XB=7.07,7.08,0.00,4.00,2.38,2.39/
&OBST XB=7.08,7.09,0.00,4.00,2.37,2.38/
&OBST XB=7.09,7.10,0.00,4.00,2.36,2.37/
&OBST XB=7.10,7.11,0.00,4.00,2.35,2.36/
&OBST XB=7.11,7.12,0.00,4.00,2.34,2.35/
&OBST XB=7.12,7.13,0.00,4.00,2.33,2.34/
&OBST XB=7.13,7.14,0.00,4.00,2.32,2.33/

```
&OBST XB=7.14,7.15,0.00,4.00,2.31,2.32/
&OBST XB=7.15,7.16,0.00,4.00,2.30,2.31/
&OBST XB=7.16,7.17,0.00,4.00,2.29,2.30/
&OBST XB=7.17,7.18,0.00,4.00,2.28,2.29/
&OBST XB=7.18,7.19,0.00,4.00,2.27,2.28/
&OBST XB=7.19,7.20,0.00,4.00,2.26,2.27/
&OBST XB=7.20,7.21,0.00,4.00,2.25,2.26/
&OBST XB=7.21,7.22,0.00,4.00,2.24,2.25/
&OBST XB=7.22,7.23,0.00,4.00,2.23,2.24/
&OBST XB=7.23,7.24,0.00,4.00,2.22,2.23/
&OBST XB=7.24,7.25,0.00,4.00,2.21,2.22/
&OBST XB=7.25,7.26,0.00,4.00,2.20,2.21/
&OBST XB=7.26,7.27,0.00,4.00,2.19,2.20/
&OBST XB=7.27,7.28,0.00,4.00,2.18,2.19/
&OBST XB=7.28,7.29,0.00,4.00,2.17,2.18/
&OBST XB=7.29,7.30,0.00,4.00,2.16,2.17/
&OBST XB=7.30,7.31,0.00,4.00,2.15,2.16/
&OBST XB=7.31,7.32,0.00,4.00,2.14,2.15/
&OBST XB=7.32,7.33,0.00,4.00,2.13,2.14/
&OBST XB=7.33,7.34,0.00,4.00,2.12,2.13/
&OBST XB=7.34,7.35,0.00,4.00,2.11,2.12/
&OBST XB=7.35,7.36,0.00,4.00,2.10,2.11/
&OBST XB=7.36,7.37,0.00,4.00,2.09,2.10/
&OBST XB=7.37,7.38,0.00,4.00,2.08,2.09/
&OBST XB=7.38,7.39,0.00,4.00,2.07,2.08/
&OBST XB=7.39,7.40,0.00,4.00,2.06,2.07/
&OBST XB=7.40,7.41,0.00,4.00,2.05,2.06/
&OBST XB=7.41,7.42,0.00,4.00,2.04,2.05/
&OBST XB=7.42,7.43,0.00,4.00,2.03,2.04/
&OBST XB=7.43,7.44,0.00,4.00,2.02,2.03/
&OBST XB=7.44,7.45,0.00,4.00,2.01,2.02/
&OBST XB=7.45,7.46,0.00,4.00,2.00,2.01/
&OBST XB=7.46,7.47,0.00,4.00,1.99,2.00/
&OBST XB=7.47,7.48,0.00,4.00,1.98,1.99/
&OBST XB=7.48,7.49,0.00,4.00,1.97,1.98/
&OBST XB=7.49,7.50,0.00,4.00,1.96,1.97/
&OBST XB=7.50,7.51,0.00,4.00,1.95,1.96/
&OBST XB=7.51,7.52,0.00,4.00,1.94,1.95/
&OBST XB=7.52,7.53,0.00,4.00,1.93,1.94/
&OBST XB=7.53,7.54,0.00,4.00,1.92,1.93/
&OBST XB=7.54,7.55,0.00,4.00,1.91,1.92/
&OBST XB=7.55,7.56,0.00,4.00,1.90,1.91/
&OBST XB=7.56,7.57,0.00,4.00,1.89,1.90/
&OBST XB=7.57,7.58,0.00,4.00,1.88,1.89/
```

&OBST XB=7.58,7.59,0.00,4.00,1.87,1.88/
&OBST XB=7.59,7.60,0.00,4.00,1.86,1.87/
&OBST XB=7.60,7.61,0.00,4.00,1.85,1.86/
&OBST XB=6.99,7.00,0.00,4.00,3.18,3.19/4TH LOUVER
&OBST XB=7.00,7.01,0.00,4.00,3.17,3.18/
&OBST XB=7.01,7.02,0.00,4.00,3.16,3.17/
&OBST XB=7.02,7.03,0.00,4.00,3.15,3.16/
&OBST XB=7.03,7.04,0.00,4.00,3.14,3.15/
&OBST XB=7.04,7.05,0.00,4.00,3.13,3.14/
&OBST XB=7.05,7.06,0.00,4.00,3.12,3.13/
&OBST XB=7.06,7.07,0.00,4.00,3.11,3.12/
&OBST XB=7.07,7.08,0.00,4.00,3.10,3.11/
&OBST XB=7.08,7.09,0.00,4.00,3.09,3.10/
&OBST XB=7.09,7.10,0.00,4.00,3.08,3.09/
&OBST XB=7.10,7.11,0.00,4.00,3.07,3.08/
&OBST XB=7.11,7.12,0.00,4.00,3.06,3.07/
&OBST XB=7.12,7.13,0.00,4.00,3.05,3.06/
&OBST XB=7.13,7.14,0.00,4.00,3.04,3.05/
&OBST XB=7.14,7.15,0.00,4.00,3.03,3.04/
&OBST XB=7.15,7.16,0.00,4.00,3.02,3.03/
&OBST XB=7.16,7.17,0.00,4.00,3.01,3.02/
&OBST XB=7.17,7.18,0.00,4.00,3.00,3.01/
&OBST XB=7.18,7.19,0.00,4.00,2.99,3.00/
&OBST XB=7.19,7.20,0.00,4.00,2.98,2.99/
&OBST XB=7.20,7.21,0.00,4.00,2.97,2.98/
&OBST XB=7.21,7.22,0.00,4.00,2.96,2.97/
&OBST XB=7.22,7.23,0.00,4.00,2.95,2.96/
&OBST XB=7.23,7.24,0.00,4.00,2.94,2.95/
&OBST XB=7.24,7.25,0.00,4.00,2.93,2.94/
&OBST XB=7.25,7.26,0.00,4.00,2.92,2.93/
&OBST XB=7.26,7.27,0.00,4.00,2.91,2.92/
&OBST XB=7.27,7.28,0.00,4.00,2.90,2.91/
&OBST XB=7.28,7.29,0.00,4.00,2.89,2.90/
&OBST XB=7.29,7.30,0.00,4.00,2.88,2.89/
&OBST XB=7.30,7.31,0.00,4.00,2.87,2.88/
&OBST XB=7.31,7.32,0.00,4.00,2.86,2.87/
&OBST XB=7.32,7.33,0.00,4.00,2.85,2.86/
&OBST XB=7.33,7.34,0.00,4.00,2.84,2.85/
&OBST XB=7.34,7.35,0.00,4.00,2.83,2.84/
&OBST XB=7.35,7.36,0.00,4.00,2.82,2.83/
&OBST XB=7.36,7.37,0.00,4.00,2.81,2.82/
&OBST XB=7.37,7.38,0.00,4.00,2.80,2.81/
&OBST XB=7.38,7.39,0.00,4.00,2.79,2.80/
&OBST XB=7.39,7.40,0.00,4.00,2.78,2.79/

&OBST XB=7.40,7.41,0.00,4.00,2.77,2.78/
&OBST XB=7.41,7.42,0.00,4.00,2.76,2.77/
&OBST XB=7.42,7.43,0.00,4.00,2.75,2.76/
&OBST XB=7.43,7.44,0.00,4.00,2.74,2.75/
&OBST XB=7.44,7.45,0.00,4.00,2.73,2.74/
&OBST XB=7.45,7.46,0.00,4.00,2.72,2.73/
&OBST XB=7.46,7.47,0.00,4.00,2.71,2.72/
&OBST XB=7.47,7.48,0.00,4.00,2.70,2.71/
&OBST XB=7.48,7.49,0.00,4.00,2.69,2.70/
&OBST XB=7.49,7.50,0.00,4.00,2.68,2.69/
&OBST XB=7.50,7.51,0.00,4.00,2.67,2.68/
&OBST XB=7.51,7.52,0.00,4.00,2.66,2.67/
&OBST XB=7.52,7.53,0.00,4.00,2.65,2.66/
&OBST XB=7.53,7.54,0.00,4.00,2.64,2.65/
&OBST XB=7.54,7.55,0.00,4.00,2.63,2.64/
&OBST XB=7.55,7.56,0.00,4.00,2.62,2.63/
&OBST XB=7.56,7.57,0.00,4.00,2.61,2.62/
&OBST XB=7.57,7.58,0.00,4.00,2.60,2.61/
&OBST XB=7.58,7.59,0.00,4.00,2.59,2.60/
&OBST XB=7.59,7.60,0.00,4.00,2.58,2.59/
&OBST XB=7.60,7.61,0.00,4.00,2.57,2.58/
&OBST XB=6.99,7.00,0.00,4.00,3.90,3.91/5TH LOUVER
&OBST XB=7.00,7.01,0.00,4.00,3.89,3.90/
&OBST XB=7.01,7.02,0.00,4.00,3.88,3.89/
&OBST XB=7.02,7.03,0.00,4.00,3.87,3.88/
&OBST XB=7.03,7.04,0.00,4.00,3.86,3.87/
&OBST XB=7.04,7.05,0.00,4.00,3.85,3.86/
&OBST XB=7.05,7.06,0.00,4.00,3.84,3.85/
&OBST XB=7.06,7.07,0.00,4.00,3.83,3.84/
&OBST XB=7.07,7.08,0.00,4.00,3.82,3.83/
&OBST XB=7.08,7.09,0.00,4.00,3.81,3.82/
&OBST XB=7.09,7.10,0.00,4.00,3.80,3.81/
&OBST XB=7.10,7.11,0.00,4.00,3.79,3.80/
&OBST XB=7.11,7.12,0.00,4.00,3.78,3.79/
&OBST XB=7.12,7.13,0.00,4.00,3.77,3.78/
&OBST XB=7.13,7.14,0.00,4.00,3.76,3.77/
&OBST XB=7.14,7.15,0.00,4.00,3.75,3.76/
&OBST XB=7.15,7.16,0.00,4.00,3.74,3.75/
&OBST XB=7.16,7.17,0.00,4.00,3.73,3.74/
&OBST XB=7.17,7.18,0.00,4.00,3.72,3.73/
&OBST XB=7.18,7.19,0.00,4.00,3.71,3.72/
&OBST XB=7.19,7.20,0.00,4.00,3.70,3.71/
&OBST XB=7.20,7.21,0.00,4.00,3.69,3.70/
&OBST XB=7.21,7.22,0.00,4.00,3.68,3.69/

&OBST XB=7.22,7.23,0.00,4.00,3.67,3.68/
&OBST XB=7.23,7.24,0.00,4.00,3.66,3.67/
&OBST XB=7.24,7.25,0.00,4.00,3.65,3.66/
&OBST XB=7.25,7.26,0.00,4.00,3.64,3.65/
&OBST XB=7.26,7.27,0.00,4.00,3.63,3.64/
&OBST XB=7.27,7.28,0.00,4.00,3.62,3.63/
&OBST XB=7.28,7.29,0.00,4.00,3.61,3.62/
&OBST XB=7.29,7.30,0.00,4.00,3.60,3.61/
&OBST XB=7.30,7.31,0.00,4.00,3.59,3.60/
&OBST XB=7.31,7.32,0.00,4.00,3.58,3.59/
&OBST XB=7.32,7.33,0.00,4.00,3.57,3.58/
&OBST XB=7.33,7.34,0.00,4.00,3.56,3.57/
&OBST XB=7.34,7.35,0.00,4.00,3.55,3.56/
&OBST XB=7.35,7.36,0.00,4.00,3.54,3.55/
&OBST XB=7.36,7.37,0.00,4.00,3.53,3.54/
&OBST XB=7.37,7.38,0.00,4.00,3.52,3.53/
&OBST XB=7.38,7.39,0.00,4.00,3.51,3.52/
&OBST XB=7.39,7.40,0.00,4.00,3.50,3.51/
&OBST XB=7.40,7.41,0.00,4.00,3.49,3.50/
&OBST XB=7.41,7.42,0.00,4.00,3.48,3.49/
&OBST XB=7.42,7.43,0.00,4.00,3.47,3.48/
&OBST XB=7.43,7.44,0.00,4.00,3.46,3.47/
&OBST XB=7.44,7.45,0.00,4.00,3.45,3.46/
&OBST XB=7.45,7.46,0.00,4.00,3.44,3.45/
&OBST XB=7.46,7.47,0.00,4.00,3.43,3.44/
&OBST XB=7.47,7.48,0.00,4.00,3.42,3.43/
&OBST XB=7.48,7.49,0.00,4.00,3.41,3.42/
&OBST XB=7.49,7.50,0.00,4.00,3.40,3.41/
&OBST XB=7.50,7.51,0.00,4.00,3.39,3.40/
&OBST XB=7.51,7.52,0.00,4.00,3.38,3.39/
&OBST XB=7.52,7.53,0.00,4.00,3.37,3.38/
&OBST XB=7.53,7.54,0.00,4.00,3.36,3.37/
&OBST XB=7.54,7.55,0.00,4.00,3.35,3.36/
&OBST XB=7.55,7.56,0.00,4.00,3.34,3.35/
&OBST XB=7.56,7.57,0.00,4.00,3.33,3.34/
&OBST XB=7.57,7.58,0.00,4.00,3.32,3.33/
&OBST XB=7.58,7.59,0.00,4.00,3.31,3.32/
&OBST XB=7.59,7.60,0.00,4.00,3.30,3.31/
&OBST XB=7.60,7.61,0.00,4.00,3.29,3.30/
&OBST XB=6.99,7.00,0.00,4.00,4.62,4.63/6TH LOUVER
&OBST XB=7.00,7.01,0.00,4.00,4.61,4.62/
&OBST XB=7.01,7.02,0.00,4.00,4.60,4.61/
&OBST XB=7.02,7.03,0.00,4.00,4.59,4.60/
&OBST XB=7.03,7.04,0.00,4.00,4.58,4.59/

```
&OBST XB=7.04,7.05,0.00,4.00,4.57,4.58/
&OBST XB=7.05,7.06,0.00,4.00,4.56,4.57/
&OBST XB=7.06,7.07,0.00,4.00,4.55,4.56/
&OBST XB=7.07,7.08,0.00,4.00,4.54,4.55/
&OBST XB=7.08,7.09,0.00,4.00,4.53,4.54/
&OBST XB=7.09,7.10,0.00,4.00,4.52,4.53/
&OBST XB=7.10,7.11,0.00,4.00,4.51,4.52/
&OBST XB=7.11,7.12,0.00,4.00,4.50,4.51/
&OBST XB=7.12,7.13,0.00,4.00,4.49,4.50/
&OBST XB=7.13,7.14,0.00,4.00,4.48,4.49/
&OBST XB=7.14,7.15,0.00,4.00,4.47,4.48/
&OBST XB=7.15,7.16,0.00,4.00,4.46,4.47/
&OBST XB=7.16,7.17,0.00,4.00,4.45,4.46/
&OBST XB=7.17,7.18,0.00,4.00,4.44,4.45/
&OBST XB=7.18,7.19,0.00,4.00,4.43,4.44/
&OBST XB=7.19,7.20,0.00,4.00,4.42,4.43/
&OBST XB=7.20,7.21,0.00,4.00,4.41,4.42/
&OBST XB=7.21,7.22,0.00,4.00,4.40,4.41/
&OBST XB=7.22,7.23,0.00,4.00,4.39,4.40/
&OBST XB=7.23,7.24,0.00,4.00,4.38,4.39/
&OBST XB=7.24,7.25,0.00,4.00,4.37,4.38/
&OBST XB=7.25,7.26,0.00,4.00,4.36,4.37/
&OBST XB=7.26,7.27,0.00,4.00,4.35,4.36/
&OBST XB=7.27,7.28,0.00,4.00,4.34,4.35/
&OBST XB=7.28,7.29,0.00,4.00,4.33,4.34/
&OBST XB=7.29,7.30,0.00,4.00,4.32,4.33/
&OBST XB=7.30,7.31,0.00,4.00,4.31,4.32/
&OBST XB=7.31,7.32,0.00,4.00,4.30,4.31/
&OBST XB=7.32,7.33,0.00,4.00,4.29,4.30/
&OBST XB=7.33,7.34,0.00,4.00,4.28,4.29/
&OBST XB=7.34,7.35,0.00,4.00,4.27,4.28/
&OBST XB=7.35,7.36,0.00,4.00,4.26,4.27/
&OBST XB=7.36,7.37,0.00,4.00,4.25,4.26/
&OBST XB=7.37,7.38,0.00,4.00,4.24,4.25/
&OBST XB=7.38,7.39,0.00,4.00,4.23,4.24/
&OBST XB=7.39,7.40,0.00,4.00,4.22,4.23/
&OBST XB=7.40,7.41,0.00,4.00,4.21,4.22/
&OBST XB=7.41,7.42,0.00,4.00,4.20,4.21/
&OBST XB=7.42,7.43,0.00,4.00,4.19,4.20/
&OBST XB=7.43,7.44,0.00,4.00,4.18,4.19/
&OBST XB=7.44,7.45,0.00,4.00,4.17,4.18/
&OBST XB=7.45,7.46,0.00,4.00,4.16,4.17/
&OBST XB=7.46,7.47,0.00,4.00,4.15,4.16/
&OBST XB=7.47,7.48,0.00,4.00,4.14,4.15/
```

```
&OBST XB=7.48,7.49,0.00,4.00,4.13,4.14/
&OBST XB=7.49,7.50,0.00,4.00,4.12,4.13/
&OBST XB=7.50,7.51,0.00,4.00,4.11,4.12/
&OBST XB=7.51,7.52,0.00,4.00,4.10,4.11/
&OBST XB=7.52,7.53,0.00,4.00,4.09,4.10/
&OBST XB=7.53,7.54,0.00,4.00,4.08,4.09/
&OBST XB=7.54,7.55,0.00,4.00,4.07,4.08/
&OBST XB=7.55,7.56,0.00,4.00,4.06,4.07/
&OBST XB=7.56,7.57,0.00,4.00,4.05,4.06/
&OBST XB=7.57,7.58,0.00,4.00,4.04,4.05/
&OBST XB=7.58,7.59,0.00,4.00,4.03,4.04/
&OBST XB=7.59,7.60,0.00,4.00,4.02,4.03/
&OBST XB=7.60,7.61,0.00,4.00,4.01,4.02/
&OBST XB=6.99,7.00,0.00,4.00,5.34,5.35/7TH LOUVER
&OBST XB=7.00,7.01,0.00,4.00,5.33,5.34/
&OBST XB=7.01,7.02,0.00,4.00,5.32,5.33/
&OBST XB=7.02,7.03,0.00,4.00,5.31,5.32/
&OBST XB=7.03,7.04,0.00,4.00,5.30,5.31/
&OBST XB=7.04,7.05,0.00,4.00,5.29,5.30/
&OBST XB=7.05,7.06,0.00,4.00,5.28,5.29/
&OBST XB=7.06,7.07,0.00,4.00,5.27,5.28/
&OBST XB=7.07,7.08,0.00,4.00,5.26,5.27/
&OBST XB=7.08,7.09,0.00,4.00,5.25,5.26/
&OBST XB=7.09,7.10,0.00,4.00,5.24,5.25/
&OBST XB=7.10,7.11,0.00,4.00,5.23,5.24/
&OBST XB=7.11,7.12,0.00,4.00,5.22,5.23/
&OBST XB=7.12,7.13,0.00,4.00,5.21,5.22/
&OBST XB=7.13,7.14,0.00,4.00,5.20,5.21/
&OBST XB=7.14,7.15,0.00,4.00,5.19,5.20/
&OBST XB=7.15,7.16,0.00,4.00,5.18,5.19/
&OBST XB=7.16,7.17,0.00,4.00,5.17,5.18/
&OBST XB=7.17,7.18,0.00,4.00,5.16,5.17/
&OBST XB=7.18,7.19,0.00,4.00,5.15,5.16/
&OBST XB=7.19,7.20,0.00,4.00,5.14,5.15/
&OBST XB=7.20,7.21,0.00,4.00,5.13,5.14/
&OBST XB=7.21,7.22,0.00,4.00,5.12,5.13/
&OBST XB=7.22,7.23,0.00,4.00,5.11,5.12/
&OBST XB=7.23,7.24,0.00,4.00,5.10,5.11/
&OBST XB=7.24,7.25,0.00,4.00,5.09,5.10/
&OBST XB=7.25,7.26,0.00,4.00,5.08,5.09/
&OBST XB=7.26,7.27,0.00,4.00,5.07,5.08/
&OBST XB=7.27,7.28,0.00,4.00,5.06,5.07/
&OBST XB=7.28,7.29,0.00,4.00,5.05,5.06/
&OBST XB=7.29,7.30,0.00,4.00,5.04,5.05/
```

&OBST XB=7.30,7.31,0.00,4.00,5.03,5.04/
&OBST XB=7.31,7.32,0.00,4.00,5.02,5.03/
&OBST XB=7.32,7.33,0.00,4.00,5.01,5.02/
&OBST XB=7.33,7.34,0.00,4.00,5.00,5.01/
&OBST XB=7.34,7.35,0.00,4.00,4.99,5.00/
&OBST XB=7.35,7.36,0.00,4.00,4.98,4.99/
&OBST XB=7.36,7.37,0.00,4.00,4.97,4.98/
&OBST XB=7.37,7.38,0.00,4.00,4.96,4.97/
&OBST XB=7.38,7.39,0.00,4.00,4.95,4.96/
&OBST XB=7.39,7.40,0.00,4.00,4.94,4.95/
&OBST XB=7.40,7.41,0.00,4.00,4.93,4.94/
&OBST XB=7.41,7.42,0.00,4.00,4.92,4.93/
&OBST XB=7.42,7.43,0.00,4.00,4.91,4.92/
&OBST XB=7.43,7.44,0.00,4.00,4.90,4.91/
&OBST XB=7.44,7.45,0.00,4.00,4.89,4.90/
&OBST XB=7.45,7.46,0.00,4.00,4.88,4.89/
&OBST XB=7.46,7.47,0.00,4.00,4.87,4.88/
&OBST XB=7.47,7.48,0.00,4.00,4.86,4.87/
&OBST XB=7.48,7.49,0.00,4.00,4.85,4.86/
&OBST XB=7.49,7.50,0.00,4.00,4.84,4.85/
&OBST XB=7.50,7.51,0.00,4.00,4.83,4.84/
&OBST XB=7.51,7.52,0.00,4.00,4.82,4.83/
&OBST XB=7.52,7.53,0.00,4.00,4.81,4.82/
&OBST XB=7.53,7.54,0.00,4.00,4.80,4.81/
&OBST XB=7.54,7.55,0.00,4.00,4.79,4.80/
&OBST XB=7.55,7.56,0.00,4.00,4.78,4.79/
&OBST XB=7.56,7.57,0.00,4.00,4.77,4.78/
&OBST XB=7.57,7.58,0.00,4.00,4.76,4.77/
&OBST XB=7.58,7.59,0.00,4.00,4.75,4.76/
&OBST XB=7.59,7.60,0.00,4.00,4.74,4.75/
&OBST XB=7.60,7.61,0.00,4.00,4.73,4.74/
&OBST XB=6.99,7.00,0.00,4.00,6.06,6.07/8TH LOUVER
&OBST XB=7.00,7.01,0.00,4.00,6.05,6.06/
&OBST XB=7.01,7.02,0.00,4.00,6.04,6.05/
&OBST XB=7.02,7.03,0.00,4.00,6.03,6.04/
&OBST XB=7.03,7.04,0.00,4.00,6.02,6.03/
&OBST XB=7.04,7.05,0.00,4.00,6.01,6.02/
&OBST XB=7.05,7.06,0.00,4.00,6.00,6.01/
&OBST XB=7.06,7.07,0.00,4.00,5.99,6.00/
&OBST XB=7.07,7.08,0.00,4.00,5.98,5.99/
&OBST XB=7.08,7.09,0.00,4.00,5.97,5.98/
&OBST XB=7.09,7.10,0.00,4.00,5.96,5.97/
&OBST XB=7.10,7.11,0.00,4.00,5.95,5.96/
&OBST XB=7.11,7.12,0.00,4.00,5.94,5.95/

```
&OBST XB=7.12,7.13,0.00,4.00,5.93,5.94/
&OBST XB=7.13,7.14,0.00,4.00,5.92,5.93/
&OBST XB=7.14,7.15,0.00,4.00,5.91,5.92/
&OBST XB=7.15,7.16,0.00,4.00,5.90,5.91/
&OBST XB=7.16,7.17,0.00,4.00,5.89,5.90/
&OBST XB=7.17,7.18,0.00,4.00,5.88,5.89/
&OBST XB=7.18,7.19,0.00,4.00,5.87,5.88/
&OBST XB=7.19,7.20,0.00,4.00,5.86,5.87/
&OBST XB=7.20,7.21,0.00,4.00,5.85,5.86/
&OBST XB=7.21,7.22,0.00,4.00,5.84,5.85/
&OBST XB=7.22,7.23,0.00,4.00,5.83,5.84/
&OBST XB=7.23,7.24,0.00,4.00,5.82,5.83/
&OBST XB=7.24,7.25,0.00,4.00,5.81,5.82/
&OBST XB=7.25,7.26,0.00,4.00,5.80,5.81/
&OBST XB=7.26,7.27,0.00,4.00,5.79,5.80/
&OBST XB=7.27,7.28,0.00,4.00,5.78,5.79/
&OBST XB=7.28,7.29,0.00,4.00,5.77,5.78/
&OBST XB=7.29,7.30,0.00,4.00,5.76,5.77/
&OBST XB=7.30,7.31,0.00,4.00,5.75,5.76/
&OBST XB=7.31,7.32,0.00,4.00,5.74,5.75/
&OBST XB=7.32,7.33,0.00,4.00,5.73,5.74/
&OBST XB=7.33,7.34,0.00,4.00,5.72,5.73/
&OBST XB=7.34,7.35,0.00,4.00,5.71,5.72/
&OBST XB=7.35,7.36,0.00,4.00,5.70,5.71/
&OBST XB=7.36,7.37,0.00,4.00,5.69,5.70/
&OBST XB=7.37,7.38,0.00,4.00,5.68,5.69/
&OBST XB=7.38,7.39,0.00,4.00,5.67,5.68/
&OBST XB=7.39,7.40,0.00,4.00,5.66,5.67/
&OBST XB=7.40,7.41,0.00,4.00,5.65,5.66/
&OBST XB=7.41,7.42,0.00,4.00,5.64,5.65/
&OBST XB=7.42,7.43,0.00,4.00,5.63,5.64/
&OBST XB=7.43,7.44,0.00,4.00,5.62,5.63/
&OBST XB=7.44,7.45,0.00,4.00,5.61,5.62/
&OBST XB=7.45,7.46,0.00,4.00,5.60,5.61/
&OBST XB=7.46,7.47,0.00,4.00,5.59,5.60/
&OBST XB=7.47,7.48,0.00,4.00,5.58,5.59/
&OBST XB=7.48,7.49,0.00,4.00,5.57,5.58/
&OBST XB=7.49,7.50,0.00,4.00,5.56,5.57/
&OBST XB=7.50,7.51,0.00,4.00,5.55,5.56/
&OBST XB=7.51,7.52,0.00,4.00,5.54,5.55/
&OBST XB=7.52,7.53,0.00,4.00,5.53,5.54/
&OBST XB=7.53,7.54,0.00,4.00,5.52,5.53/
&OBST XB=7.54,7.55,0.00,4.00,5.51,5.52/
&OBST XB=7.55,7.56,0.00,4.00,5.50,5.51/
```

&OBST XB=7.56,7.57,0.00,4.00,5.49,5.50/
&OBST XB=7.57,7.58,0.00,4.00,5.48,5.49/
&OBST XB=7.58,7.59,0.00,4.00,5.47,5.48/
&OBST XB=7.59,7.60,0.00,4.00,5.46,5.47/
&OBST XB=7.60,7.61,0.00,4.00,5.45,5.46/
&OBST XB=6.99,7.00,0.00,4.00,6.78,6.79/9TH LOUVER
&OBST XB=7.00,7.01,0.00,4.00,6.77,6.78/
&OBST XB=7.01,7.02,0.00,4.00,6.76,6.77/
&OBST XB=7.02,7.03,0.00,4.00,6.75,6.76/
&OBST XB=7.03,7.04,0.00,4.00,6.74,6.75/
&OBST XB=7.04,7.05,0.00,4.00,6.73,6.74/
&OBST XB=7.05,7.06,0.00,4.00,6.72,6.73/
&OBST XB=7.06,7.07,0.00,4.00,6.71,6.72/
&OBST XB=7.07,7.08,0.00,4.00,6.70,6.71/
&OBST XB=7.08,7.09,0.00,4.00,6.69,6.70/
&OBST XB=7.09,7.10,0.00,4.00,6.68,6.69/
&OBST XB=7.10,7.11,0.00,4.00,6.67,6.68/
&OBST XB=7.11,7.12,0.00,4.00,6.66,6.67/
&OBST XB=7.12,7.13,0.00,4.00,6.65,6.66/
&OBST XB=7.13,7.14,0.00,4.00,6.64,6.65/
&OBST XB=7.14,7.15,0.00,4.00,6.63,6.64/
&OBST XB=7.15,7.16,0.00,4.00,6.62,6.63/
&OBST XB=7.16,7.17,0.00,4.00,6.61,6.62/
&OBST XB=7.17,7.18,0.00,4.00,6.60,6.61/
&OBST XB=7.18,7.19,0.00,4.00,6.59,6.60/
&OBST XB=7.19,7.20,0.00,4.00,6.58,6.59/
&OBST XB=7.20,7.21,0.00,4.00,6.57,6.58/
&OBST XB=7.21,7.22,0.00,4.00,6.56,6.57/
&OBST XB=7.22,7.23,0.00,4.00,6.55,6.56/
&OBST XB=7.23,7.24,0.00,4.00,6.54,6.55/
&OBST XB=7.24,7.25,0.00,4.00,6.53,6.54/
&OBST XB=7.25,7.26,0.00,4.00,6.52,6.53/
&OBST XB=7.26,7.27,0.00,4.00,6.51,6.52/
&OBST XB=7.27,7.28,0.00,4.00,6.50,6.51/
&OBST XB=7.28,7.29,0.00,4.00,6.49,6.50/
&OBST XB=7.29,7.30,0.00,4.00,6.48,6.49/
&OBST XB=7.30,7.31,0.00,4.00,6.47,6.48/
&OBST XB=7.31,7.32,0.00,4.00,6.46,6.47/
&OBST XB=7.32,7.33,0.00,4.00,6.45,6.46/
&OBST XB=7.33,7.34,0.00,4.00,6.44,6.45/
&OBST XB=7.34,7.35,0.00,4.00,6.43,6.44/
&OBST XB=7.35,7.36,0.00,4.00,6.42,6.43/
&OBST XB=7.36,7.37,0.00,4.00,6.41,6.42/
&OBST XB=7.37,7.38,0.00,4.00,6.40,6.41/

&OBST XB=7.38,7.39,0.00,4.00,6.39,6.40/
&OBST XB=7.39,7.40,0.00,4.00,6.38,6.39/
&OBST XB=7.40,7.41,0.00,4.00,6.37,6.38/
&OBST XB=7.41,7.42,0.00,4.00,6.36,6.37/
&OBST XB=7.42,7.43,0.00,4.00,6.35,6.36/
&OBST XB=7.43,7.44,0.00,4.00,6.34,6.35/
&OBST XB=7.44,7.45,0.00,4.00,6.33,6.34/
&OBST XB=7.45,7.46,0.00,4.00,6.32,6.33/
&OBST XB=7.46,7.47,0.00,4.00,6.31,6.32/
&OBST XB=7.47,7.48,0.00,4.00,6.30,6.31/
&OBST XB=7.48,7.49,0.00,4.00,6.29,6.30/
&OBST XB=7.49,7.50,0.00,4.00,6.28,6.29/
&OBST XB=7.50,7.51,0.00,4.00,6.27,6.28/
&OBST XB=7.51,7.52,0.00,4.00,6.26,6.27/
&OBST XB=7.52,7.53,0.00,4.00,6.25,6.26/
&OBST XB=7.53,7.54,0.00,4.00,6.24,6.25/
&OBST XB=7.54,7.55,0.00,4.00,6.23,6.24/
&OBST XB=7.55,7.56,0.00,4.00,6.22,6.23/
&OBST XB=7.56,7.57,0.00,4.00,6.21,6.22/
&OBST XB=7.57,7.58,0.00,4.00,6.20,6.21/
&OBST XB=7.58,7.59,0.00,4.00,6.19,6.20/
&OBST XB=7.59,7.60,0.00,4.00,6.18,6.19/
&OBST XB=7.60,7.61,0.00,4.00,6.17,6.18/
&OBST XB=6.99,7.00,0.00,4.00,7.50,7.51/10TH LOUVER
&OBST XB=7.00,7.01,0.00,4.00,7.49,7.50/
&OBST XB=7.01,7.02,0.00,4.00,7.48,7.49/
&OBST XB=7.02,7.03,0.00,4.00,7.47,7.48/
&OBST XB=7.03,7.04,0.00,4.00,7.46,7.47/
&OBST XB=7.04,7.05,0.00,4.00,7.45,7.46/
&OBST XB=7.05,7.06,0.00,4.00,7.44,7.45/
&OBST XB=7.06,7.07,0.00,4.00,7.43,7.44/
&OBST XB=7.07,7.08,0.00,4.00,7.42,7.43/
&OBST XB=7.08,7.09,0.00,4.00,7.41,7.42/
&OBST XB=7.09,7.10,0.00,4.00,7.40,7.41/
&OBST XB=7.10,7.11,0.00,4.00,7.39,7.40/
&OBST XB=7.11,7.12,0.00,4.00,7.38,7.39/
&OBST XB=7.12,7.13,0.00,4.00,7.37,7.38/
&OBST XB=7.13,7.14,0.00,4.00,7.36,7.37/
&OBST XB=7.14,7.15,0.00,4.00,7.35,7.36/
&OBST XB=7.15,7.16,0.00,4.00,7.34,7.35/
&OBST XB=7.16,7.17,0.00,4.00,7.33,7.34/
&OBST XB=7.17,7.18,0.00,4.00,7.32,7.33/
&OBST XB=7.18,7.19,0.00,4.00,7.31,7.32/
&OBST XB=7.19,7.20,0.00,4.00,7.30,7.31/

```
&OBST XB=7.20,7.21,0.00,4.00,7.29,7.30/
&OBST XB=7.21,7.22,0.00,4.00,7.28,7.29/
&OBST XB=7.22,7.23,0.00,4.00,7.27,7.28/
&OBST XB=7.23,7.24,0.00,4.00,7.26,7.27/
&OBST XB=7.24,7.25,0.00,4.00,7.25,7.26/
&OBST XB=7.25,7.26,0.00,4.00,7.24,7.25/
&OBST XB=7.26,7.27,0.00,4.00,7.23,7.24/
&OBST XB=7.27,7.28,0.00,4.00,7.22,7.23/
&OBST XB=7.28,7.29,0.00,4.00,7.21,7.22/
&OBST XB=7.29,7.30,0.00,4.00,7.20,7.21/
&OBST XB=7.30,7.31,0.00,4.00,7.19,7.20/
&OBST XB=7.31,7.32,0.00,4.00,7.18,7.19/
&OBST XB=7.32,7.33,0.00,4.00,7.17,7.18/
&OBST XB=7.33,7.34,0.00,4.00,7.16,7.17/
&OBST XB=7.34,7.35,0.00,4.00,7.15,7.16/
&OBST XB=7.35,7.36,0.00,4.00,7.14,7.15/
&OBST XB=7.36,7.37,0.00,4.00,7.13,7.14/
&OBST XB=7.37,7.38,0.00,4.00,7.12,7.13/
&OBST XB=7.38,7.39,0.00,4.00,7.11,7.12/
&OBST XB=7.39,7.40,0.00,4.00,7.10,7.11/
&OBST XB=7.40,7.41,0.00,4.00,7.09,7.10/
&OBST XB=7.41,7.42,0.00,4.00,7.08,7.09/
&OBST XB=7.42,7.43,0.00,4.00,7.07,7.08/
&OBST XB=7.43,7.44,0.00,4.00,7.06,7.07/
&OBST XB=7.44,7.45,0.00,4.00,7.05,7.06/
&OBST XB=7.45,7.46,0.00,4.00,7.04,7.05/
&OBST XB=7.46,7.47,0.00,4.00,7.03,7.04/
&OBST XB=7.47,7.48,0.00,4.00,7.02,7.03/
&OBST XB=7.48,7.49,0.00,4.00,7.01,7.02/
&OBST XB=7.49,7.50,0.00,4.00,7.00,7.01/
&OBST XB=7.50,7.51,0.00,4.00,6.99,7.00/
&OBST XB=7.51,7.52,0.00,4.00,6.98,6.99/
&OBST XB=7.52,7.53,0.00,4.00,6.97,6.98/
&OBST XB=7.53,7.54,0.00,4.00,6.96,6.97/
&OBST XB=7.54,7.55,0.00,4.00,6.95,6.96/
&OBST XB=7.55,7.56,0.00,4.00,6.94,6.95/
&OBST XB=7.56,7.57,0.00,4.00,6.93,6.94/
&OBST XB=7.57,7.58,0.00,4.00,6.92,6.93/
&OBST XB=7.58,7.59,0.00,4.00,6.91,6.92/
&OBST XB=7.59,7.60,0.00,4.00,6.90,6.91/
&OBST XB=7.60,7.61,0.00,4.00,6.89,6.90/

&SLCF PBY=2.00, QUANTITY='TEMPERATURE'/
&SLCF PBX=3.00, QUANTITY='TEMPERATURE'/
```

```
&SLCF PBX=6.00, QUANTITY='TEMPERATURE'/
&SLCF PBY=2.00, QUANTITY='VELOCITY', VECTOR=.TRUE./
&SLCF PBX=3.00, QUANTITY='VELOCITY', VECTOR=.TRUE./
&SLCF PBX=6.00, QUANTITY='VELOCITY', VECTOR=.TRUE./
&SLCF PBY=2.00, QUANTITY='VISIBILITY'/
&DEVC XB=5.90,5.90,0.00,4.00,5.10,7.00, QUANTITY='MASS FLOW -'/
&DEVC XB=5.90,5.90,0.00,4.00,1.40,2.40, QUANTITY='MASS FLOW +'/
&DEVC XB=6.00,6.99,0.00,4.00,7.51,7.51, QUANTITY='MASS FLOW +'/
&DEVC XB=7.61,7.61,0.00,4.00,0.00,6.89, QUANTITY='MASS FLOW +'/
&DEVC ID='TC2_1', XYZ=2.90,2.00,4.50, QUANTITY='TEMPERATURE'/
&DEVC ID='TC2_2', XYZ=2.90,2.00,4.90, QUANTITY='TEMPERATURE'/
&DEVC ID='TC2_3', XYZ=2.90,2.00,5.30, QUANTITY='TEMPERATURE'/
&DEVC ID='TC2_4', XYZ=2.90,2.00,5.70, QUANTITY='TEMPERATURE'/
&DEVC ID='TC2_5', XYZ=2.90,2.00,6.10, QUANTITY='TEMPERATURE'/
&DEVC ID='TC2_6', XYZ=2.90,2.00,6.50, QUANTITY='TEMPERATURE'/
&DEVC ID='TC2_7', XYZ=2.90,2.00,6.90, QUANTITY='TEMPERATURE'/
&DEVC ID='TC2_8', XYZ=2.90,2.00,7.30, QUANTITY='TEMPERATURE'/
&DEVC ID='TC2_9', XYZ=2.90,2.00,7.70, QUANTITY='TEMPERATURE'/
&DEVC ID='TO1_1', XYZ=5.90,2.00,1.50, QUANTITY='TEMPERATURE'/
&DEVC ID='TO1_2', XYZ=5.90,2.00,1.60, QUANTITY='TEMPERATURE'/
&DEVC ID='TO1_3', XYZ=5.90,2.00,1.70, QUANTITY='TEMPERATURE'/
&DEVC ID='TO1_4', XYZ=5.90,2.00,1.80, QUANTITY='TEMPERATURE'/
&DEVC ID='TO1_5', XYZ=5.90,2.00,1.90, QUANTITY='TEMPERATURE'/
&DEVC ID='TO1_6', XYZ=5.90,2.00,2.00, QUANTITY='TEMPERATURE'/
&DEVC ID='TO1_7', XYZ=5.90,2.00,2.10, QUANTITY='TEMPERATURE'/
&DEVC ID='TO1_8', XYZ=5.90,2.00,2.20, QUANTITY='TEMPERATURE'/
&DEVC ID='TO1_9', XYZ=5.90,2.00,2.30, QUANTITY='TEMPERATURE'/
&DEVC ID='TO2_1', XYZ=5.90,2.00,5.20, QUANTITY='TEMPERATURE'/
&DEVC ID='TO2_2', XYZ=5.90,2.00,5.30, QUANTITY='TEMPERATURE'/
&DEVC ID='TO2_3', XYZ=5.90,2.00,5.40, QUANTITY='TEMPERATURE'/
&DEVC ID='TO2_4', XYZ=5.90,2.00,5.50, QUANTITY='TEMPERATURE'/
&DEVC ID='TO2_5', XYZ=5.90,2.00,5.60, QUANTITY='TEMPERATURE'/
&DEVC ID='TO2_6', XYZ=5.90,2.00,5.70, QUANTITY='TEMPERATURE'/
&DEVC ID='TO2_7', XYZ=5.90,2.00,5.80, QUANTITY='TEMPERATURE'/
&DEVC ID='TO2_8', XYZ=5.90,2.00,5.90, QUANTITY='TEMPERATURE'/
&DEVC ID='TO2_9', XYZ=5.90,2.00,6.00, QUANTITY='TEMPERATURE'/
&DEVC ID='TO2_10', XYZ=5.90,2.00,6.10, QUANTITY='TEMPERATURE'/
&DEVC ID='TO2_11', XYZ=5.90,2.00,6.20, QUANTITY='TEMPERATURE'/
&DEVC ID='TO2_12', XYZ=5.90,2.00,6.30, QUANTITY='TEMPERATURE'/
&DEVC ID='TO2_13', XYZ=5.90,2.00,6.40, QUANTITY='TEMPERATURE'/
&DEVC ID='TO2_14', XYZ=5.90,2.00,6.50, QUANTITY='TEMPERATURE'/
&DEVC ID='TO2_15', XYZ=5.90,2.00,6.60, QUANTITY='TEMPERATURE'/
&DEVC ID='TO2_16', XYZ=5.90,2.00,6.70, QUANTITY='TEMPERATURE'/
&DEVC ID='TO2_17', XYZ=5.90,2.00,6.80, QUANTITY='TEMPERATURE'/
```

```
&DEVC ID='TO2_18', XYZ=5.90,2.00,6.90, QUANTITY='TEMPERATURE'/
&DEVC ID='VO1_1', XYZ=5.90,2.00,1.50, QUANTITY='U-VELOCITY'/
&DEVC ID='VO1_2', XYZ=5.90,2.00,1.60, QUANTITY='U-VELOCITY'/
&DEVC ID='VO1_3', XYZ=5.90,2.00,1.70, QUANTITY='U-VELOCITY'/
&DEVC ID='VO1_4', XYZ=5.90,2.00,1.80, QUANTITY='U-VELOCITY'/
&DEVC ID='VO1_5', XYZ=5.90,2.00,1.90, QUANTITY='U-VELOCITY'/
&DEVC ID='VO1_6', XYZ=5.90,2.00,2.00, QUANTITY='U-VELOCITY'/
&DEVC ID='VO1_7', XYZ=5.90,2.00,2.10, QUANTITY='U-VELOCITY'/
&DEVC ID='VO1_8', XYZ=5.90,2.00,2.20, QUANTITY='U-VELOCITY'/
&DEVC ID='VO1_9', XYZ=5.90,2.00,2.30, QUANTITY='U-VELOCITY'/
&DEVC ID='VO2_1', XYZ=5.90,2.00,5.20, QUANTITY='U-VELOCITY'/
&DEVC ID='VO2_2', XYZ=5.90,2.00,5.30, QUANTITY='U-VELOCITY'/
&DEVC ID='VO2_3', XYZ=5.90,2.00,5.40, QUANTITY='U-VELOCITY'/
&DEVC ID='VO2_4', XYZ=5.90,2.00,5.50, QUANTITY='U-VELOCITY'/
&DEVC ID='VO2_5', XYZ=5.90,2.00,5.60, QUANTITY='U-VELOCITY'/
&DEVC ID='VO2_6', XYZ=5.90,2.00,5.70, QUANTITY='U-VELOCITY'/
&DEVC ID='VO2_7', XYZ=5.90,2.00,5.80, QUANTITY='U-VELOCITY'/
&DEVC ID='VO2_8', XYZ=5.90,2.00,5.90, QUANTITY='U-VELOCITY'/
&DEVC ID='VO2_9', XYZ=5.90,2.00,6.00, QUANTITY='U-VELOCITY'/
&DEVC ID='VO2_10', XYZ=5.90,2.00,6.10, QUANTITY='U-VELOCITY'/
&DEVC ID='VO2_11', XYZ=5.90,2.00,6.20, QUANTITY='U-VELOCITY'/
&DEVC ID='VO2_12', XYZ=5.90,2.00,6.30, QUANTITY='U-VELOCITY'/
&DEVC ID='VO2_13', XYZ=5.90,2.00,6.40, QUANTITY='U-VELOCITY'/
&DEVC ID='VO2_14', XYZ=5.90,2.00,6.50, QUANTITY='U-VELOCITY'/
&DEVC ID='VO2_15', XYZ=5.90,2.00,6.60, QUANTITY='U-VELOCITY'/
&DEVC ID='VO2_16', XYZ=5.90,2.00,6.70, QUANTITY='U-VELOCITY'/
&DEVC ID='VO2_17', XYZ=5.90,2.00,6.80, QUANTITY='U-VELOCITY'/
&DEVC ID='VO2_18', XYZ=5.90,2.00,6.90, QUANTITY='U-VELOCITY'/
&DEVC ID='VC2_1', XYZ=2.90,2.00,4.30, QUANTITY='U-VELOCITY'/
&DEVC ID='VC2_2', XYZ=2.90,2.00,4.50, QUANTITY='U-VELOCITY'/
&DEVC ID='VC2_3', XYZ=2.90,2.00,4.70, QUANTITY='U-VELOCITY'/
&DEVC ID='VC2_4', XYZ=2.90,2.00,4.90, QUANTITY='U-VELOCITY'/
&DEVC ID='VC2_5', XYZ=2.90,2.00,5.10, QUANTITY='U-VELOCITY'/
&DEVC ID='VC2_6', XYZ=2.90,2.00,5.30, QUANTITY='U-VELOCITY'/
&DEVC ID='VC2_7', XYZ=2.90,2.00,5.50, QUANTITY='U-VELOCITY'/
&DEVC ID='VC2_8', XYZ=2.90,2.00,5.70, QUANTITY='U-VELOCITY'/
&DEVC ID='VC2_9', XYZ=2.90,2.00,5.90, QUANTITY='U-VELOCITY'/
&DEVC ID='VC2_10', XYZ=2.90,2.00,6.10, QUANTITY='U-VELOCITY'/
&DEVC ID='VC2_11', XYZ=2.90,2.00,6.30, QUANTITY='U-VELOCITY'/
&DEVC ID='VC2_12', XYZ=2.90,2.00,6.50, QUANTITY='U-VELOCITY'/
&DEVC ID='VC2_13', XYZ=2.90,2.00,6.70, QUANTITY='U-VELOCITY'/
&DEVC ID='VC2_14', XYZ=2.90,2.00,6.90, QUANTITY='U-VELOCITY'/
&DEVC ID='VC2_15', XYZ=2.90,2.00,7.10, QUANTITY='U-VELOCITY'/
&DEVC ID='VC2_16', XYZ=2.90,2.00,7.30, QUANTITY='U-VELOCITY'/
```

```
&DEVC ID='VC2_17', XYZ=2.90,2.00,7.50, QUANTITY='U-VELOCITY'/
&DEVC ID='VC2_18', XYZ=2.90,2.00,7.70, QUANTITY='U-VELOCITY'/
&DEVC ID='VC2_19', XYZ=2.90,2.00,7.90, QUANTITY='U-VELOCITY'/

&DEVC ID='MFC2_1', XYZ=2.90,2.00,4.30, QUANTITY='MASS FRACTION',
SPEC_ID='SOOT'/
&DEVC ID='MFC2_2', XYZ=2.90,2.00,4.50, QUANTITY='MASS FRACTION',
SPEC_ID='SOOT'/
&DEVC ID='MFC2_3', XYZ=2.90,2.00,4.70, QUANTITY='MASS FRACTION',
SPEC_ID='SOOT'/
&DEVC ID='MFC2_4', XYZ=2.90,2.00,4.90, QUANTITY='MASS FRACTION',
SPEC_ID='SOOT'/
&DEVC ID='MFC2_5', XYZ=2.90,2.00,5.10, QUANTITY='MASS FRACTION',
SPEC_ID='SOOT'/
&DEVC ID='MFC2_6', XYZ=2.90,2.00,5.30, QUANTITY='MASS FRACTION',
SPEC_ID='SOOT'/
&DEVC ID='MFC2_7', XYZ=2.90,2.00,5.50, QUANTITY='MASS FRACTION',
SPEC_ID='SOOT'/
&DEVC ID='MFC2_8', XYZ=2.90,2.00,5.70, QUANTITY='MASS FRACTION',
SPEC_ID='SOOT'/
&DEVC ID='MFC2_9', XYZ=2.90,2.00,5.90, QUANTITY='MASS FRACTION',
SPEC_ID='SOOT'/
&DEVC ID='MFC2_10', XYZ=2.90,2.00,6.10, QUANTITY='MASS FRACTION',
SPEC_ID='SOOT'/
&DEVC ID='MFC2_11', XYZ=2.90,2.00,6.30, QUANTITY='MASS FRACTION',
SPEC_ID='SOOT'/
&DEVC ID='MFC2_12', XYZ=2.90,2.00,6.50, QUANTITY='MASS FRACTION',
SPEC_ID='SOOT'/
&DEVC ID='MFC2_13', XYZ=2.90,2.00,6.70, QUANTITY='MASS FRACTION',
SPEC_ID='SOOT'/
&DEVC ID='MFC2_14', XYZ=2.90,2.00,6.90, QUANTITY='MASS FRACTION',
SPEC_ID='SOOT'/
&DEVC ID='MFC2_15', XYZ=2.90,2.00,7.10, QUANTITY='MASS FRACTION',
SPEC_ID='SOOT'/
&DEVC ID='MFC2_16', XYZ=2.90,2.00,7.30, QUANTITY='MASS FRACTION',
SPEC_ID='SOOT'/
&DEVC ID='MFC2_17', XYZ=2.90,2.00,7.50, QUANTITY='MASS FRACTION',
SPEC_ID='SOOT'/
&DEVC ID='MFC2_18', XYZ=2.90,2.00,7.70, QUANTITY='MASS FRACTION',
SPEC_ID='SOOT'/
&DEVC ID='MFC2_19', XYZ=2.90,2.00,7.90, QUANTITY='MASS FRACTION',
SPEC_ID='SOOT'/

&TAIL/
```

APPENDIX B: Locations of Devices in FDS Simulations

As introduced in 2.3.2, devices are set in FDS simulations to record the values of velocity, temperature and mass fraction at points along the center line of first floor opening (O1_1-9), second floor opening (O2_1-18) and second floor compartment (C2_1-18). Locations of these points are listed in Figure A.1 and Table A.1. The names of these devices are shown in the output files of FDS and also used in graphs plotted in Chapter 3.

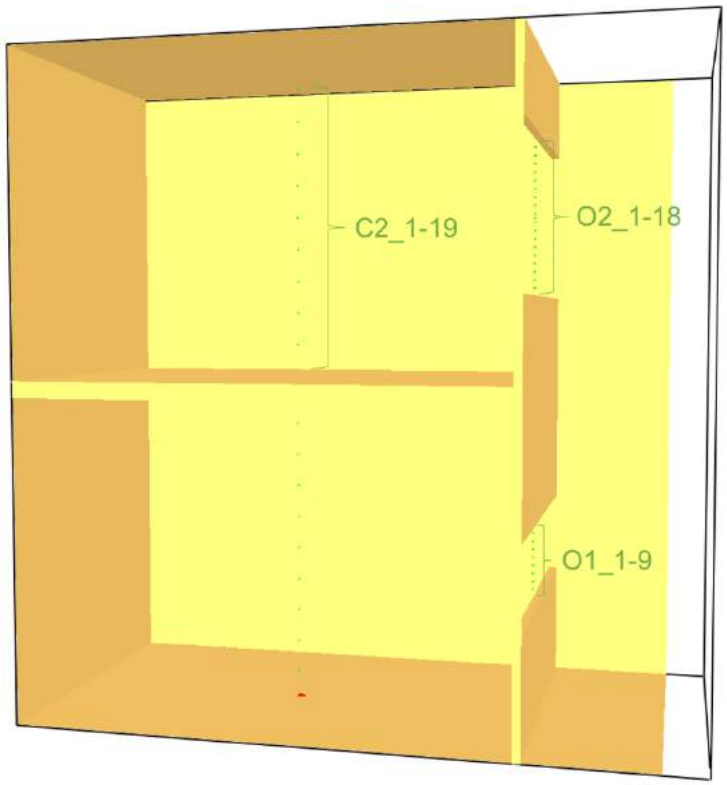

Figure B.1 Locations of Devices in FDS Simulations

		Height from Ground (m)	Name of Devices		
			Velocity	Temperature	Mass Fraction
First Floor Opening	O1_1	1.50	VO1_1	TO1_1	-
	O1_2	1.60	VO1_2	TO1_2	-
	O1_3	1.70	VO1_3	TO1_3	-
	O1_4	1.80	VO1_4	TO1_4	-
	O1_5	1.90	VO1_5	TO1_5	-
	O1_6	2.00	VO1_6	TO1_6	-
	O1_7	2.10	VO1_7	TO1_7	-
	O1_8	2.20	VO1_8	TO1_8	-
	O1_9	2.30	VO1_9	TO1_9	-

Second Floor Opening	O2_1	5.20	VO2_1	TO2_1	-
	O2_2	5.30	VO2_2	TO2_2	-
	O2_3	5.40	VO2_3	TO2_3	-
	O2_4	5.50	VO2_4	TO2_4	-
	O2_5	5.60	VO2_5	TO2_5	-
	O2_6	5.70	VO2_6	TO2_6	-
	O2_7	5.80	VO2_7	TO2_7	-
	O2_8	5.90	VO2_8	TO2_8	-
	O2_9	6.00	VO2_9	TO2_9	-
	O2_10	6.10	VO2_10	TO2_10	-
	O2_11	6.20	VO2_11	TO2_11	-
	O2_12	6.30	VO2_12	TO2_12	-
	O2_13	6.40	VO2_13	TO2_13	-
	O2_14	6.50	VO2_14	TO2_14	-
	O2_15	6.60	VO2_15	TO2_15	-
	O2_16	6.70	VO2_16	TO2_16	-
	O2_17	6.80	VO2_17	TO2_17	-
	O2_18	6.90	VO2_18	TO2_18	-
Second Floor Center	C2_1	4.30	VC2_1	-	MFC2_1
	C2_2	4.50	VC2_2	TC2_1	MFC2_2
	C2_3	4.70	VC2_3	-	MFC2_3
	C2_4	4.90	VC2_4	TC2_2	MFC2_4
	C2_5	5.10	VC2_5	-	MFC2_5
	C2_6	5.30	VC2_6	TC2_3	MFC2_6
	C2_7	5.50	VC2_7		MFC2_7
	C2_8	5.70	VC2_8	TC2_4	MFC2_8
	C2_9	5.90	VC2_9	-	MFC2_9
	C2_10	6.10	VC2_10	TC2_5	MFC2_10
	C2_11	6.30	VC2_11	-	MFC2_11
	C2_12	6.50	VC2_12	TC2_6	MFC2_12
	C2_13	6.70	VC2_13	-	MFC2_13
	C2_14	6.90	VC2_14	TC2_7	MFC2_14
	C2_15	7.10	VC2_15	-	MFC2_15
	C2_16	7.30	VC2_16	TC2_8	MFC2_16
	C2_17	7.50	VC2_17	-	MFC2_17
	C2_18	7.70	VC2_18	TC2_9	MFC2_18
	C2_19	7.90	VC2_19	-	MFC2_19

Table B.1 Locations of Devices in FDS Simulations

APPENDIX C: Output Plots of FDS Simulations

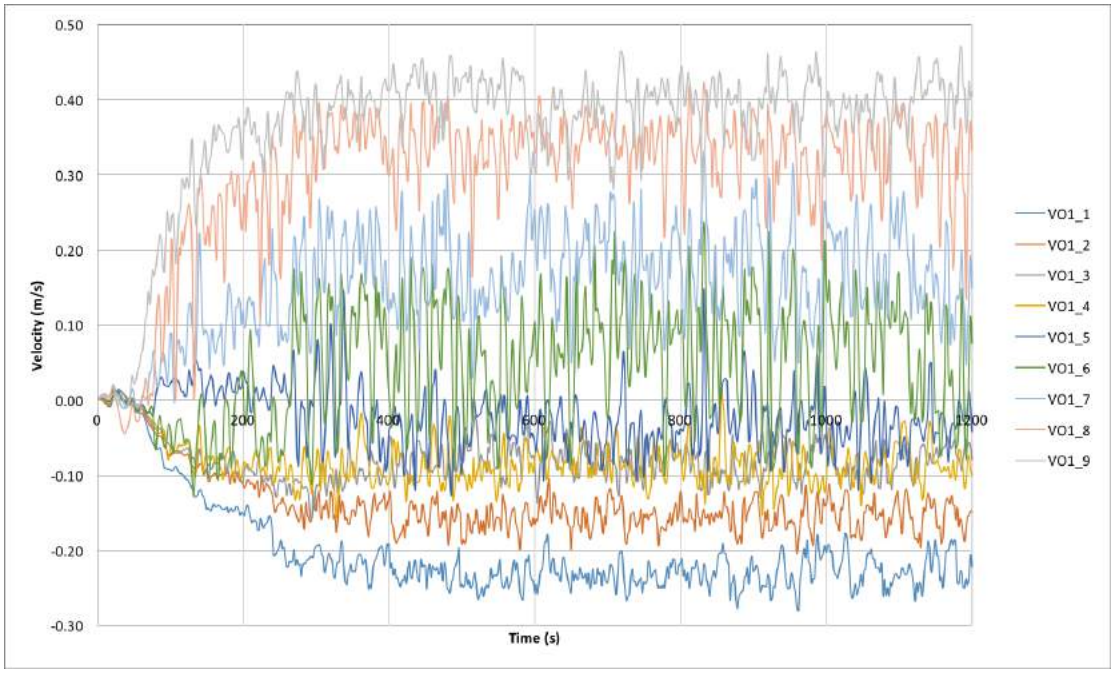

Figure C.1 Velocities along the Center Line of the First Floor Opening in M2

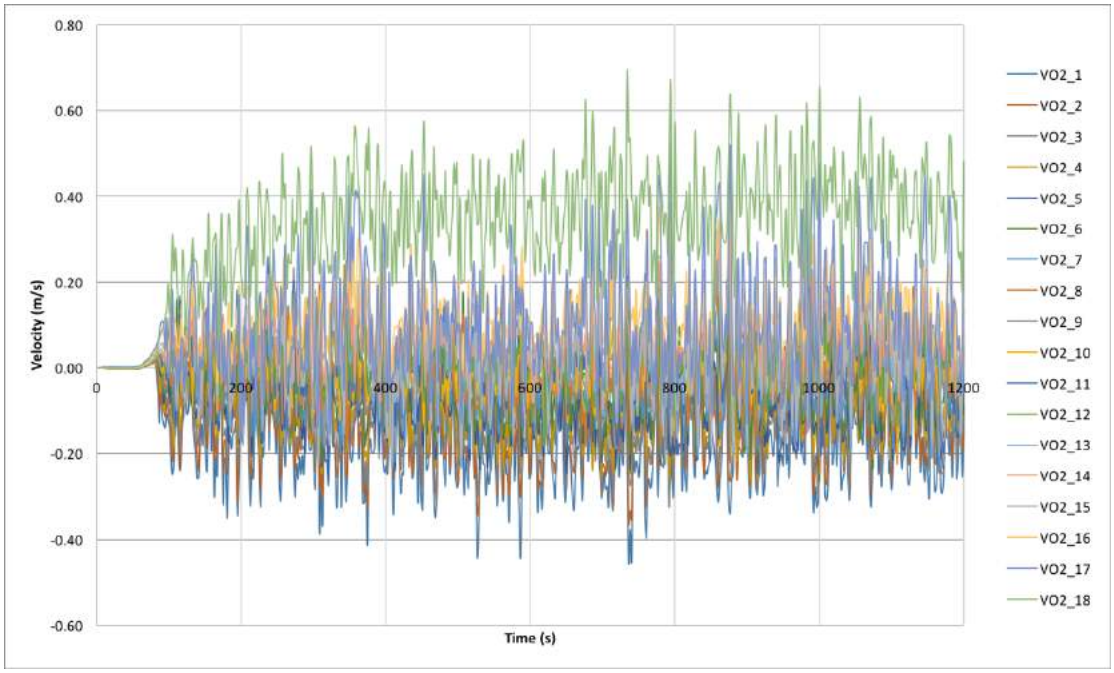

Figure C.2 Velocities along the Center Line of the Second Floor Opening in M2

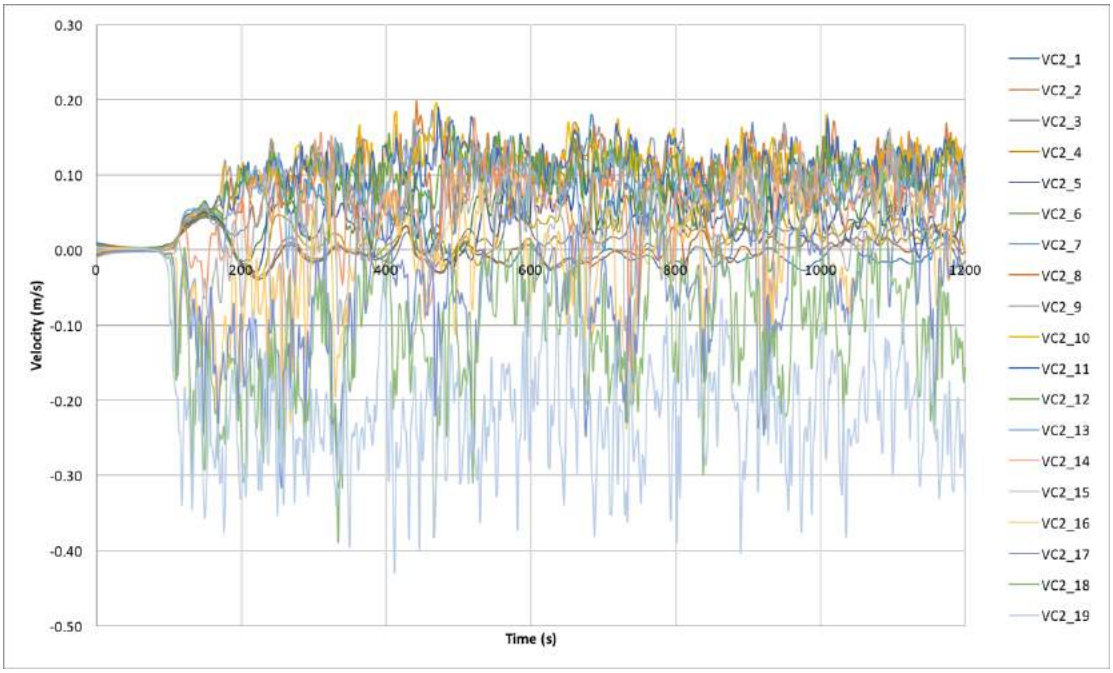

Figure C.3 Velocities along the Center Line of the Second Floor Compartment in M2

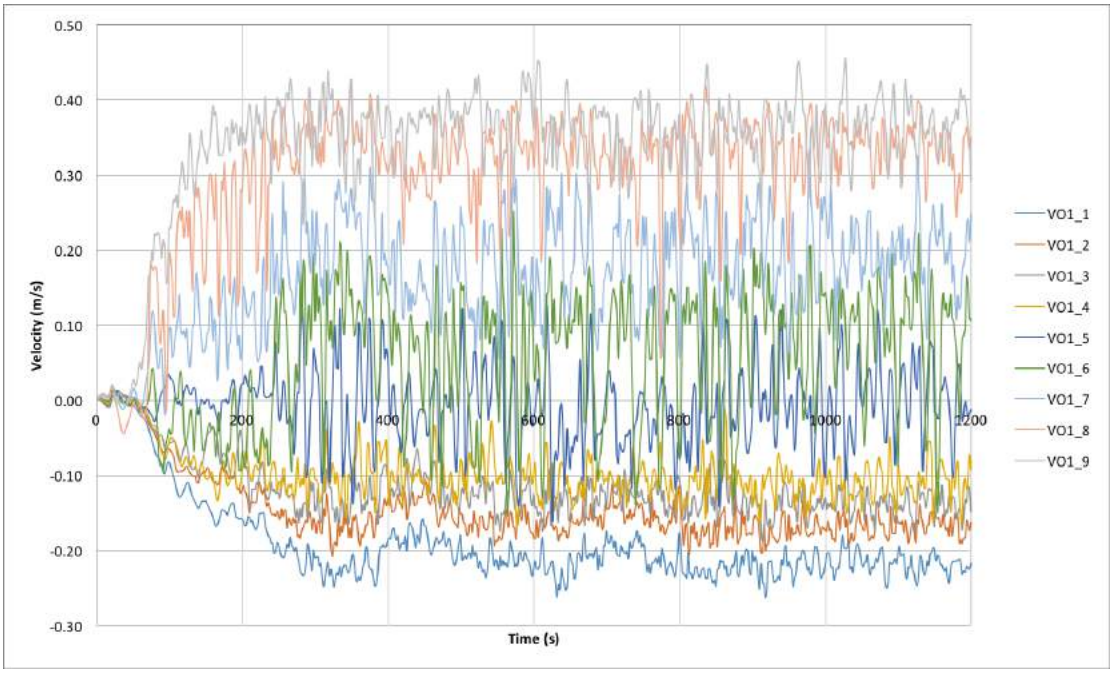

Figure C.4 Velocities along the Center Line of the First Floor Opening in M3

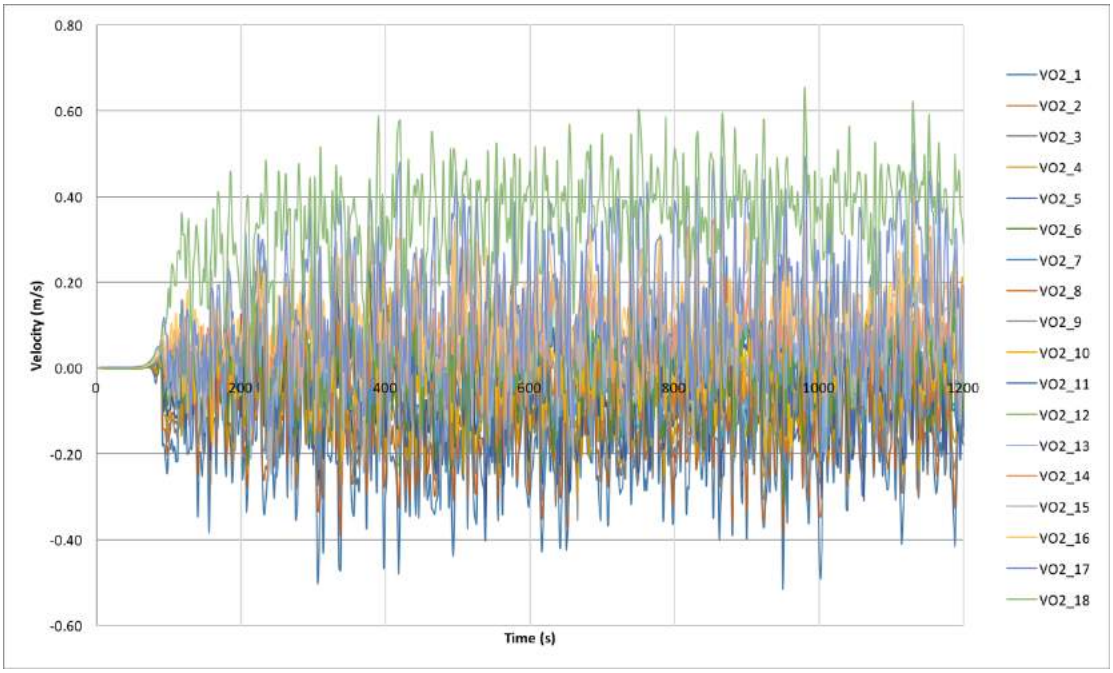

Figure C.5 Velocities along the Center Line of the Second Floor Opening in M3

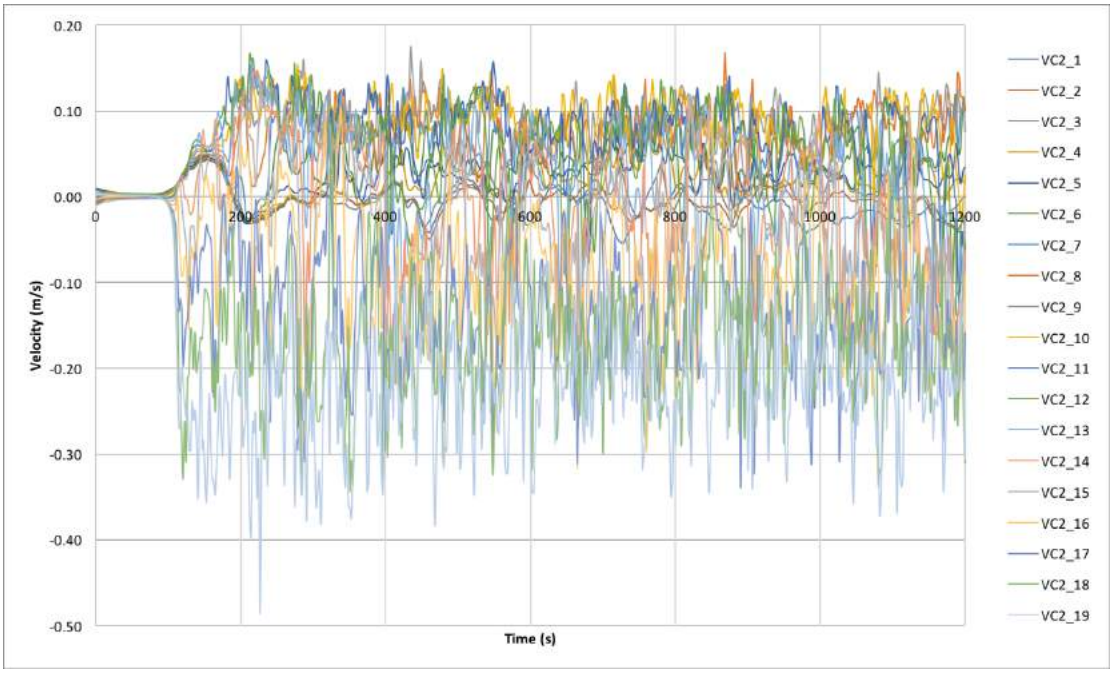

Figure C.6 Velocities along the Center Line of the Second Floor Compartment in M3

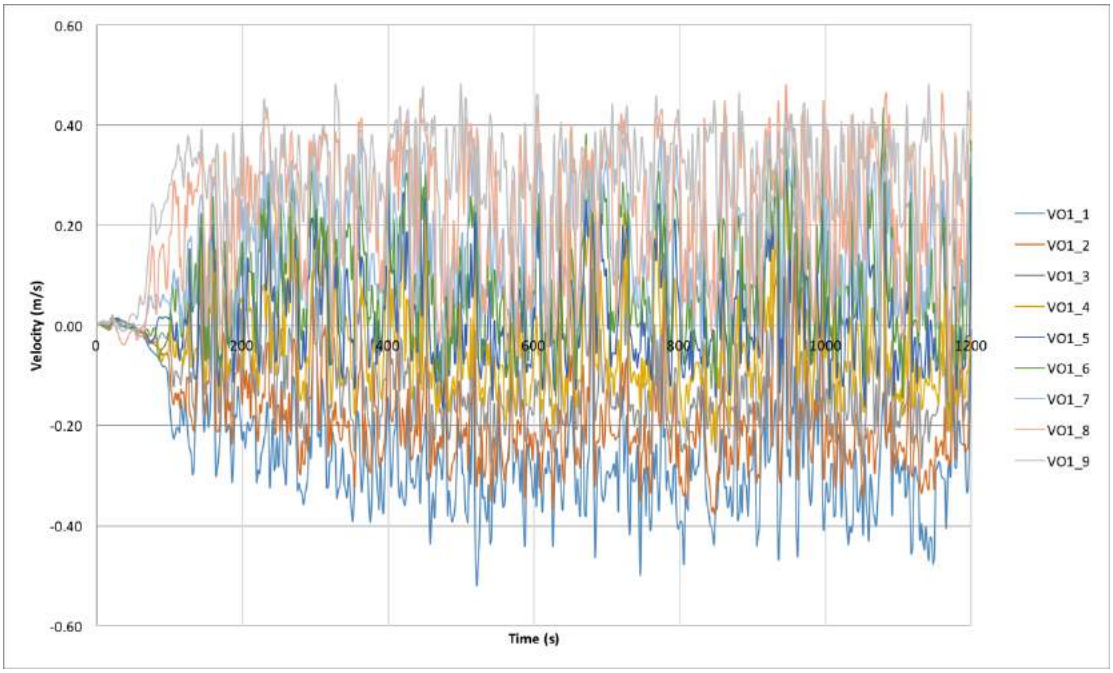

Figure C.7 Velocities along the Center Line of the First Floor Opening in M4

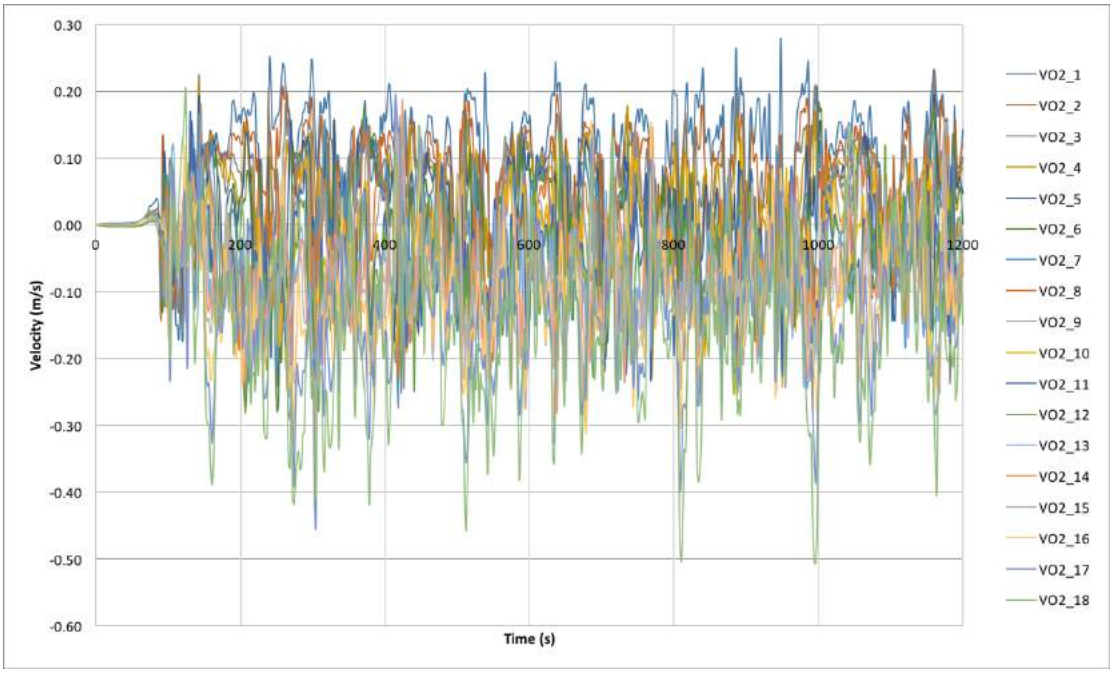

Figure C.8 Velocities along the Center Line of the Second Floor Opening in M4

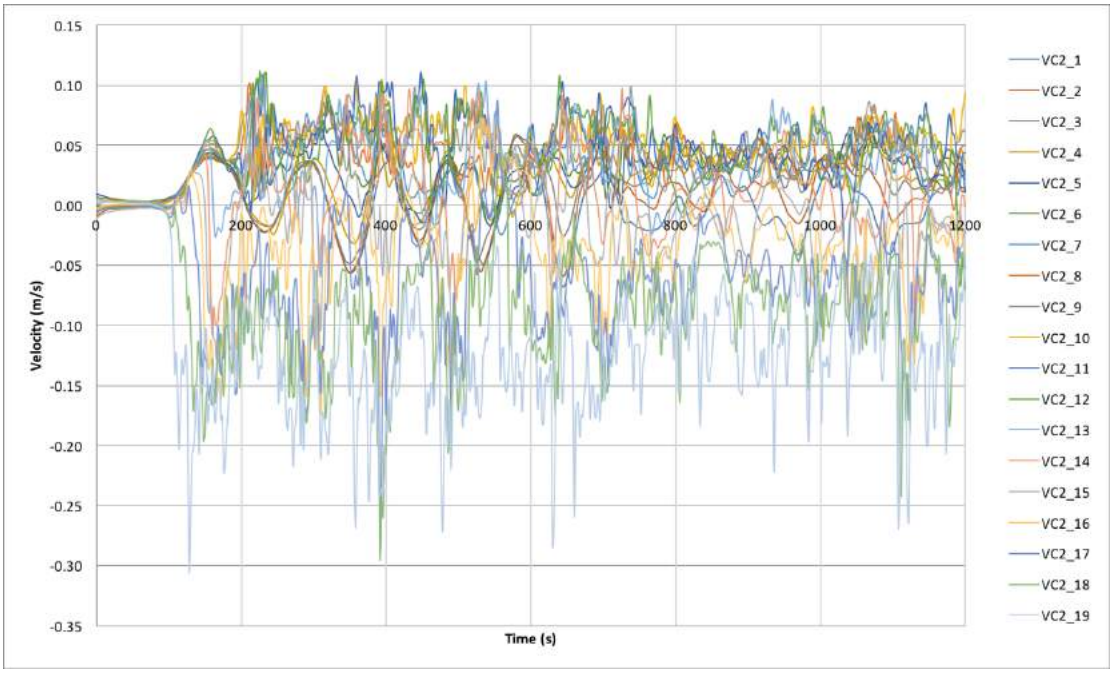

Figure C.9 Velocities along the Center Line of the Second Floor Compartment in M4

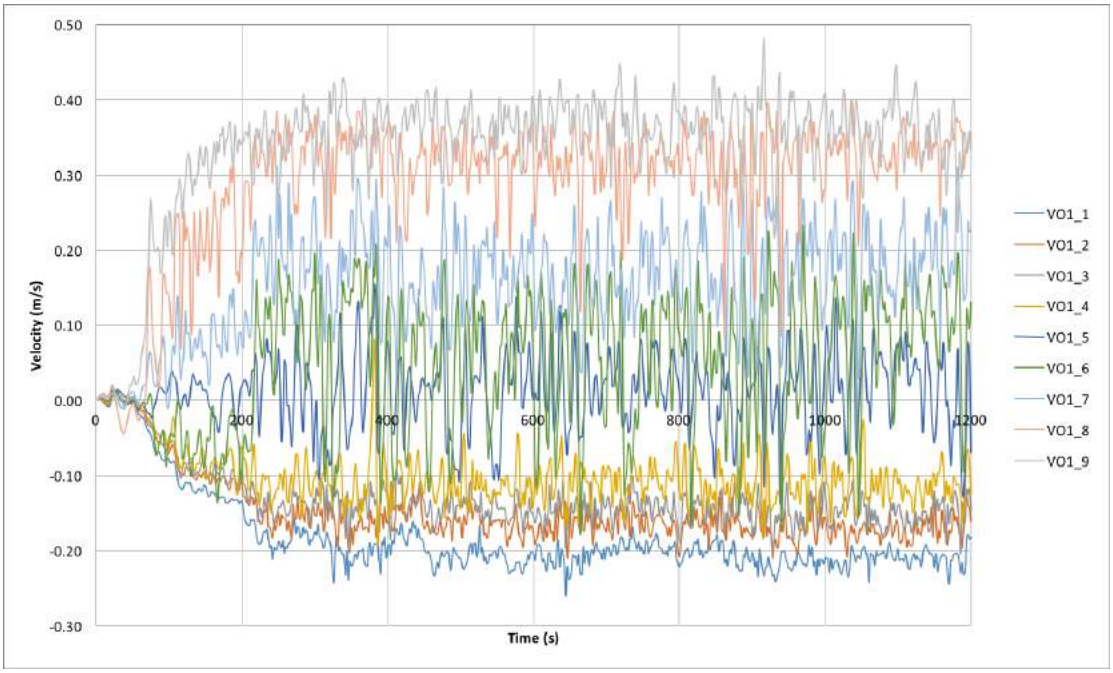

Figure C.10 Velocities along the Center Line of the First Floor Opening in M5

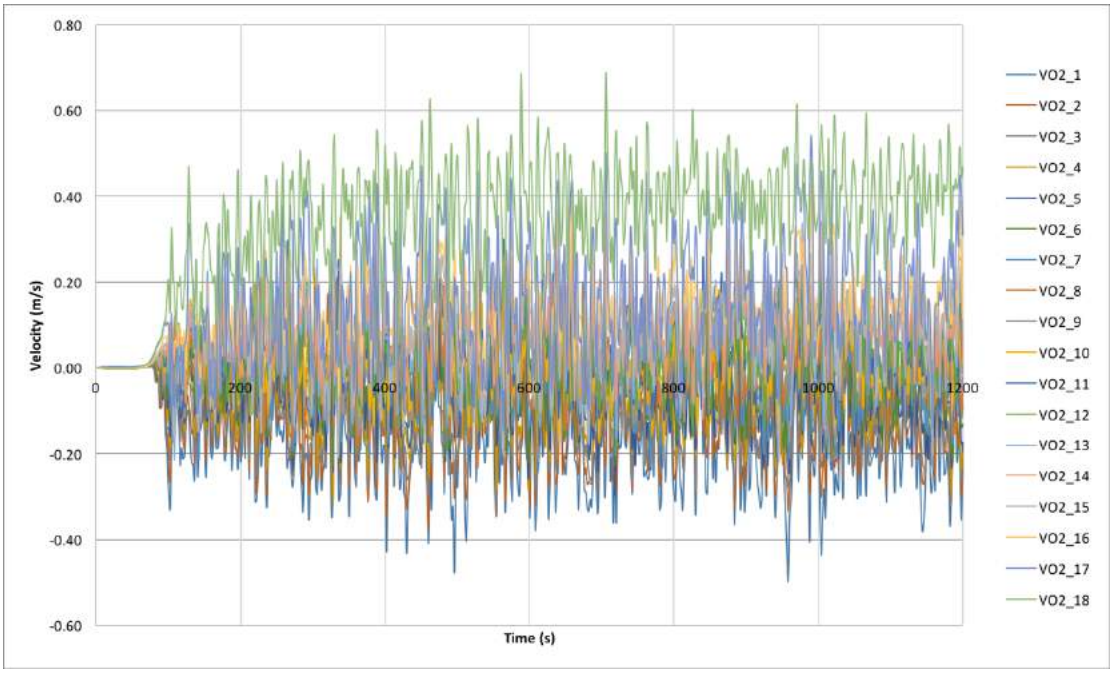

Figure C.11 Velocities along the Center Line of the Second Floor Opening in M5

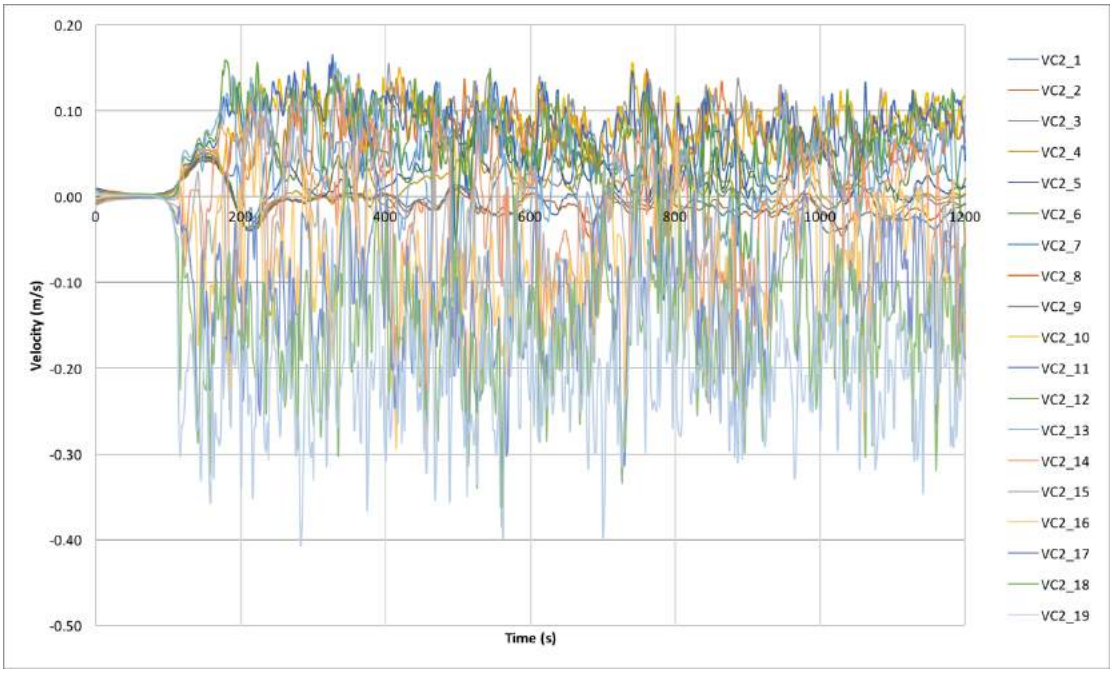

Figure C.12 Velocities along the Center Line of the Second Floor Compartment in M5

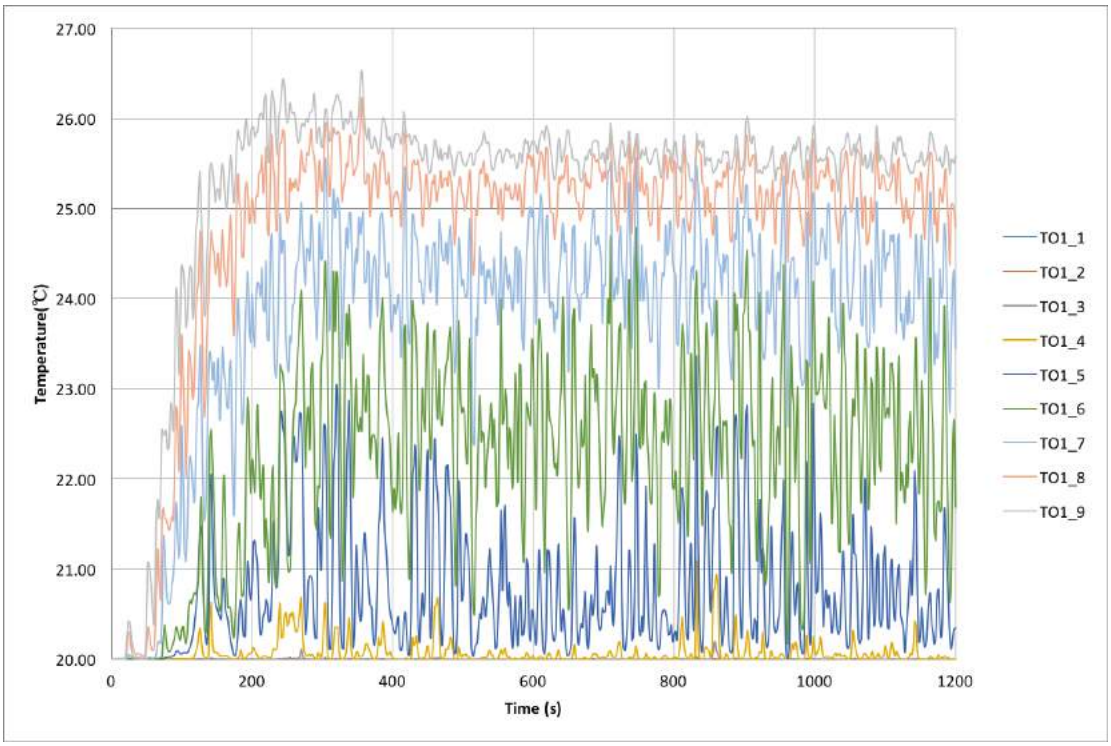

Figure C.13 Temperatures along the Center Line of the First Floor Opening in M2

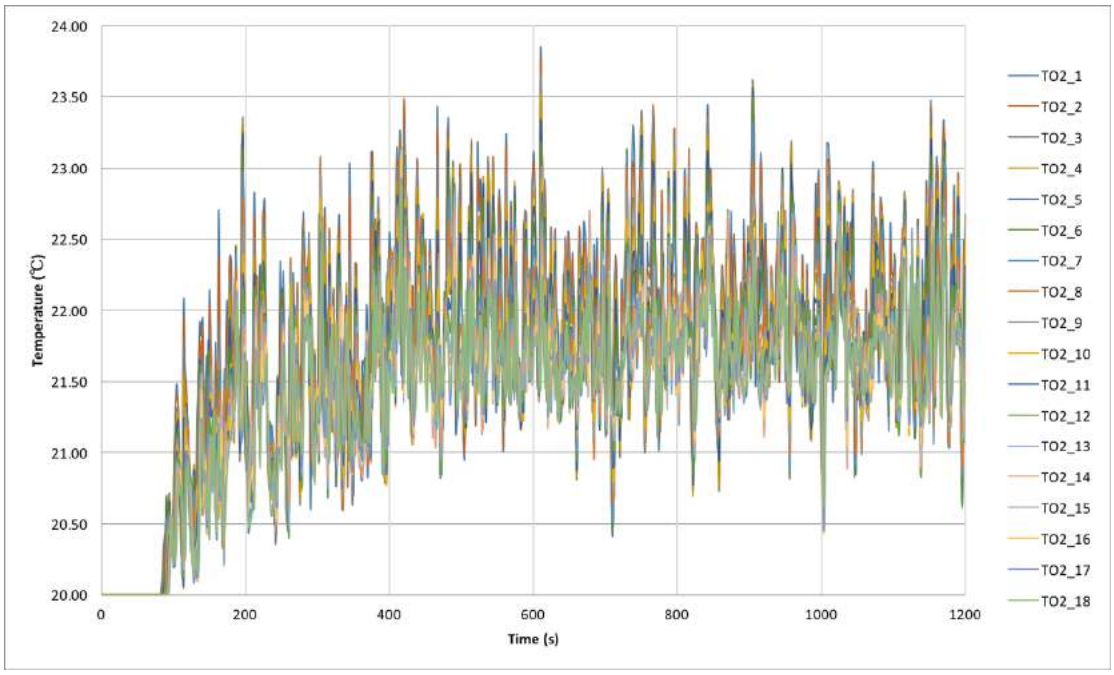

Figure C.14 Temperatures along the Center Line of the Second Floor Opening in M2

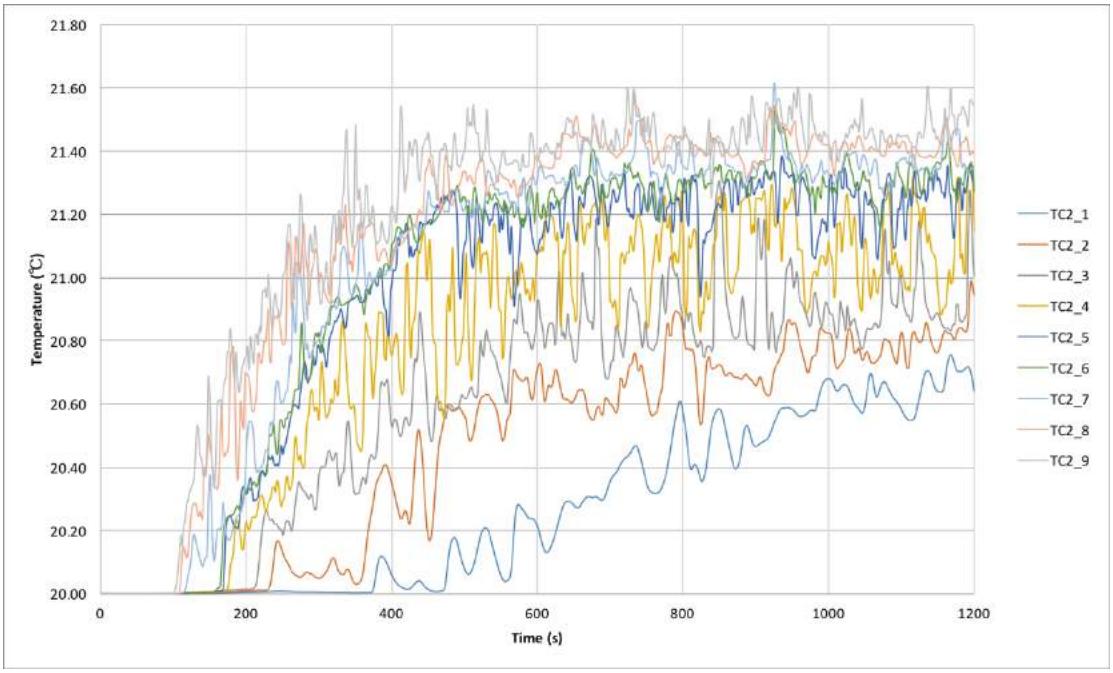

Figure C.15 Temperatures along the Center Line of the Second Floor Enclosure in M2

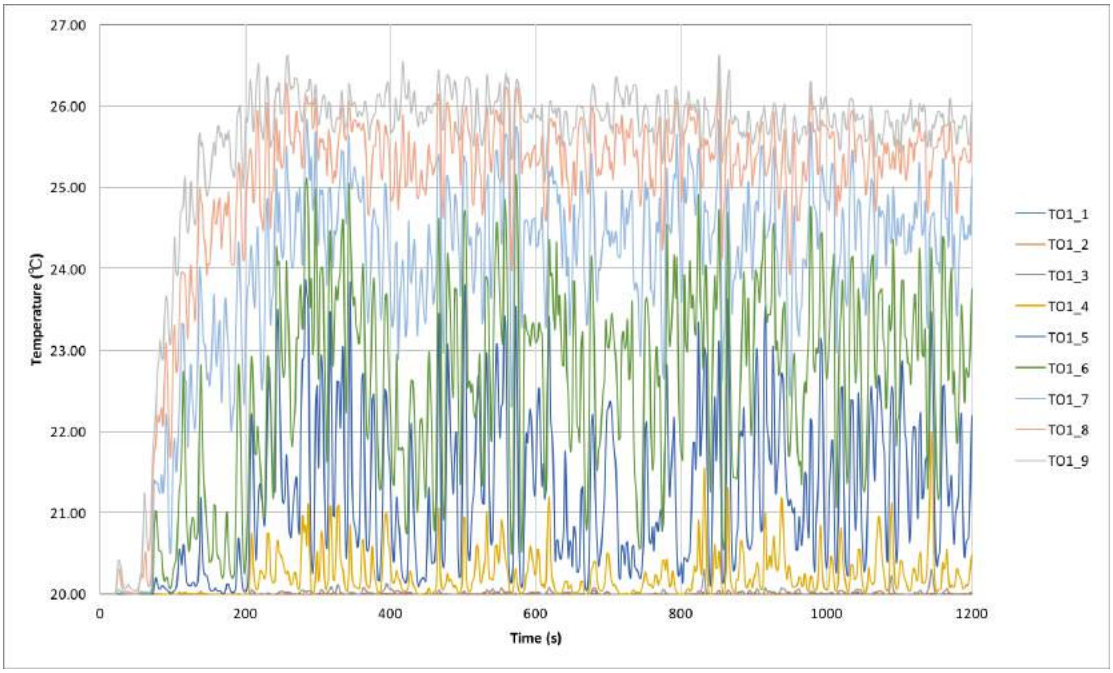

Figure C.16 Temperatures along the Center Line of the First Floor Opening in M3

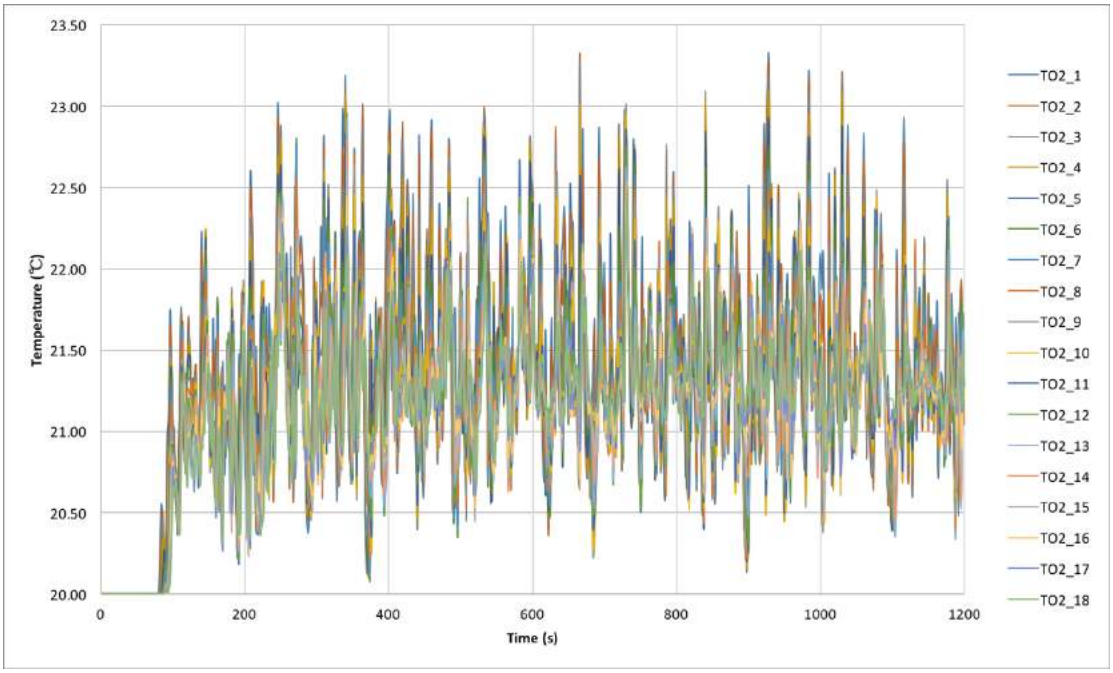

Figure C.17 Temperatures along the Center Line of the Second Floor Opening in M3

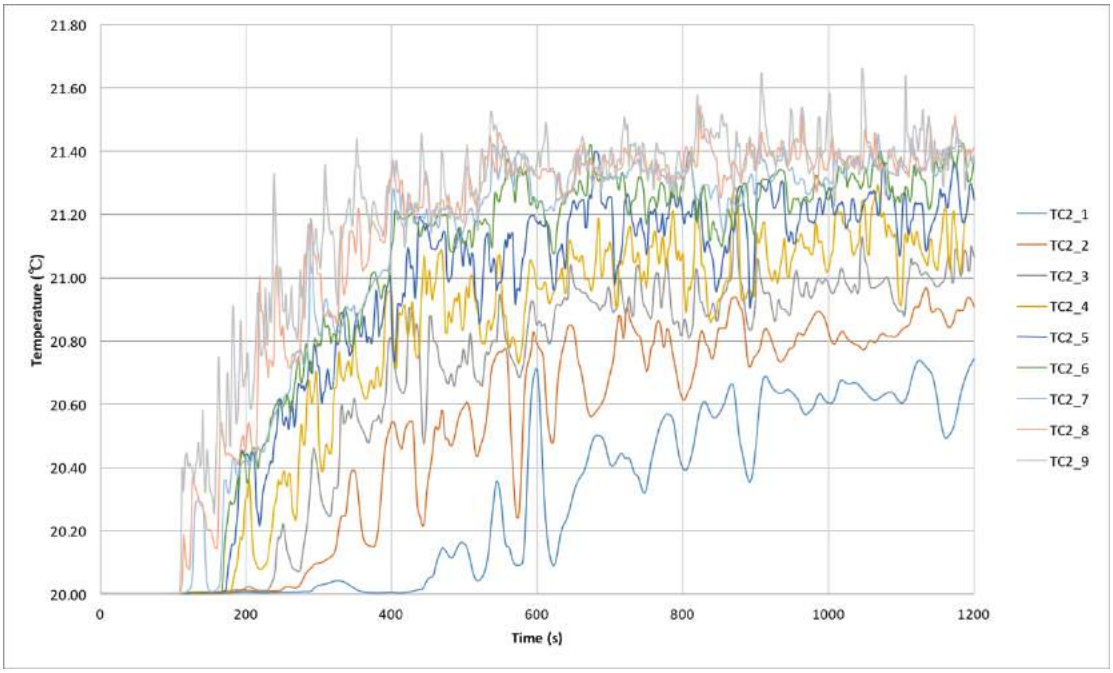

Figure C.18 Temperatures along the Center Line of the Second Floor Enclosure in M3

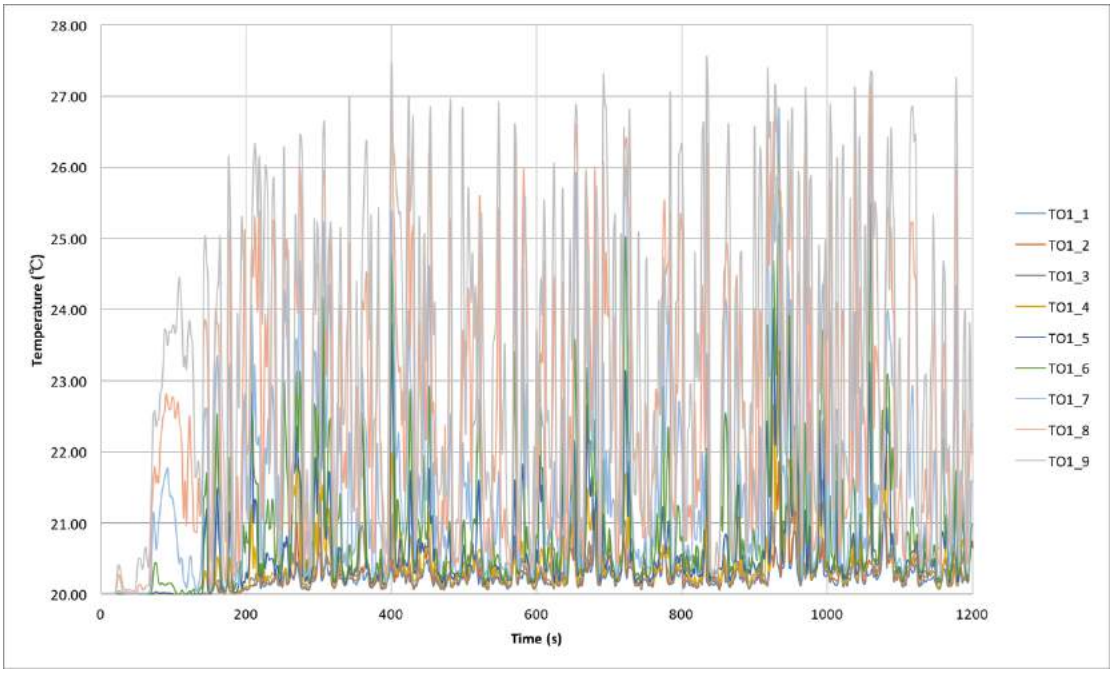

Figure C.19 Temperatures along the Center Line of the First Floor Opening in M4

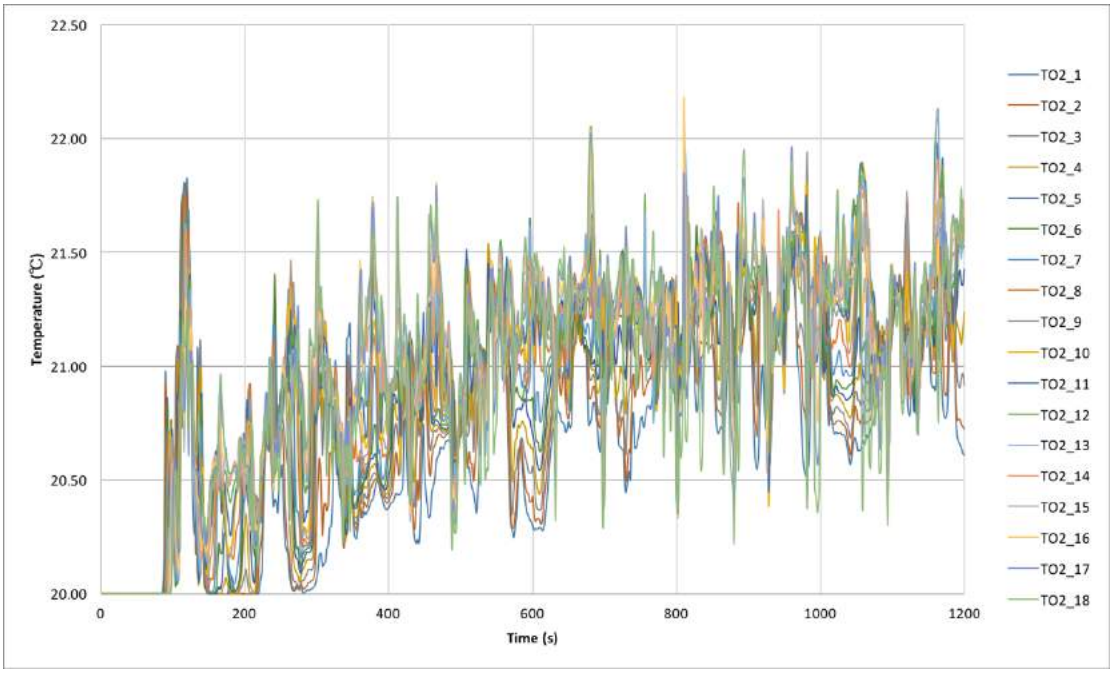

Figure C.20 Temperatures along the Center Line of the Second Floor Opening in M4

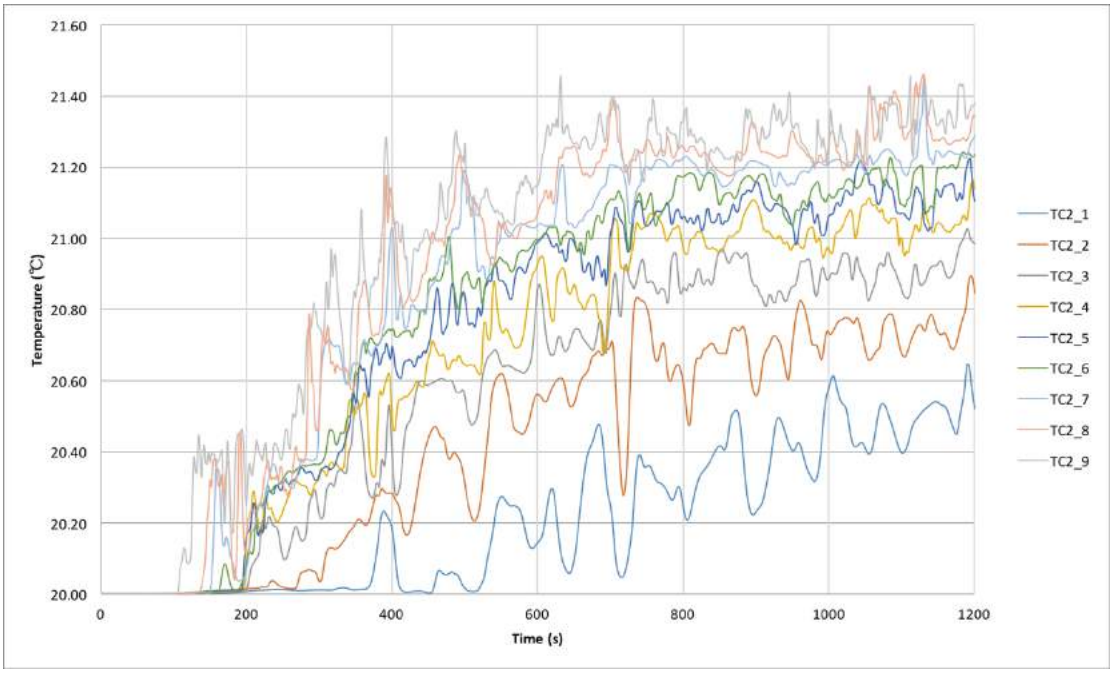

Figure C.21 Temperatures along the Center Line of the Second Floor Enclosure in M4

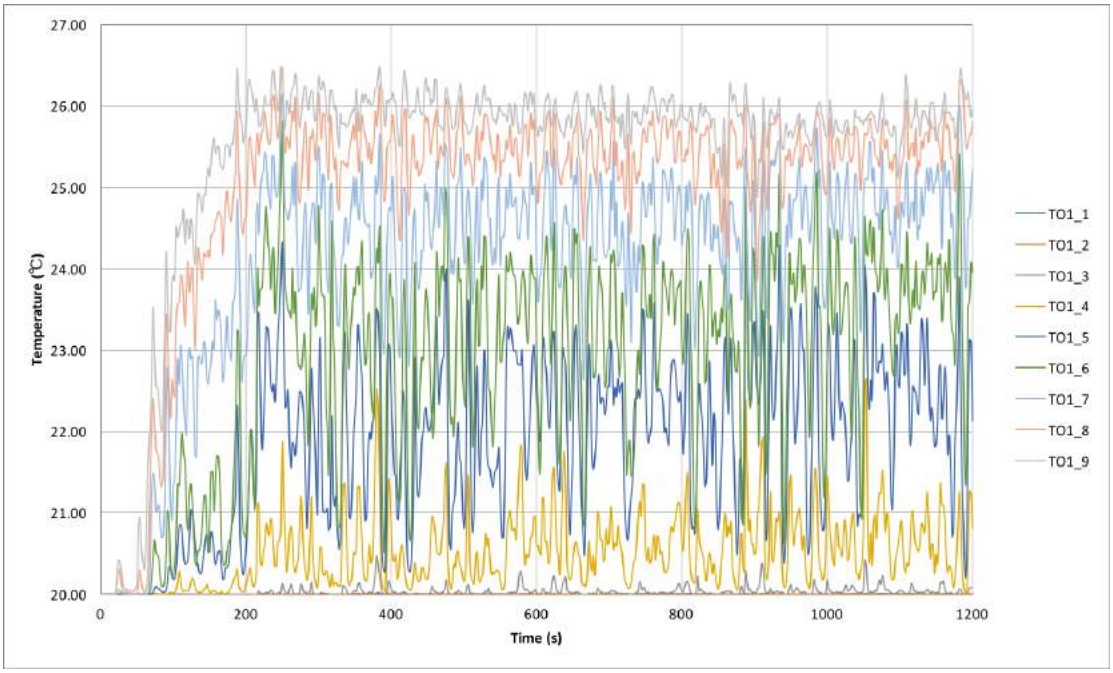

Figure C.22 Temperatures along the Center Line of the First Floor Opening in M5

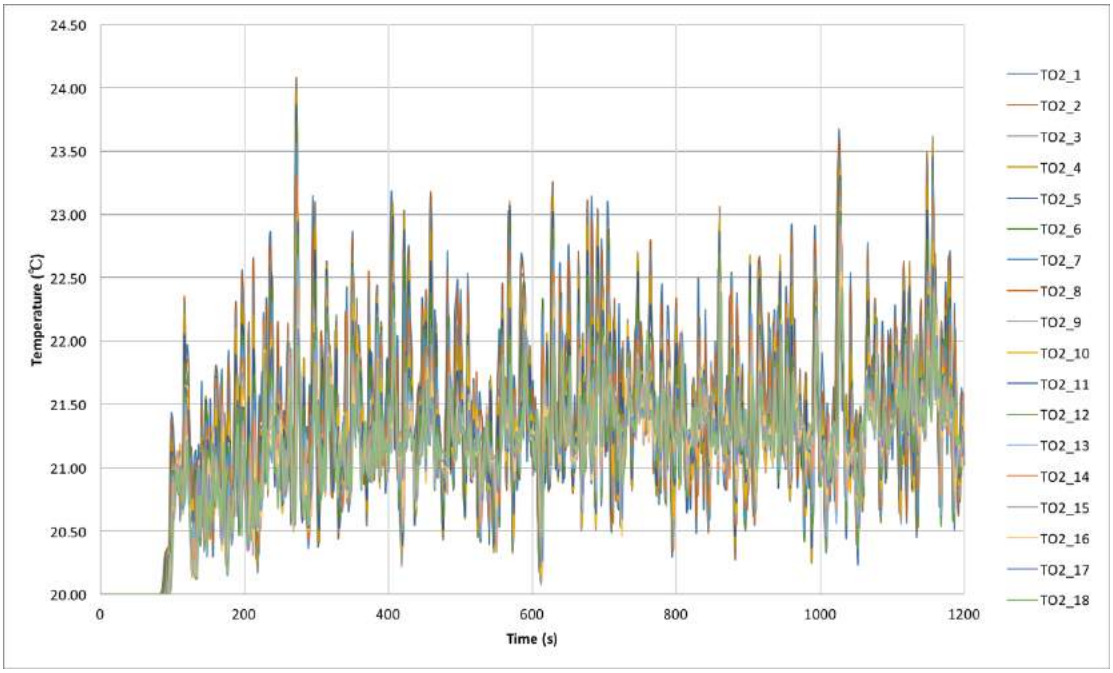

Figure C.23 Temperatures along the Center Line of the Second Floor Opening in M5

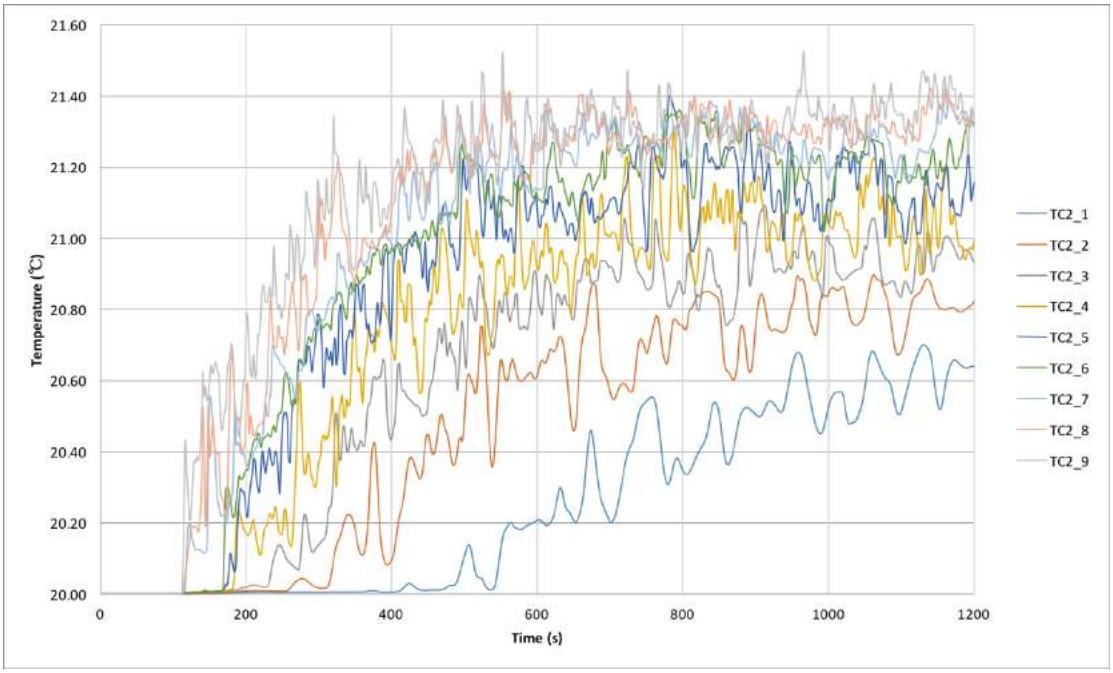

Figure C.24 Temperatures along the Center Line of the Second Floor Enclosure in M5

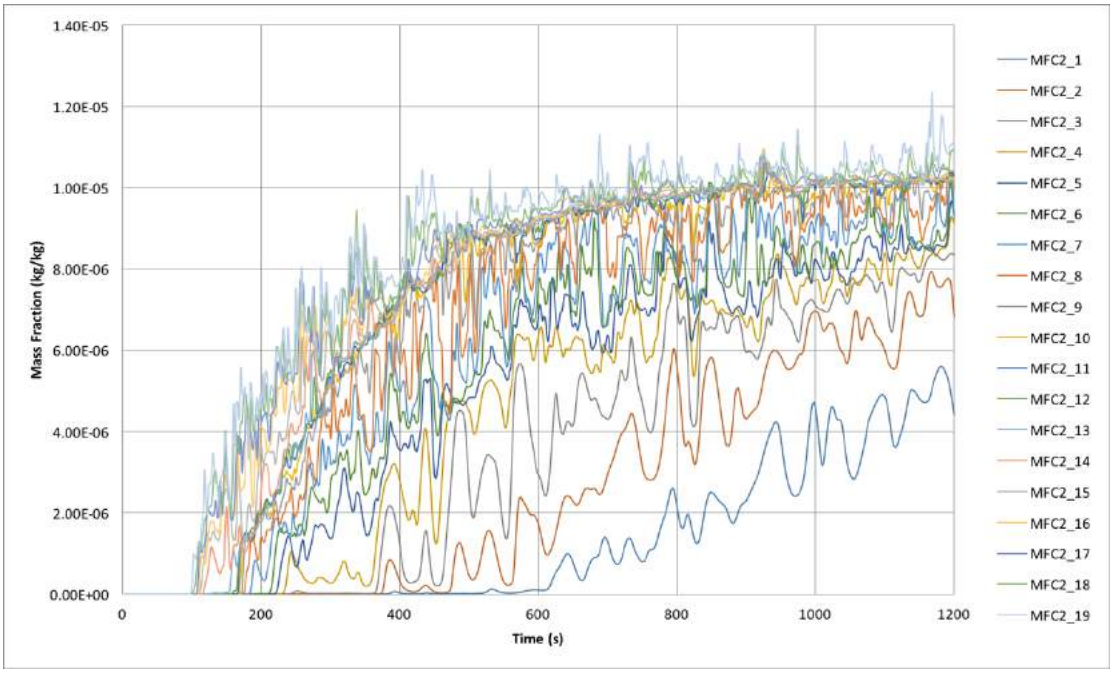

Figure C.25 Mass Fraction along the Center Line of the Second Floor Enclosure in M2

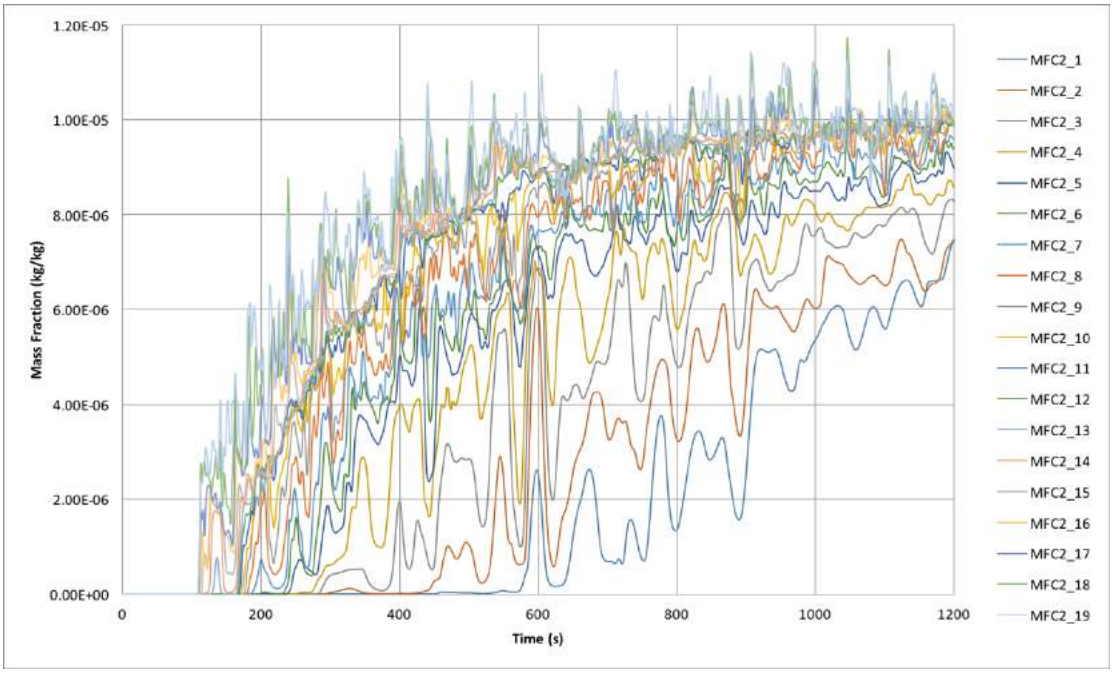

Figure C.26 Mass Fraction along the Center Line of the Second Floor Enclosure in M3

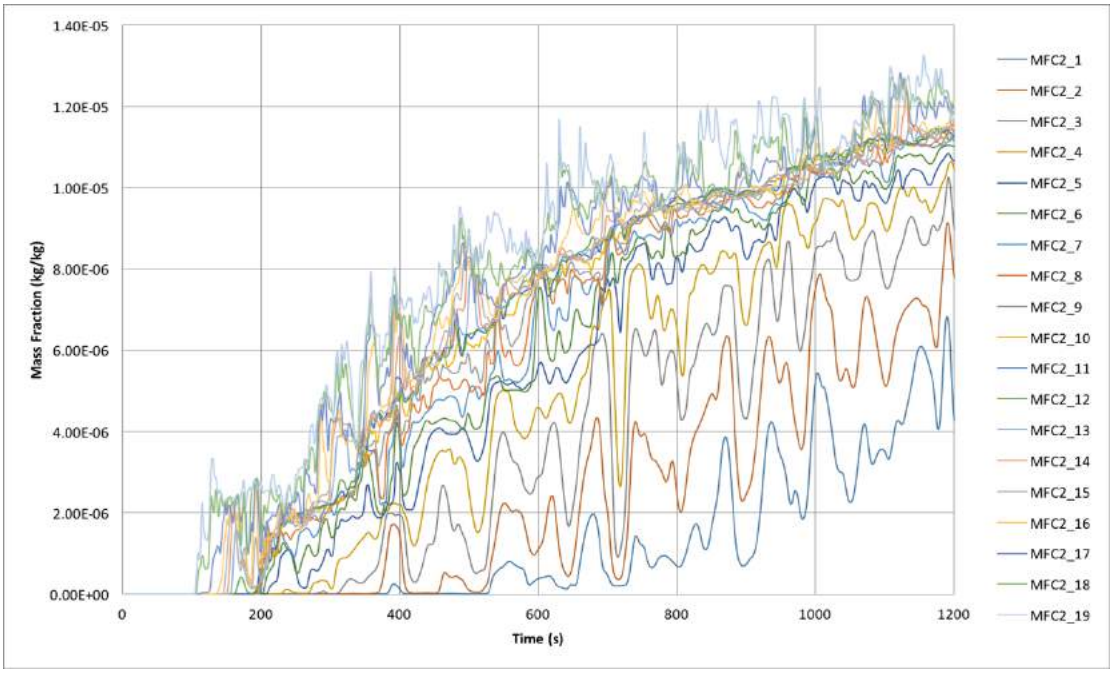

Figure C.27 Mass Fraction along the Center Line of the Second Floor Enclosure in M4

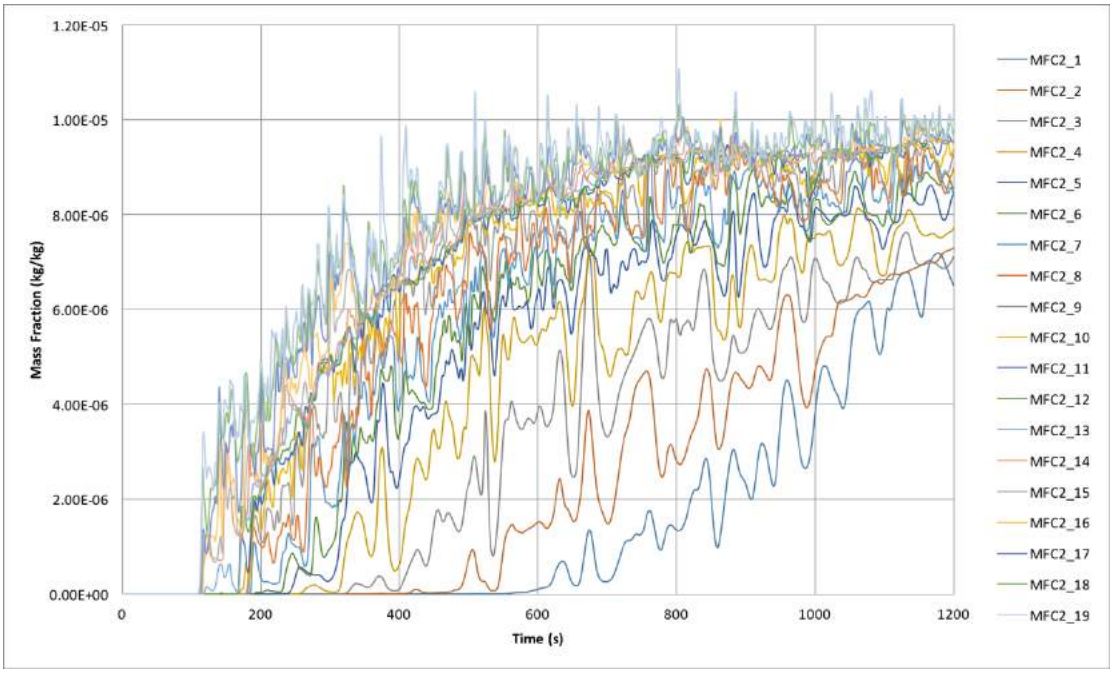

Figure C.28 Mass Fraction along the Center Line of the Second Floor Enclosure in M5

APPENDIX D: Mean Velocity Values Exported from PIV System

Height (m)	Velocity (m/s)			
	M1	M2	M3	M4
0.055	-0.02845041	-0.02052213	-0.03508422	-0.01613167
0.065	-0.01660030	-0.00821663	-0.01968277	-0.01051133
0.075	-0.00940439	-0.00211664	-0.01078755	-0.00791668
0.085	-0.00232621	0.00335545	-0.00431672	-0.00490197
0.095	0.00527030	0.00875311	0.00352953	-0.00079843
0.105	0.01319117	0.01514728	0.01112234	0.00357927
0.115	0.02117283	0.02222085	0.01815001	0.01096979
0.125	0.03028814	0.02920855	0.02647147	0.02202409

Table D.1 Mean Velocity Values at Steady State at the Center Line of Second Floor Opening Exported from PIV Experiments for M1 to M4